Doctoral Dissertation

Metabolomic analysis of immunoglobulin G (IgG)-producing Chinese hamster lung-YN cells in glucose-regulated fed-batch cultures

Puriwat Sukwattananipaat

October 2024

Department of Biotechnology,
Graduate School of Engineering,
Osaka University

Table of Contents

Table of Contents (continued)

Table of Contents (continued)

Table of Contents (continued)

Abbreviations

ALDH7A1: Aldehyde dehydrogenase 7A1, **AOC1**: Amiloride-sensitive amine oxidase, **ARG-2**: Arginase-2, **ASL**: Argininosuccinate lyase, **ASS**: Argininosuccinate synthetase, **ATP**: adenosine triphosphate, **BHMT***:* Betaine-homocysteine S-methyltransferase, **CBS**: cystathionine β-synthetase, **CHO**: Chinese hamster ovary, **CHL**: Chinese hamster lung, **COVID-19**: Coronavirus disease 2019, **CTH**: cystathionine γ-lyase, **Del**: decline stage of cell growth, **DO**: dissolved oxygen, **DMNT1**: DNA (cytosine-5-)-methyltransferase 1, **Ear:** early stage of cell growth, **ELISA**: enzyme linked immunosorbent assay, **Exp**: exponential stage of cell growth, **FBS**: fetal bovine serum, **FDA**: the United States Food and Drug Administration, **GABA:** gamma-aminobutyrate; 4-aminobutyrate, **GC**: gas chromatography, **GMP**: Good Manufacturing Practice, **GNMT**: Glycine N-methyltransferase, **GlnC**: glutamine consumption stage, **GlnP**: glutamine production stage, **GlnR**: glutamine re-consumption stage, **GA**: Glutaminase, **GS**: Glutamine synthetase, **HMT**: Human Metabolome Technologies, **Ig**: immunoglobulin, **IgG**: immunoglobulin G, **IMDM**: Iscove's modified Dulbecco medium, **KEGG**: Kyoto Encyclopedia of Genes and Genomes, **LC**: liquid chromatography, **LC-MS/MS**: liquid chromatography with tandem mass spectrometry, **mAb**: monoclonal antibody, **MAT2A**: methionine adenosyltransferase 2A, **mRNA**: messenger ribonucleic acid, **MS**: mass spectrometry, **NIR**: near infrared, **NMR**: Nuclear magnetic resonance, **NNMT**: Nicotinamide N-methyltransferase, **OAT**: Ornithine aminotransferase, **OCT**: Ornithine carbamoyl transferase, **ODC**: Ornithine decarboxylase, **P5CD**: pyrroline-5-carboxylate dehydrogenase, **P5CR**: Pyrroline 5-carboxylase reductase, **P5CS**: pyrroline-5-carboxylate synthetase, **PAT**: process analytical technology, **PCA**: principal component analysis, **PID**: proportional-integral-derivative, **RMSEP**: root mean square error of prediction, **SAH**: S-

adenosylhomocysteine, **SAHH**: adenosyl homocysteinase, **SAM**: S-adenosylmethionine, **Sta**: stationary stage of cell growth, **TCA**: tricarboxylic acid, **VCC**: viable cell concentration,

Nomenclatures

μ_{max}	maximum specific cell growth rate (d^{-1})
ΔGlc	a difference between target point of glucose concentration (3.0 g/L) and off-line measured glucose concentration (-)
F_{Glc}	scheduled glucose feed amount (L)
$F_{Glc\ mod}$	modified glucose feed amount (L)
G_{con}	weight of consumed glucose (g)
Glc_{feed}	glucose concentration in glucose feed solution (g/L)
Glc	extracellular glucose concentration from off-line measurement (g/L)
Glc^*	extracellular glucose concentration from in-line NIR measurement (g/L)
Gln	extracellular glutamine concentration (mmol/L)
IgG	extracellular IgG concentration (mg/L)
Lac	extracellular lactate concentration (g/L)
n	number of samples (-)
q_{glc}	specific glucose consumption rate ($pmol \cdot cell^{-1} \cdot d^{-1}$)
q_{gln}	specific glutamine consumption rate ($pmol \cdot cell^{-1} \cdot d^{-1}$)
q_{lac}	specific lactate consumption rate ($pmol \cdot cell^{-1} \cdot d^{-1}$)
q_p	specific IgG production rate ($pg \cdot cell^{-1} \cdot d^{-1}$)
t	time (d)
V	culture volume (L)
$V_{glc\ feed}$	glucose feed volume (L)
$V_{other\ feeds}$	supplied volume including feed medium and basic solution (L)
X_v	viable cell concentration (cell/L)
X_t	total cell concentration (cell/L)
$\int(X_v/X_t)\ dt$	integral viable cell concentration ($cell^{-1} \cdot d^{-1}$)

Chapter 1:

General introduction

Chapter 1: General introduction

1.1 Monoclonal antibody (mAb) and immunoglobulin (Ig)G production

Monoclonal antibodies (mAbs) are proteins that have a particular binding ability to one target called an epitope (Tabll et al., 2015). The mAbs are advantageous due to their applications. For instance, several mAbs are currently used as therapeutic medicines for curing cancers, infectious diseases, and autoimmune disorders (Castelli et al., 2019). Additionally, mAbs are applied for clinical diagnostic tools (Waldmann, 1991). For example, a rapid antigen test kit for coronavirus disease 2019 (COVID-19) diagnosis was developed based on murine-derived mAb conjugated with gold nanoparticles (Salcedo et al., 2022). Due to their versatility, the demand for mAb has grown over the decade. The ratio of mAb products in the protein-based biopharmaceutical industry has been increasing since 2011. The portion of mAbs sales gradually increased from 49.9% in 2011 to 80.2% in 2021 (Fig. 1) and hiked worldwide sales to over 217 billion United States dollars in the same years (Walsh and Walsh, 2022).

Among mAb products, recombinant immunoglobulin G (IgG) is the most approved and sold antibody serotype. The IgG subclass is approximately 90% of the commercial mAbs available in the United States and Europe (Tang et al., 2021). The majority of IgG in available mAb products may be caused by the fact that IgG is the most antibody available in human serum among five antibody serotypes, consisting of immunoglobulin A, D, E, G, and M (Vidarsson et al., 2014). Therefore, abundant research uses IgG-expressing systems as a study model, including this research.

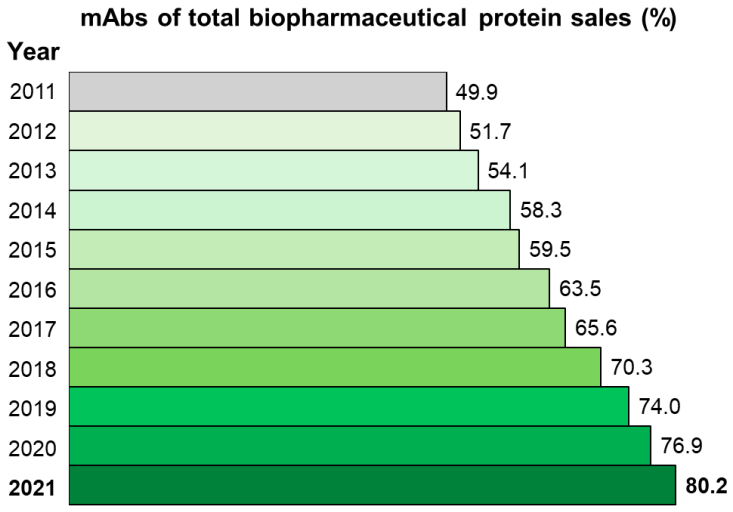

Figure 1. Rasing trends the antibody demand in the biopharmaceutical global market. The annual records of monoclonal antibody sales were described as a percentage of total protein-based biopharmaceutical products from 2011 to 2021. Redesigned from Walsh and Walsh, 2022.

1.2 Chinese hamster ovary cells, the major expression host in the mAb production

Chinese hamster ovary (CHO) cells are an immortalized cell line that was isolated from ovarian epithelial of Chinese hamster (*Cricetulus griseus*) biopsy (Puck et al., 1958). Then, the CHO-K1 cell line was the first CHO strain successfully generated from the parental CHO subclone and reported in 1968 (Lewis et al., 2013). So far, varieties of CHO cell lineages have been constructed with unique properties. For example, CHO-DG44 cells are a dihydrofolate reductase-deficient CHO cell line, which allows the methotrexate selection system, which is a non-antibiotic usage system (Reinhart et al., 2018). CHO-S cells are a commonly used CHO cell line on the industrial scale. This CHO cell line is well-adapted to serum-free suspension culture while providing high volumetric production (Tihanyi and Nyitray, 2020). CHO-MK cells are a new isolated CHO cell line capable of high productivity in a brief time (Masuda et al., 2024).

In 1987, CHO cells were applied as an expression host for the first time for human tissue plasminogen activator production that was approved by the United States Food and Drug Administration (FDA) (Finkle et al., 1988; Bryan et al., 2021; Walsh and Walsh, 2022). Nowadays, CHO cells have become the most widely used expression host in a plenty of recombinant proteins, including monoclonal antibodies (Geng et al., 2024). The report from the National Institution of Health Science of Japan in 2022 showed that CHO cells were the major (69%) expression hosts for approval antibody products in Japan, the United States of America, and Europe (Fig. 2). The desires of CHO cell usage are attributed to their characteristics. For instance, CHO cells have human-like N-glycosylation modification (Spadiut et al., 2014), which can affect immunogenic response and safety (Boune et al., 2020). Moreover, CHO cells are resistant to several families of pathogenic viruses such as coxsackievirus B3, influenza, and hepatitis virus (Berting et al., 2010; Horie et al., 2022). In addition, CHO cells can adapt to serum-free cultivation, conduct scaling-up processes, and produce therapeutic antibodies up to 10 g/L, which are certified by the Good Manufacturing Practice (GMP) regulation (Omasa et al., 2010).

Although CHO cells have been versatile in the biopharmaceutical industry over decades, using CHO cells still faces some limitations and requires further cell line improvement or optional expression host development. For instance, CHO cells have a longer proliferation process compared to non-mammalian expression hosts such as bacteria and fungi (Jiang et al., 2019; Sandomenico et al., 2020). The low growth rate of CHO cells leads to extending the duration of upstream bioprocess, especially 3–9 months for stable cell clone generation, resulting in expanding cell line development processes, raising cost, and loading of laboratory work (Rajendra et al., 2016; Poulain et al., 2019).

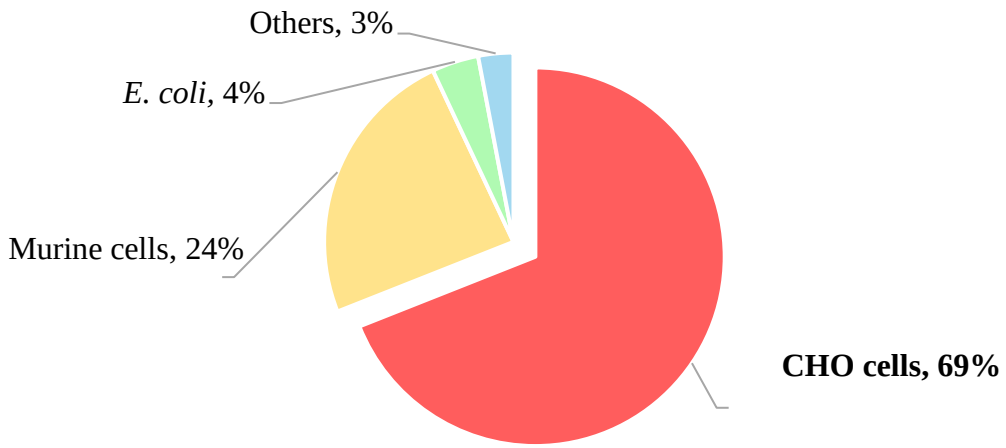

Figure 2. Ratio of expression hosts in therapeutic antibodies production in 2022. Approval antibody products were recorded in Japan, the US, and Europe. Redesigned from (List of antibody drugs approved in the US, Japan, and Europe, [National Institutes of Health, Japan]., March 13, 2024).

1.3 Chinese hamster lung – YN cells, an optional rapid-proliferating expression host for the mAb production

As a challenge to CHO cells in terms of their slow growth, developing a fast-growing mammalian expression concept has been executed. Chinese hamster lung (CHL)-YN cells (RIKEN Bioresource Cell Bank, RCB5004) are a new cell line originated from lung fibroblast cells by Dr. Yamano-Adachi Noriko, reported in 2020. The CHL-YN cells were isolated from the lung tissue of a female Chinese hamster, and then an immortalized cell pool was generated from the primary cell culture by spontaneous transformation with Iscove's modified Dulbecco medium and 20% fetal bovine serum. Then, CHL-YN cells were able to cultivate into a serum-free condition. CHL-YN cells could be cultivated over five hundred days and cryopreserved. Besides that, CHL-YN cells were certified for biosafety tests such as mycoplasma detection tests, viral

contamination, and sterility testing. CHL-YN cells have already been deposited at the RIKEN RBC cell bank (Yamano-Adachi et al., 2020).

Considering their characteristics, CHL-YN cells have comparable properties to CHO-K1 cells in many aspects, such as chromosomal translocation pattern, over 50% transfection efficiency, and glycosylation profiles on the mAb product. Intriguingly, CHL-YN cells could grow rapidly in a serum-free chemically defined medium. The doubling time is approximately 10.74 hours (Table 1), which doubles faster than CHO-K1 cells when cultivated in the same condition. Additionally, CHL-YN cell culture investigation indicated that CHL-YN cells have different metabolic backgrounds compared to CHO-K1 cells. For instance, a previous study in flask-batch cultivation revealed that CHL-YN cells had lower glucose consumption rates than CHO-K1 cells (Fig. 3). Intriguingly, CHL-YN cells had strong glutamine production ability, which is distinct from several CHO cell lines. Extracellular glutamine concentration rose after it was dropped without any supplementation (Fig. 4A). Besides that, RNA-sequencing analysis showed that glutamine synthetase, an enzyme converting glutamate and ammonium into glutamine, in CHL-YN cells was expressed at a higher level than CHO-K1 cells (Fig. 4B). Glutamine is a nonessential amino acid that is considered an essential energy source for cancer and immortalized cells due to an overrate of glutamine consumption beyond glutamine biosynthesis (Ritacco et al., 2018; Yoo et al., 2020). Therefore, these prominent properties of CHL-YN cells could conduce to the development of CHL-YN cells as an optional expression host for mAb production.

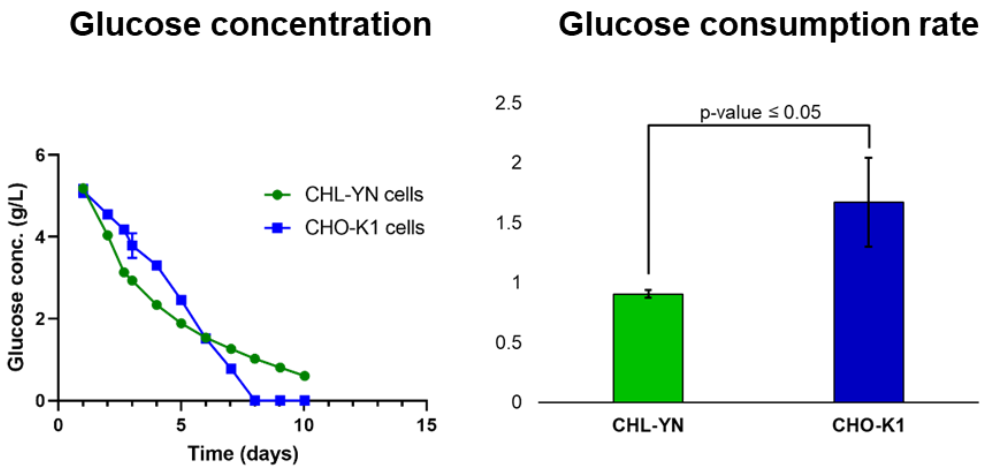

Figure 3. Glucose profiles from flask-batch CHL-YN and CHO-K1 cell cultures. (Left) Time course of extracellular glucose concentration. (Right) Specific glucose consumption was calculated from the exponential phase of cell growth during 24–64 hours. Statistical analysis is performed via the student's *T*-test (Master thesis of Sukwattananipaat, 2020).

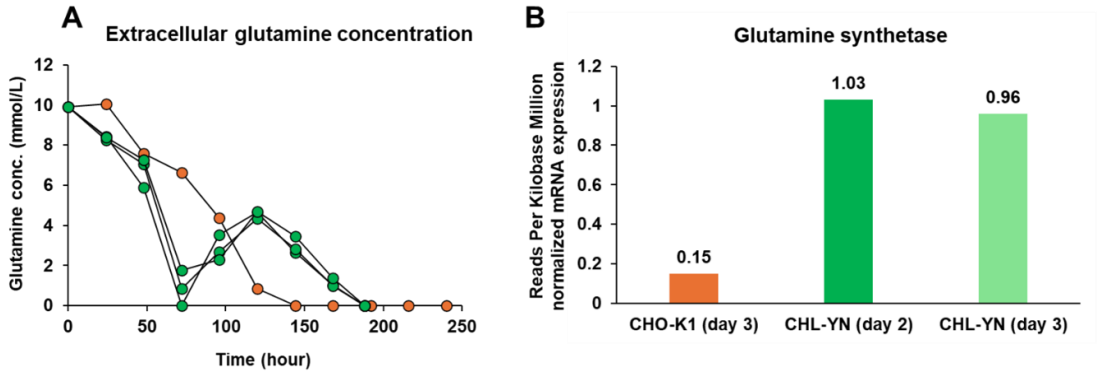

Figure 4. CHL-YN cells investigation revealed their glutamine production capability. **A)** Time-course of extracellular glutamine concentration in cell cultures. Green dots represent the CHL-YN cell samples, while orange dots represent the CHO-K1 cell samples. **B)** Reads per Kilobase per million mapped reads normalized mRNA-sequencing information shows the availability of glutamine synthetase gene expression. Redesigned from (Yamano-Adachi et al., 2020).

Table 1. Comparison of specific cell growth and IgG productivity between the CHL-YN and CHO-K1 cells cultivating in 500-mLErlenmeyer flasks. Both cells were cultivated in EX-CELL® CD CHO Fusion medium containing 6 mM L-glutamine (Yamano-Adachi et al., 2020).

Cell type	CHL-YN	CHO-K1
Specific growth rate (h^{-1})	0.0645 ± 0.0012	0.0326 ± 0.0005
Doubling time (h)	10.7 ± 0.2	21.3 ± 0.3
Specific production rate ($pg \cdot cell^{-1} \cdot day^{-1}$)	0.255 ± 0.012	0.124 ± 0.023
Final IgG concentration (mg/L)	7.13 ± 0.29	6.05 ± 0.73

1.4 Metabolomics approach, an investigative tool on cell culture components

As the previous studies (Yamano-Adachi et al., 2020; Thesis of Sukwattananipaat, 2020) did not provide comprehensive investigation on distinct glucose and glutamine metabolic backgrounds, in this study, metabolomics analysis was proposed for investigating metabolic profiles of IgG-producing CHL-YN cells compared to CHO-K1 cells, particularly in glucose and glutamine metabolisms. Metabolomics is an omics method that is the systematic identification and quantitation of all metabolites in a biological sample (Idle and Gonzalez, 2007). Metabolomics can be used for exploring a variety of samples and be beneficially applied to various fields such as food components, microbiome study, medical design, disorder diagnosis, and cell cultures (Castelli et al., 2021; Selamat et al., 2021; Bauermeister et al., 2022).

Regarding metabolomics analysis applied for cell cultivations, many researchers conducted metabolomics approaches aiming at exploring the cell cultures under various conditions. For instance, Pereira et al. (2018) gathered and reviewed key metabolites that become limited or over-accumulated during CHO cell cultivation and critically affect cell survival and production abilities

(Fig. 5). As several studies in CHO cells revealed that several central energy intermediates and associated metabolites have been considered as critical factors impacting the cell culture performance, such as several amino acids, TCA cycle intermediates, and inhibitory metabolites (Coulet et al., 2022; Lai et al., 2022), investigation of these metabolites in IgG-producing CHL-YN cell cultures can contribute to understanding the cellular metabolic states and requirements, leading to the development of cell cultivation strategies such as tailoring culture conditions, medium optimization, and feed strategy design. Thus, a metabolomics study for IgG-producing CHL-YN cell cultures is required.

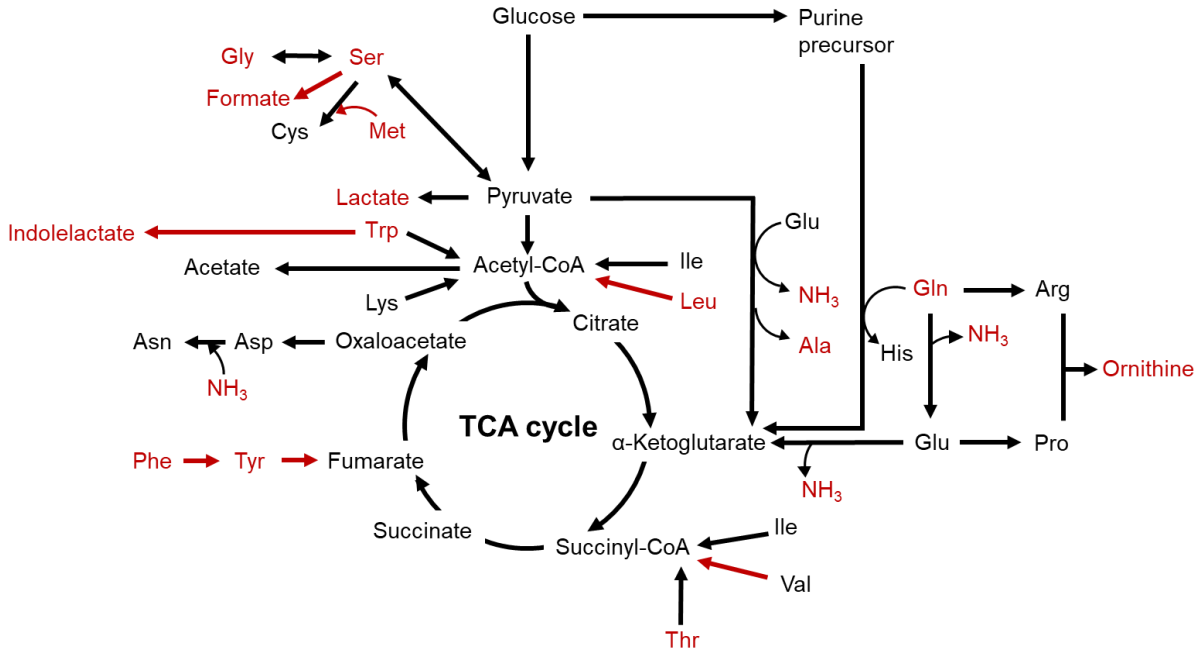

Figure 5. Overview of main metabolic pathways of CHO cells. Red items represent metabolites that are able to cause inhibitory effects, particularly when accumulating at high concentrations, and red arrows indicate the availability of intermediates that could provide inhibitory effects when accumulating at high concentrations. Information originated from (Pereira et al., 2018).

The workflow of metabolomics typically includes five major steps: sample collection, sample preparation, sample analysis, data processing and analysis, and biochemical interpretation. First, samples are gathered and quenched to minimize the metabolic changes. After that, metabolites are extracted from the sample matrices and treated with internal standards. Then, metabolites of prepared samples are separated and detected with chromatography and mass spectrometry. The raw measurement data is normalized and processed by statistical analysis and biochemical interpretation (Dettmer et al., 2007; Clish, 2015).

Considering the sample analysis instruments, several technologies can be applied by providing different pros and cons. Nuclear magnetic resonance (NMR) spectrometry, gas chromatography (GC)-mass spectrometry (MS), and liquid chromatography (LC)-MS are usually used in metabolomics studies. NMR spectroscopy can detect up to hundreds of metabolites covering carbohydrates, organic acids, and amino acids with simple detection needs. However, the limitation of NMR is that it is less sensitive than the MS system. Besides that, molecular weight increased from the NMR technique causes difficulty in identifying long hydrocarbons such as fatty acids. Comparing MS systems such as LC-MS and GC-MS, although both MS methods are able to detect up to thousands of metabolites, including compounds detectable via the NMR, the LC-MS detection has a wider range of detection over the GC-MS, such as thermolabile, polar metabolites, and high-molecular-weight compounds without derivatization (Tian et al., 2016). Additionally, capillary electrophoresis (CE)-MS is also applied to metabolomics analysis. This approach can provide high sensitivity and resolution while requiring a small volume of samples. In addition, the CE-MS technique is applicable for analyzing polyamines and sugar phosphates (Kałuzna-Czaplińska, 2011; Ramautar et al., 2019). Therefore, this study using a combination of

CE-MS and LC-MS approaches for IgG-producing CHL-YN cell cultures via targeted metabolomics analyses.

1.5 Serum-free fed-batch cultivation, the most used operation for mAb production

In order to perform metabolomics analysis, serum-free fed-batch operation was considered as a study model. In mAb production, a serum-free system is a commonly used cultivation platform in modern mammalian cell-based manufacturing. Serum is a fetal bovine-derived supplement fluid used in the earliest mammalian cell cultures, which contains growth factors, hormones, and nutrients for supporting cell growth. However, serum usage increases the contamination risk, such as bovine and transmissible spongiform encephalopathy, commonly known as mad cow disease infected by prion. In addition, it is difficult to control the variability and cost of serum production. Moreover, serum components can be obstructive in the purification steps (Baker, 2016; Ritacco et al., 2018; Li et al., 2021). Hence, serum-free systems have been developed and utilized in mammalian cell cultivation to avoid these undesired issues for over 20 years.

Serum-free fed-batch cultivation is typically selected for a practical operation mode in the industrial mAb bioprocess. Fed-batch is a culture process that supplies additional feed such as carbon sources, amino acids, and trace elements to prevent nutrient deprivation during cultivation. Feeding could promote cell growth and improve volumetric productivity or titer. The advantages of fed-batch performance are a well-developed procedure, large-scale compatibility, and well-balanced performance between simplicity and production yield (Huang et al., 2010; Mellahi et al., 2019; Xu et al., 2023). Recently, a prominent fed-batch strategy called intensified fed-batch is becoming noticeable. This process first prepares a high concentration seed train in the pre-culture,

generally by perfusion method. Subsequently, inoculating the high cell seeding to the fed-batch operation in the production bioreactor. This strategy could provide enhancement of the final mAb production while retaining the quality of glycosylation patterns. (Xu et al., 2020; Xiang et al., 2023). Although the fed-batch is a methodology that is extensively utilized and well-developed for several mAb-producing CHO cells, this operation has never been constructed for CHL-YN cells.

1.6 Development of glucose feeding strategies, the initiative progress on fed-batch CHL-YN cell culture

For the first step of fed-batch process development, feeding design for CHL-YN is crucial and influential in cell culture and production performance (Xu et al., 2023). Amidst several feed components, glucose is the top priority to consider since it is a primary energy source that is rapidly consumed in the exponential phase of cell growth. Glucose is uptaken and catabolized through glycolysis and the tricarboxylic acid (TCA) cycle. Then, adenosine triphosphate (ATP) is produced from oxidative phosphorylation in the electron transport chain in the mitochondrial membrane (Park et al., 2022). Besides that, glucose is a source that finally turns into biomass and a product. Although glucose is an important nutrient, overwhelming glucose supplementation leads to regression of CHO cell culture performance (Lee et al., 2015). The high glucose feed enhances lactate production, which is known as a toxic byproduct inhibiting cell growth. Hence, a limited glucose control strategy has been investigated and developed. Lu et al. reported that maintaining glucose above 0.22 g/L could cultivate the erythropoietin-producing CHO cells without energy shortage. Nevertheless, low glucose maintenance has a possibility of approaching zero, which also critically affects cell viability. To avoid glucose depletion during the cultivation, glucose

concentration control is recommended to be set at 2–3 g/L. (Lu et al., 2005; Ritacco et al., 2018; Chakrabarti et al., 2022; Xu et al., 2023).

1.7 Overview of the dissertation and relationship between chapters

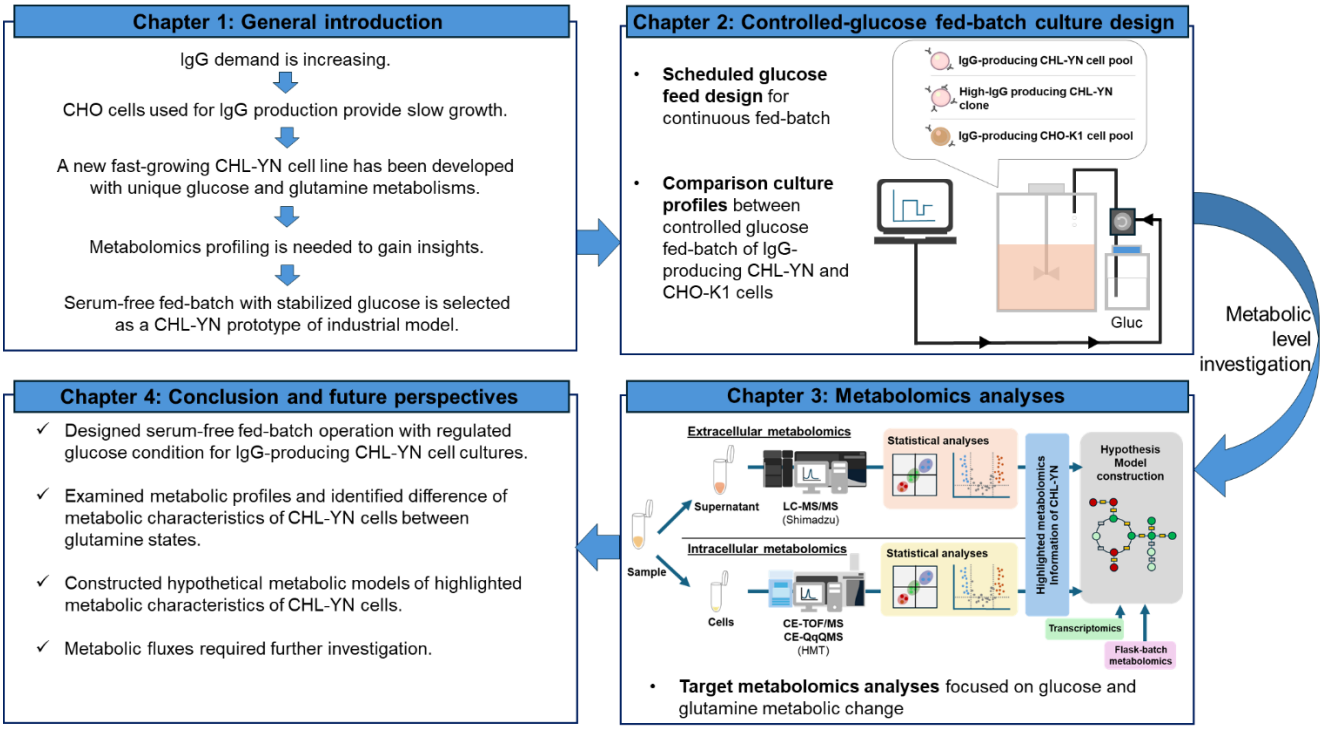

Figure 6. Dissertation outline.

The outline of this dissertation is presented in Fig. 6. In Chapter 1, general information, importances, novelties, and objectives of this dissertation were described. As the demand for IgG is gradually increasing over the past decade, challenges on improving IgG production processes become further intensive. CHO cell lines are the most used expression host for IgG production with found of slow growth compared to non-mammalian types. Their slow growth can lead to

prolonging cell line development process and increase in cost, resources, and laboratory workforces' usage. Hence, new fast-growing CHL-YN cells, have been developed with retaining IgG production abilities as well as CHO cells. Intriguingly, the previous study revealed unique glucose and glutamine metabolisms in CHL-YN cells compared to CHO-K1 cells. However, the previous study did not provide investigation on further metabolites associated with glucose and glutamine metabolism. Aiming at gaining insight of these metabolic incidents, this study proposed targeted metabolomics analyses specifically focusing on glucose and glutamine metabolisms. Considering the cultivation model for the metabolomics investigation, serum-free fed-batch operation was selected for this study because of their ordinarily used in the industrial IgG production. Besides that, regulable extracellular glucose condition was further determined in the fed-batch cultures to avoid unfavored conditions, which may be critical impact cell performance and productivity, such as glucose deprivation and excessive glucose supplementation. However, IgG-producing CHL-YN cell cultures required specifically developed serum-free fed-batch operation with glucose feed strategy tailoring in accordance with their cellular requirements. Therefore, this study proposed two research novelties. Firstly, I developed a serum-free fed-batch culture method with glucose feeding strategy tailoring for IgG-producing CHL-YN cells. Secondly, metabolomics analyses were conducted aimed at gaining psychological knowledge particularly glucose, glutamine, and associated metabolisms.

In Chapter 2, development serum-free fed-batch operation for IgG-producing CHL-YN cell cultures were proposed for being a cultivation model of the metabolomics study. Besides that, continuous glucose feeding strategy was designed aiming at achieving regulable glucose condition within the target range. The scheduled glucose feeding strategy was also determined for a high IgG-producing CHL-YN clone and IgG-producing CHO-K1 cell cultures. Then, the cultivation

profiles, including viable cell count; viability; extracellular critical metabolic components; and IgG production, were investigated and compared between each cell type. From this chapter, glucose consumption patterns of IgG-producing CHL-YN cells were fluctuated in accordance with glutamine metabolism. During the first glutamine metabolic shift from consumption to production, immediately reduced glucose consumption was observed in CHL-YN cells. After that, cell viability and productivity were dropped during the glutamine production stage. Thus, to elaborate the metabolic incidents during the first glutamine metabolic shift, deeper-level investigation such as metabolomics analysis would be suggested for the next chapter to achieve broader metabolic aspects of glucose and glutamine metabolisms.

In Chapter 3, combinations of targeted CE-MS and LC-MS metabolomics analyses were performed aimed at achieving comprehensive glycolysis, TCA cycle, and amino acid metabolisms. Samples collected from IgG-producing CHL-YN and CHO-K1 heterogeneous cell pools and a high IgG-producing CHL-YN clone covering the first metabolic shift and representing each cell stage on basis of cell growth (Vodopivec et al., 2019). Metabolic results were clustered and analyzed by statistical analyses. Then, comparison between sample groups were presented and interpreted. Finally, further omics information from relevant studies were considered and hypothetical metabolic models were created.

Eventually, in Chapter 4, studies on fed-batch culture development for IgG-producing CHL-YN cells and their metabolomics were concluded. Furthermore, the limitations of this study and future perspectives were also mentioned in this chapter.

Chapter 2:

Development of continuous glucose feeding for IgG-producing CHL-YN cell cultures in serum-free fed-batch cultures

Chapter 2: Development of continuous glucose feeding for IgG-producing CHL-YN cell cultures in serum-free fed-batch cultures

2.1 Introduction

As previously mentioned in Chapter 1, serum-free fed-batch cultivation is the most favored operation mode for industrial mAb production. Therefore, this study first aimed to apply CHL-YN cells into a serum-free fed-batch culture. The previous study reported lower glucose consumption of CHL-YN cells compared to CHO-K1 cells. Here, I designed glucose feed strategies based on CHL-YN cell metabolism.

Feeding methods in the fed-batch operation mainly execute with two methods: bolus and continuous feeds. Bolus feeding is a method that periodically provides supplements, whereas continuous feeding gradually supplies the nutrients into the system. Despite the simplicity and inexpensiveness provided by bolus feed utilization, continuous feeding is preferred. Since bolus feeding swiftly inputs concentrated nutrients to the cell cultivation, especially high feed volume, the culture environment tends to be changed, such as pH and osmolarity. Immediate shift of cell culture conditions leads to raised cellular oxidative stresses and affects the cell cycle and productivity. (Xiao et al., 2021; Romanova et al., 2022; Xu et al., 2023). As described in Chapter 1, excessive glucose supplementation can lead to negative effects on cell cultures, including high lactate accumulation and high osmotic pressures (Lee et al., 2015; Gowtham et al., 2017). Therefore, I developed the continuous feeding procedure for the CHL-YN cell cultures. Additionally, continuous glucose feeding strategy for cell cultures can be advantageous in product quality such as glycosylation attributes of IgG products. Insufficient glucose feeding leads to

limitation of glycosylation precursors. In addition, low glucose feeding may risk glucose depletion, which had reported the correlation between glucose depletion and non-glycosylated monoclonal antibody products (Liu et al., 2014; Villacrés et al., 2015). On the other hand, extravagant glucose feeding could increase lactate accumulation and osmolarity, which could disrupt glycosylation profiles as well (Horvat et al., 2020; Xu et al., 2023).

Here, IgG-producing CHL-YN cells cultivated in serum-free fed-batch were performed in a stirred-tank bioreactor Yokogawa BR1000. The first goal of this research was to develop a schedule of continuous glucose feed methodology for stabilizing the extracellular glucose concentration in the target range of 2.0–4.0 g/L along with the cultivation process. Then, the scheduled glucose feed design was ensured by application to a high IgG-producing clone of CHL-YN cells. Finally, this study also compared cell culture profiles to IgG-producing CHO-K1 cells, the most currently common IgG-expressing host.

2.2 Materials and Methods

2.2.1 Cell lines, media, and flask-batch culture conditions

The models of this study were suspension CHL-YN and CHO-K1 cells harboring genes for producing trastuzumab, an anti-HER2 immunoglobulin G1 (IgG1). The heterogeneous IgG-producing cell pools were kindly supported by Associate Professor Yamano-Adachi Noriko (Yamano-Adachi et al. 2020). Cultivation and cell passaging were conducted on a serum-free platform, which included a chemically defined EX-CELL® media series (Merck, Rahway, NJ, USA), 6 mM L-glutamine (Fujifilm Wako Pure, Osaka, Japan), and 5 μg/mL puromycin (InvivoGen, San Diego, CA, USA). The EX-CELL® CD CHO Fusion medium was first used in

the initial stages of both cell cultures during flask-batch cultivation; subsequently, the EX-CELL® Advanced CHO Fed-batch medium was used instead of the third cell passage in order to introduce cells to fed-batch conditions. Both cell cultures were inoculated in a Corning® Polycarbonate Erlenmeyer flask (Corning Inc., Corning, NY, USA), which contained 20 mL of working volume for passaging and 100 mL of preculture for bioreactor cultivation. Both flask-scale cell cultures were grown in a Climo-shaker ISFI-X incubator (Kühner, Birsfelden, Switzerland), which was set to 37.0 °C temperature, 5% carbon dioxide gas, 80% humidity, and a 90-rpm rotary shaking speed. Living cell counts (VCC) and viability were determined using a Vi-CELL™ XR cell viability analyzer (Beckman Coulter, Brea, CA, USA). The precultures of both cell lines were fifth cell passaged cultures with 100 U/mL penicillin and 100 μg/mL streptomycin (Thermo Fisher Scientific, Waltham, MA, USA). Fed-batch-adapted cultures did not provide feed medium after starting cultivation.

2.2.2 Single clone isolation

The IgG-producing CHL-YN cell pool was screened for high IgG-producing clone selection via a limiting dilution procedure. Exponentially grown CHL-YN cell culture was serially diluted with a 1:1 mixture of EX-CELL® CD CHO fusion medium and conditioned medium. Conditioned medium was prepared from filtration-based sterilized supernatants of late exponential CHL-YN cell cultures. IgG-producing CHL-YN cell concentration was diluted to 0.5 cells/mL, then 200 μL diluted cell cultures were transferred to a 96-well cultivation plate and incubated in a static incubator (PHC Corporation, Tokyo, Japan) at 37.0 °C temperature and 5% carbon dioxide gas setting. After 4 h of incubation, the cells were expected to reach the bottom of the well, and single cells were marked by light microscopy CKX31 (Olympus Life Science, Tokyo, Japan). After

incubation for 7 days, single IgG-producing CHL-YN colonies were observed again to ensure the achievement of a single clone. The 100 µL supernatant of each clone was collected to measure the IgG concentration via sandwich enzyme-linked immunosorbent assay (ELISA) to search for the clone with the highest IgG production. All single clones were transferred to 6-well plates and scaled up for flask-scale cultivation. Ultimately, all IgG-producing CHL-YN clones were expanded and stored at -80 °C. Among the 17 isolated clones, the B-08 clone displayed the highest IgG production.

2.2.3 BR1000 bioreactor fed-batch cultivations and cell culture analyses

2.2.3.1 Cell cultivations

The Advanced Control Bioreactor System BR1000, a glass stirred-tank type (Yokogawa Electric Corp., Tokyo, Japan), was selected as a cultivation platform for this study. Firstly, the inlet and outlet silicon tubes and containers were connected to the glass tank. Then, in-line sensors were calibrated and sterilized together with the bioreactor by autoclaving. Then, medium and supplements were added into the clean tank. After that, the precultures from the flask batch were inoculated in the medium containing the components in Table 2. After seeding, bioreactor conditions were monitored as shown in Table 3. All parameters were started real-time monitoring by the data logger software after the first sample collection at 3 h after inoculation. Off-line sample collection timepoints were relied on cell lines. For IgG-producing CHL-YN cell culture experiments, sample collection was executed every 12 h. and more often during glutamine metabolic change. While samples of IgG-producing CHO-K1 cell culture experiments were collected every 24 h.

Table 2. The 2000 mL cultivation components in serum-free fed-batch operation.

Parameters	Setting value
Basal medium	EX-CELL® Advanced CHO Fed-batch medium (Merck)
Supplements	6 mM L-glutamine (Fujifilm Wako Pure), 5 μg/mL puromycin (InvivoGen), and 100 U/mL Penicillin-Streptomycin (Thermo Fisher Scientific)
Cell inoculum	1.0×10^6 cells/mL of IgG-producing CHL-YN preculture or 5.0×10^6 cells/mL of IgG-producing CHO-K1 preculture

Table 3. The BR1000 bioreactor culture conditions for serum-free fed-batch cultivation.

Parameters	Setting value
Temperature	37.0 °C
pH control	7.17–7.22
Buffer system	Carbon dioxide (CO_2) gas (acid) and 1 mol/L Sterilized sodium hydrogen carbonate ($NaHCO_3$) solution (base)
Upper ventilation	Air + 5% CO_2 gas flow rate: 100 mL/min (SCCM)
Lower ventilation	100% Oxygen (O_2) gas with Microsparger (flow rate: 0–100 mL/min)
Dissolved oxygen (DO)	Not below 3.4 mg/L

Table 3. Continued

Parameters	Setting value
Agitation speed	80–180 rpm, Cascade mode (The agitation speed is automatically increased or decreased agitation by 5 rpm to assist DO adjustment. The operation executed when target of O_2 flow rate at 10.0 SCCM.)

2.2.3.2 Cell count and viability measurement

Fresh samples collected at the sampling timepoint were immediately measured without any treatments for quantifying viable cell concentration (VCC) and viability by the Vi-CELL™ XR cell count machine (Beckman Coulter). Measured cell concentration above 10.0×10^6 cells/mL is required dilution. The samples would be diluted by using fresh EX-CELL® Advanced Fed-batch medium.

2.2.3.3 Extracellular metabolite concentration measurement

Collected samples were centrifuged using 14,000 ×*g*, 5 min, and 4 °C conditions to separate the cell pellet and supernatant. The supernatant could be stored at -80 °C. To detect concentrations of critical metabolites in cell cultures consisting of glucose, glutamine, glutamate, lactate, and ammonium, a biochemical analyzer YSI2950 (Xylem Inc., Yellow Springs, OH, USA) was prosecuted.

2.2.3.4 IgG concentration measurement

To determine IgG concentrations in the cell culture, sandwich ELISA was conducted. The procedure was previously mentioned (Onitsuka et al., 2012) using the reagents mentioned in Table 4. The standard IgG concentration curve was estimated from a serial dilution of purified IgG as a known-concentration reference. Absorbance at 405 nm was detected via an Enspire™ 2300 Multilabel Reader (Perkin Elmer, Waltham, MA, USA).

Table 4. The sandwich-ELISA reagent list.

ELISA reagents	Reagent name
Primary antibody	Goat-anti-human IgG Fc fragment (Bethyl Laboratories, Montgomery, TX, USA)
Secondary antibody	Horseradish peroxidase-conjugated goat anti-human IgG Fc fragment (Bethyl Laboratories)
Coating buffer	KPL Coating solution concentrate (Seracare Life Sciences, Milford, MA, USA)
Blocking buffer	Albumin, from bovine serum, fraction V, pH7.0 (Fujifilm Wako Pure)
Enzymatic reaction substrate	KPL ABTS® Peroxidase Substrate system (Seracare Life Sciences)
Enzymatic reaction stop solution	KPL ABTS® Peroxidase Stop solution (Seracare Life Sciences)
Washing solution	TWEEN® 20 (Merck), Sodium Chloride, NaCl (Fujifilm Wako Pure)

2.2.4 Feeding operation and glucose feed strategies

The nutrient supplementary system for all fed-batch cultures included two independent feed solutions: a feed medium and concentrated glucose solution. Feeding medium used in this study was EX-CELL® Advanced CHO feed 1, without glucose and glutamine (Merck). The feed medium was prepared following the Merck company instructions, and then sterilization was conducted via a 0.2 μm vacuum filtration system (Corning Inc.). The solution was kept at 4 °C to prevent degradation. After the batch cultivation for 48 h, the feeding operation was started. The rate of the sterile feed medium was fixed at 50 mL/d, which is 2.5% V/V/d of the initial culture volume. During the cultivation, feed medium was kept in an ice box. The feed was gradually supplied until the cultivation terminated.

Sterile glucose solution was continuously input into the cell cultures with two strategies: automated and scheduled modes. The automated glucose feeding system was first used as the preliminary IgG-producing CHL-YN cultures. Then, the glucose profiles from the preliminary IgG-producing CHL-YN cell cultures were applied for evaluating glucose feed rate schedule for IgG-producing CHL-YN cell pool. The achievement of glucose feed strategies was to control extracellular glucose concentration within the target range of 3.0±1.0 g/L along with the cultivation. The concentrated glucose solution for the bioreactor cultures contained 30% W/V of D-glucose (Fujifilm Wako Pure). Sterilization was then conducted after solution preparation via a 0.2 μm vacuum filtration system (Corning Inc.).

2.2.4.1 Automated glucose feed strategy (preliminary cultures)

The automated glucose delivery system was a feature provided in the BR1000 bioreactor system. This system includes dual in-line sensors and a process-control algorithm. The two in-line sensors are a near-infrared (NIR) sensor for measuring extracellular glucose and lactate concentrations and a capacitance sensor for measuring viable cell concentrations (VCC). These sensors require reference models specifying a cell type and collective data for improving the measurement. Therefore, the preliminary fed-batch cultivation using bolus feeding was first conducted to introduce off-line measurement of glucose, lactate, and VCC data. Then, the additional data was collected in another culture using an automatic system to refine the reference model. The process controller is a close-loop system based on the model predictive control, named proportional-integral-derivative (PID) system (Fig 7). (Sakaki et al., 2023). This controller combines mass balance equations and kinetics of glucose and VCC models to automatically generate the amount of glucose feeding. Here, this automatic system was used only with IgG-producing CHL-YN cell pool culture. Construction models for IgG-producing CHL-YN cell cultures were kindly supported by Yokogawa Electric Corp. The automated operation was run since Day 1 of the cultivation.

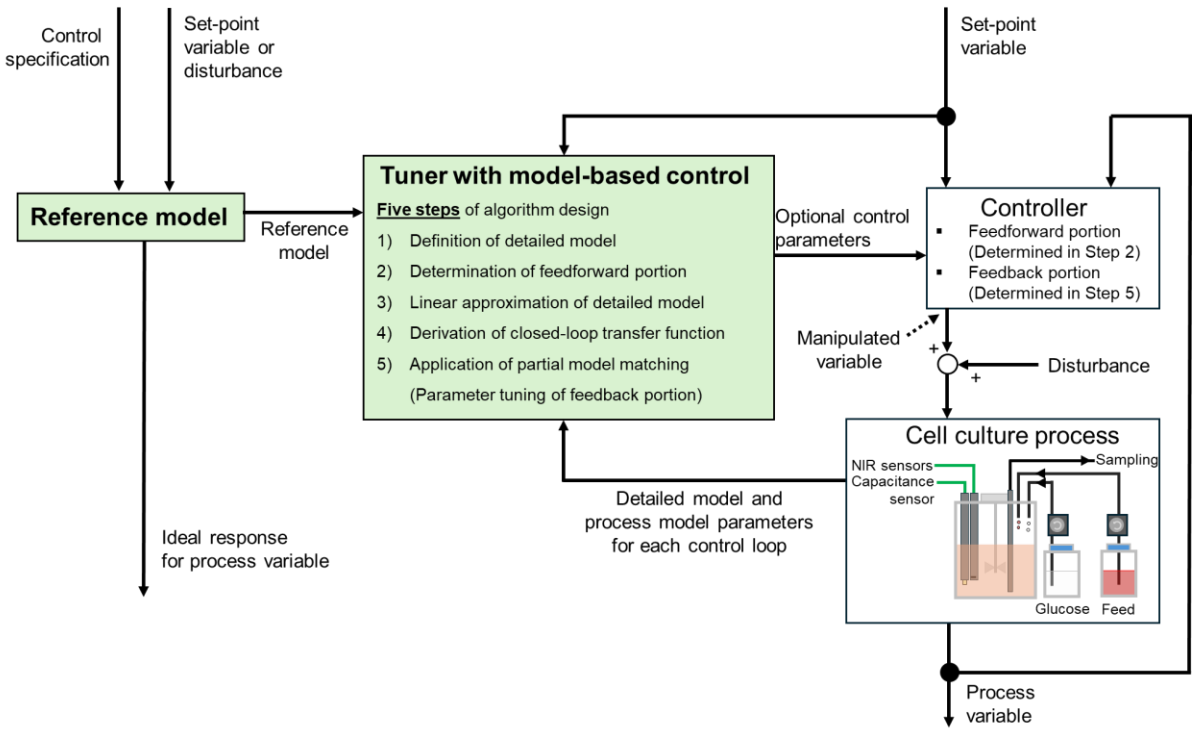

Figure 7. Overview of automated control system. Redesigned from (Sakaki et al., 2023).

2.2.4.2 Scheduled glucose feed strategy

The scheduled glucose feed strategy is generated based on the calculation of the feeding glucose amount following specific glucose consumption activities. This feed strategy only used data from off-line metabolic measurements. Glucose feed operation was begun at approximately Day 2, when off-line measurement of extracellular glucose concentration was ~4.5 g/L. The amount of glucose supply was computed by **equation 1, equation 2, and equation 3**, aiming to finalize the extracellular glucose concentration at 3.0 g/L. After receiving the amount of glucose supply at each sampling timepoint, the total glucose feed amount was evaluated and then illustrated in the time-course plot. Eventually, the linear regression methodology was used to find out the average glucose feed rates.

Using the off-line data to discover the consumed glucose amount;

$$G_{con} = Glc_n V_n - Glc_{n-1} V_{n-1} + Glc_{feed} V_{glc\ feed} \quad (1)$$

Then, the glucose feed volume would be calculated by the following equation;

$$Glc_n\left(V_{n-1} + V_{glc\ feed} + V_{other\ feeds}\right) = Glc_{n-1} V_{n-1} - G_{con} + Glc_{feed} V_{glc\ feed} \quad (2)$$

As I set the expected culture conditions at Glc_{n} = 3.0 g/L and Glc_{feed} = 300.0 g/L;

$$V_{glc\ feed} = \frac{3V_{n-1} + 3V_{other\ feeds} - Glc_{n-1} V_{n-1} + G_{con}}{297} \quad (3)$$

Where G_{con} represents the weight of consumed glucose in grams (g) unit, which is estimated as the loss from the cultivation system. Whilst Glc_n is the concentration of glucose in grams per liter (g/L) unit at the time n, and V is the volume of cell culture in liters (L) units. The Glc_{feed} is the concentration of glucose feed, which is fixed at 300.0 g/L, while the $V_{\text{gluc feed}}$ is the volume of glucose feed in L units. The $V_{\text{other feeds}}$ represents the volume (L) of other supplements excluding glucose, including EX-CELL® Advanced CHO feed 1 and $NaHCO_3$ solution.

Additionally, to encounter biological variability on each cell culture, which reflects the different metabolic profiles on each cultivation batch, glucose feed rate modification was further determined during the cultivation. The adjustment of glucose feed amounts was calculated using **equation 4**.

$$F_{Glc\ mod} = F_{Glc} + \left(\frac{\Delta Glc \cdot V}{Glc}\right) \quad (4)$$

Where $F_{\text{Glc mod}}$ is an adjusted glucose feed amount (L), F_{Glc} is a glucose feed amount (L), which is achieved from the linear regression, ΔGlc is a difference between target point of glucose

concentration (3.0 g/L) and off-line measured glucose concentration, *V* is cultivation volume (L), and *Glc* is glucose concentration (g/L).

To deliver the glucose supply, peristatic pumps and operation were provided with the BR1000 system. This calculation was kindly supported by Dr. Hiroaki Yamanaka, a staff member of Yokogawa Electric Corp.

2.2.5 Specific growth, productivity, and metabolic consumption rate calculations

Specific growth, specific IgG productivity, and extracellular metabolites metabolic rates were calculated following the previous articles (Omasa et al., 1992; Yamano-Adachi et al., 2020; Samy et al., 2020). The specific growth rate (μ) was evaluated based on linear regression. The integral viable cell concentration (*IVCC;* $\int(X_v/X_t)dt$) was calculated by **equation 5**. Then, the maximum specific growth rate (μ_{max}) was evaluated from exponential growth data plots (24–72 h of CHL-YN cells and 24–96 h of CHO-K1 cells), which represented the best-fit curve of **equation 6**. The doubling time was later calculated from the μ_{max} via **equation 7**.

$$\int(X_v/X_t)dt = \sum_{i=0}^{n} \frac{(X_{v_i}+X_{v_{i-1}})}{2} \times \frac{(t_i-t_{i-1})}{24} \quad (5)$$

$$\mu_{max} = \frac{\ln(X_n)-ln(X_{n-1})}{\int_{n-1}^{n}(X_v/X_t)dt} \quad (6)$$

$$T_d = \frac{\ln(2)}{\mu_{max}} \quad (7)$$

Where $\int(X_v/X_t)dt$ is an integral viable cell concentration, X_v is a viable cell concentration at a time point, *t* represents the timepoint in a unit of hours. μ_{max} is the maximum specific growth rate, *X* is the total cell concentration, and T_d is doubling time.

Specific productivity (q_p) was estimated following **equation 8** using linear regression to find a slope of the plot between IgG concentration and *IVCC*.

$$q_p = \frac{(IgG_n - IgG_{n-1})}{\int_{n-1}^{n}(X_V)dt} \quad (8)$$

Where q_p is specific productivity, IgG is IgG concentration, and X_v is a viable cell concentration.

Specific glucose consumption rate (q_{glc}), specific glutamine consumption rate (q_{gln}), and specific lactate consumption rate (q_{lac}) were calculated from **equations 9–11**, respectively. Since the results showed the fluctuation of the glucose and glutamine concentration trends, q_{glc}, q_{lac} and q_{gln} from different phases of CHL-YN cell cultures and two phases of CHO-K1 cell cultures were separately calculated.

$$q_{glc} = \frac{-(V_n \cdot Glc_n) - (V_{n-1} \cdot Glc_{n-1}) + \int (V_{feed} \cdot Glc_{feed})dt}{\int_{n-1}^{n}(V \cdot X_V)dt} \quad (9)$$

$$q_{gln} = \frac{(V_n \cdot Gln_n) - (V_{n-1} \cdot Gln_{n-1})}{\int_{n-1}^{n}(V \cdot X_V)dt} \quad (10)$$

$$q_{lac} = \frac{(V_n \cdot Lac_n) - (V_{n-1} \cdot Lac_{n-1})}{\int_{n-1}^{n}(V \cdot X_V)dt} \quad (11)$$

Where q_{glc} is a specific glucose consumption rate, V is culture volume, V_{feed} is feed volume, Glc is glucose concentration, Glc_{feed} is glucose concentration in a glucose supply solution (300.0 g/L), X_v is a viable cell concentration, q_{gln} is a specific glutamine consumption rate, and Gln is glutamine concentration. q_{lac} is a specific lactate consumption rate, and Lac is lactate concentration. Statistical significance was determined by unpaired two-tailed student's T-test (p-value ≥ 0.05) following the previous study (Samy et al., 2020).

2.3 Results

2.3.1 Scheduled glucose feeding evaluation

The scheduled glucose feed strategy for IgG-producing CHL-YN cell cultures was established on the basis of consumed glucose calculation and estimation of the amount of glucose feeding that could finalize the concentration at 3.00 g/L. Results from the preliminary automated culture (automated-1 culture) were used as reference data (**Supporting information 1A-B**). As a result, the glucose feed schedule for IgG-producing CHL-YN cell cultures was divided into three different rates: 31.9 mL/d on Day 2–3.5, 8.62 mL/d on Day 4–5.5, and 18.0 mL/d on Day 6 onward. As the glucose feed evaluation, the swing of glucose feed rates was observed. Consideration on extracellular metabolite analysis, the result revealed remarkable patterns of extracellular glutamine concentrations from the automated-1 CHL-YN cell culture. Glutamine concentrations of CHL-YN cells were found in three different stages during the cultivation process. Glutamine concentration was first sharply fallen during Days 0–3 of the cultivation. When the glutamine concentration reached close to 0 mM, which represents the glutamine depletion stage, the glutamine concentration was then increased. This incident could be noticeable during Days 3–5 of the automated CHL-YN cultivation (**Supporting information 1B**). Lastly, glutamine was dropped again after Day 5 of cultivation (Fig. 8). From these results, it suggests that glucose feeding for IgG-producing CHL-YN cell culture was in accordance with glutamine metabolism. After glutamine metabolic shift for approximately 12 hours, glucose was also turned.

Performing the preliminary of scheduled glucose feed for IgG-producing CHL-YN cell culture could stabilize glucose feeding. However, glucose concentrations were still over the target range (**Supporting information 2).** Hence, the adjustment of the glucose feed rate equation had been applied to scheduled glucose feed evaluation. As a result, in the scheduled-1 and scheduled-

2 cultures, glucose concentrations could be controlled in the desired range at 3.00 ± 1.00 g/L (Fig. 9).

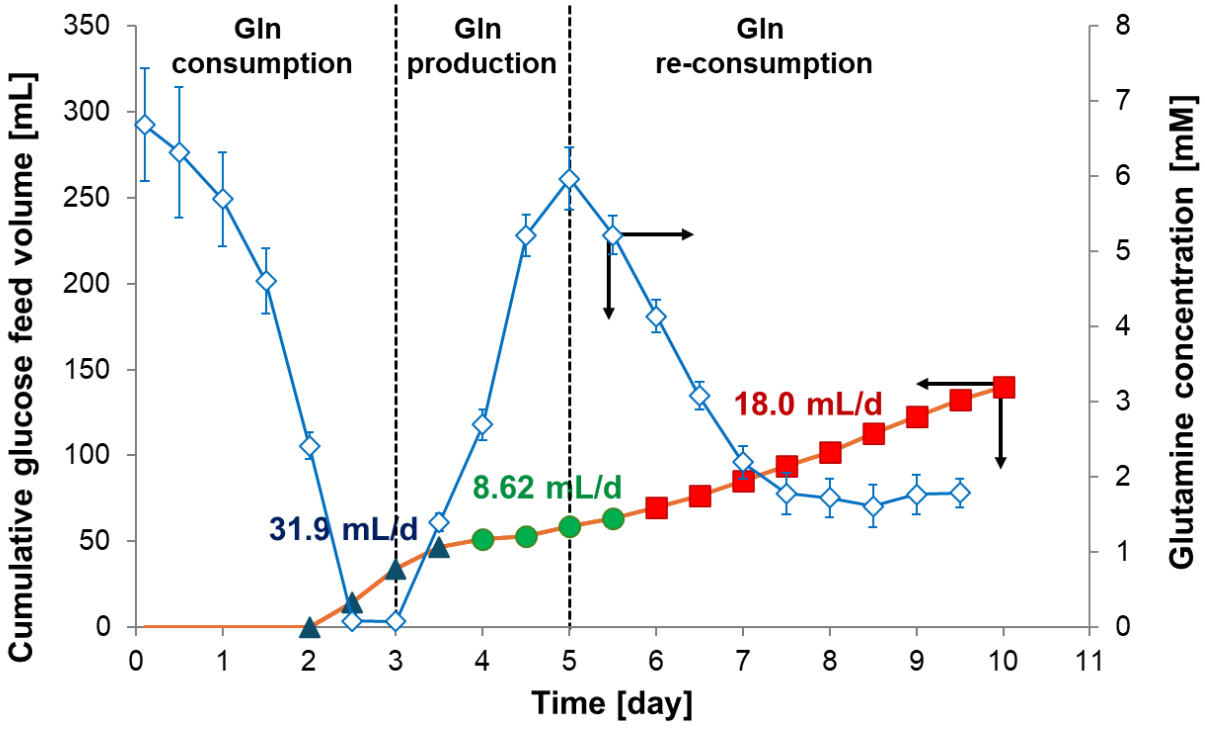

Figure 8. Schedule of glucose feed rates evaluated from the automated glucose feed method applied for IgG-producing CHL-YN cell culture (Automated-1, data available at **supporting information 1A-B**). The time-course of predicted glucose feed volume is expected to finalize extracellular glucose concentration at 3.00 g/L. Black-dashed lines represented turning points of glutamine concentration that occurred in the time-course glutamine plot.

To ensure this scheduled glucose feed strategy, this procedure was also applied for fed-batch cultures of the high IgG-producing CHL-YN B-08 clone. Calculations from preliminary B-08 culture showed three distinct glucose feed rates: 24.3 mL/d on Day 2–4, 8.62 mL/d on Day 4–6, and 18.0 mL/d on Day 6 onward. This feed evaluation, together with the adjustment of the

glucose feed rate equation, could successfully regulate extracellular glucose concentrations in the desired range (3.00 ± 1.00 g/L) as well as results from the CHL-YN cell pool cultures (Fig. 10).

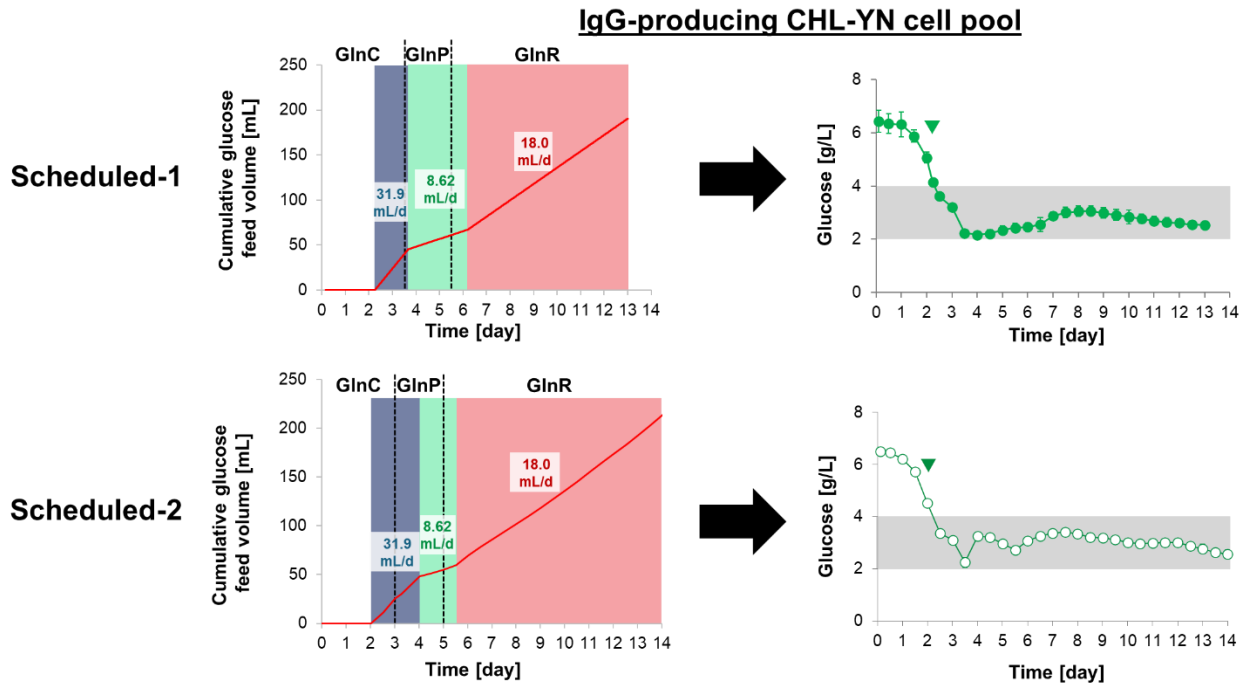

Figure 9. Scheduled glucose feed strategy applied for IgG-producing CHL-YN heterogeneous cell pool cultures. (Left) Time-course of cumulative glucose feed amount on each bioreactor run. Three-different colors (blue, green, and red) represent three distinct glucose feed rates following the change of glutamine metabolism (glutamine consumption, GlnC; glutamine production, GlnP; glutamine re-consumption, GlnR). Black-dashed lines represented turning points of glutamine concentration that occurred in the time-course glutamine plot.

Overall, results from both the IgG-producing CHL-YN heterogeneous cell pool and the B-08 clone suggest that dynamic three glucose feed rates providing for CHL-YN cells could regulate glucose levels along with the cultivation. However, biological variability was observed among

each bioreactor run, resulting in different glucose and glutamine consumption. Hence, scheduling the glucose feed adjustment by fixing a timepoint was preferred. As all results indicate, it is concluded that glucose concentration could be successfully regulated when glucose feed rates were set at 31.9 mL/d approximately on Day 2–4, 8.62 mL/d approximately on Day 4–6, and 18.0 mL/d approximately on Day 6 onward for CHL-YN cell pool cultivations, while 24.3 mL/d approximately on Day 2–4, 8.62 mL/d approximately on Day 4–6, and 18.0 mL/d approximately on Day 6 onward for CHL-YN B-08 clone cultivations.

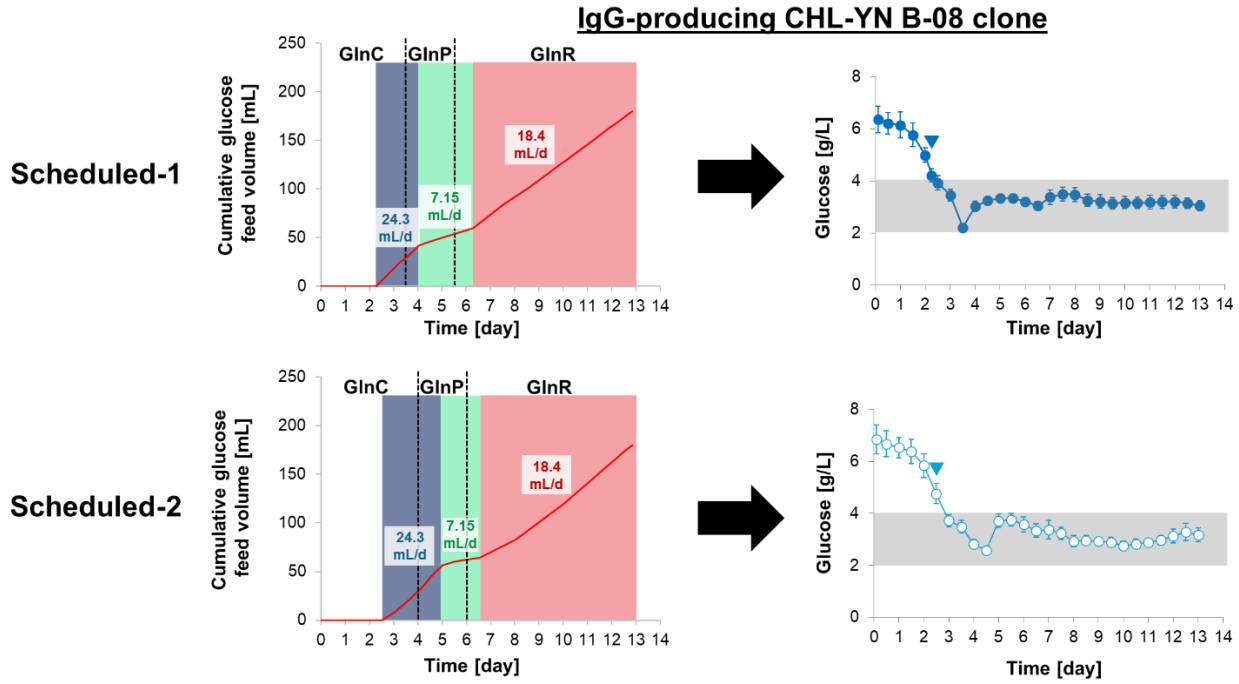

Figure 10. Scheduled glucose feed strategy applied for high IgG-producing CHL-YN B-08 clone cultures. (Left) Time-course of cumulative glucose feed amount on each bioreactor run. Three-different colors (blue, green, and red) represent three distinct glucose feed rates following the change of glutamine metabolism (glutamine consumption, GlnC; glutamine production, GlnP; glutamine re-consumption; GlnR). Black-dashed lines represented turning points of glutamine concentration that occurred in the time-course glutamine plot.

Not only CHL-YN cell cultures but also IgG-producing CHO-K1 cells were cultivated by using the scheduled glucose feed strategy. From a preliminary bolus culture of IgG-producing CHO-K1 cells, glucose feed rates were evaluated at 21.5 mL/d on Day 2 onward. With this glucose feeding schedule, extracellular glucose concentrations of IgG-producing CHO-K1 cells could be roughly regulated. In scheduled-1 of the CHO-K1 culture, undesired concentrations, which were out of the range of 3.00 ± 1.00 g/L, were occasionally observed. Whereas scheduled-2 of CHO-K1 culture showed successfully regulated glucose levels in the target range (Fig. 11). From these results, it suggests the difference in glucose consumption features between CHL-YN and CHO-K1 cells.

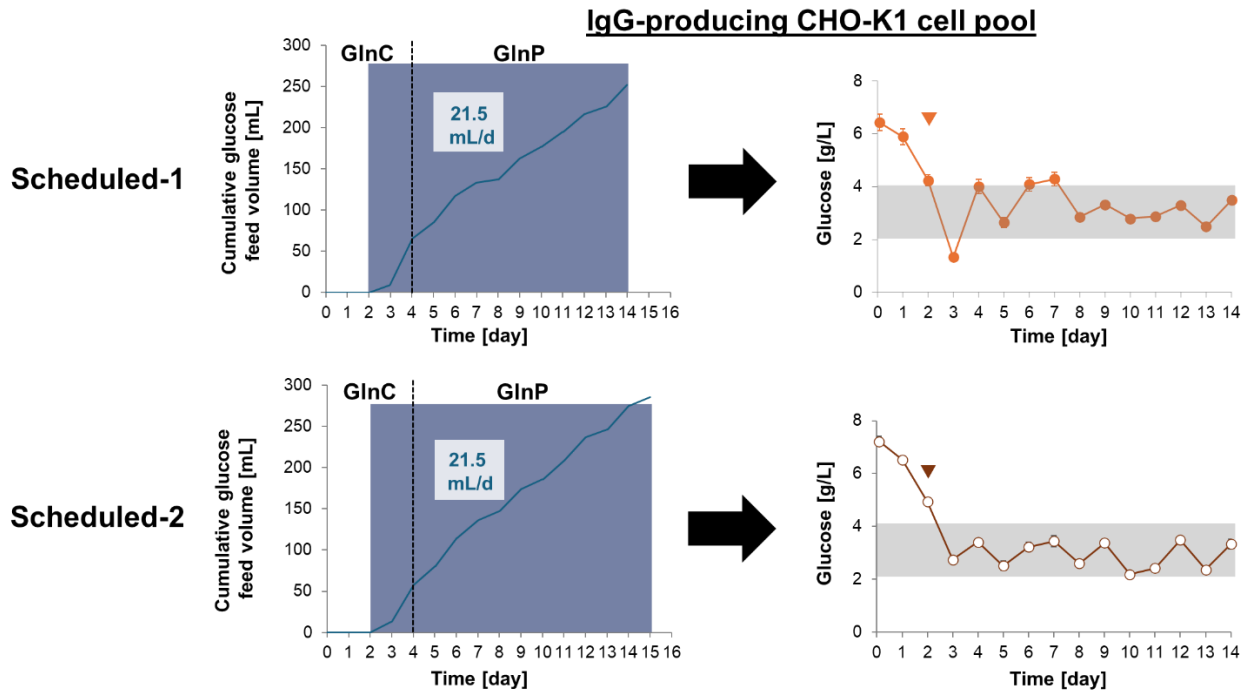

Figure 11. Scheduled glucose feed strategy applied for high IgG-producing CHO-K1 heterogeneous cell pool cultures. (Left) Time-course of cumulative glucose feed amount on each bioreactor run. Three-different colors (blue, green, and red) represent three distinct glucose feed rates following the change of glutamine metabolism (glutamine consumption, GlnC; glutamine

production, GlnP; glutamine re-consumption, GlnR). Black-dashed lines represented turning points of glutamine concentration that occurred in the time-course glutamine plot.

2.3.2 Comparison controlled-glucose fed-batch cultivation profiles between cell types

Cell cultivation results from the scheduled glucose feed strategy usage for fed-batch cultures showed advantages of regulated glucose levels. CHL-YN cell cultures with regulable glucose concentration showed alleviation of viability decrease during late cultivation. With this condition, IgG-producing CHL-YN cells, both heterogeneous cell pool and B-08 clone, reached the maximum viable cell concentration on Day 4 and subsequently declined until culture termination on Days 13–14. Considering cell viability, CHL-YN cells began to fall sharply on Days 4–6, then gradually dropped until becoming below 70.0% of viability, which is a criterion for terminating the cell culture (Fig. 12A–B). The scheduled glucose feeding for CHL-YN cell cultures showed a slight improvement in cell performance compared to the preliminary automated glucose feeding by extending the cultivation from 9.5 days to 13–14 days. This pattern of CHL-YN cell viability showed different characteristics when compared to CHO-K1 cells. The viable CHO-K1 cell concentration reached its peak on Day 6, whilst the cell viability decreased during Days 6–8 and remained over 70.0% until 14 days of cultivation (Fig. 12C).

Investigation on extracellular metabolites revealed unique characteristics of CHL-YN cells. Glutamine showed fluctuation, which was mainly divided into four stages: glutamine consumption approximately on Day 0–3.5; glutamine production approximately on Day 3.5–5.5; glutamine re-consumption approximately on Day 5.5–8; and glutamine stability approximately on Day 8 onward. Whereas glutamine profiles of CHO-K1 cell cultures were shown

at two stages: glutamine consumption approximately on Day 0–4; and glutamine production approximately on Day 4 onward. These glutamine profiles concurred with glutamate and ammonium profiles of both CHL-YN and CHO-K1 cell cultures. In CHL-YN cell cultures, glutamate and ammonium were initially increased approximately on Day 0–3, subsequently tremendously fell approximately on Day 3–4. Glutamate was shown depletion approximately on Day 4 of cultivation, while ammonium depletion was not found. Then, glutamate showed in low concentrations until the end of cultivation. While ammonium increased from approximately Day 4–8 and slightly decreased approximately on Day 8 onward. This incident was also observed in CHO cells, showing the turnover point of glutamine, glutamate, and ammonium on Day 4 (Fig. 13A).

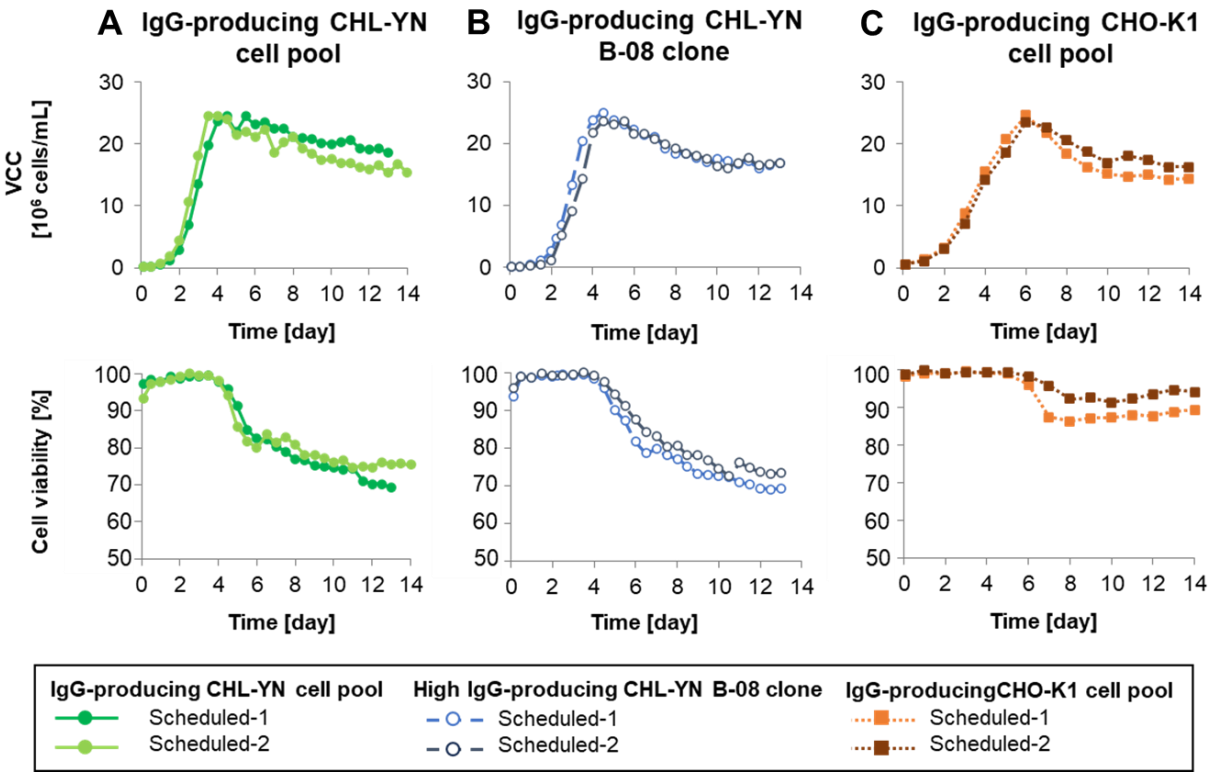

Figure 12. Time-course of cell profiles, including viable cell concentration (VCC) and cell viability, cultivated by fed-batch operation with scheduled glucose feeding manner. **A)** IgG-

producing CHL-YN heterogeneous cell pool. **B)** High IgG-producing CHL-YN B-08 clone. **C)** IgG-producing CHO-K1 heterogeneous cell pool. Cell cultures were sampling and counting living cells. These plots have been published and are available in Sukwattananipaat et al., 2024.

During the change of glutamine metabolism, lactate shift was also presented in both CHL-YN and CHO-K1 cell cultures. In CHL-YN cell cultures, lactate shift was observed approximately on Day 3.5. Whereas the lactate shift of CHO-K1 cell cultures was available approximately on Day 5. A lactate drop to very low concentrations was found in CHL-YN cell cultures (Fig. 13B).

In addition, IgG production showed in different ways across cell lines. IgG production of CHL-YN heterogeneous cell pool cultures reached the maximum concentration on the final day of cultivation at 67.9±1.7 and 62.0±1.8 mg/L, whereas high IgG-producing CHL-YN B-08 clone cultures were shown to have about 2-fold higher IgG production. The maximum IgG concentrations of the B-08 cultures were 146±18 mg/L and 134±4 mg/L on the final day of cultivation. Moreover, the final IgG production of CHO-K1 heterogeneous cell pool cultures was shown at lower concentrations (16.8±2.7 and 18.4±1.4 mg/L) compared to CHL-YN cells (Fig. 13C).

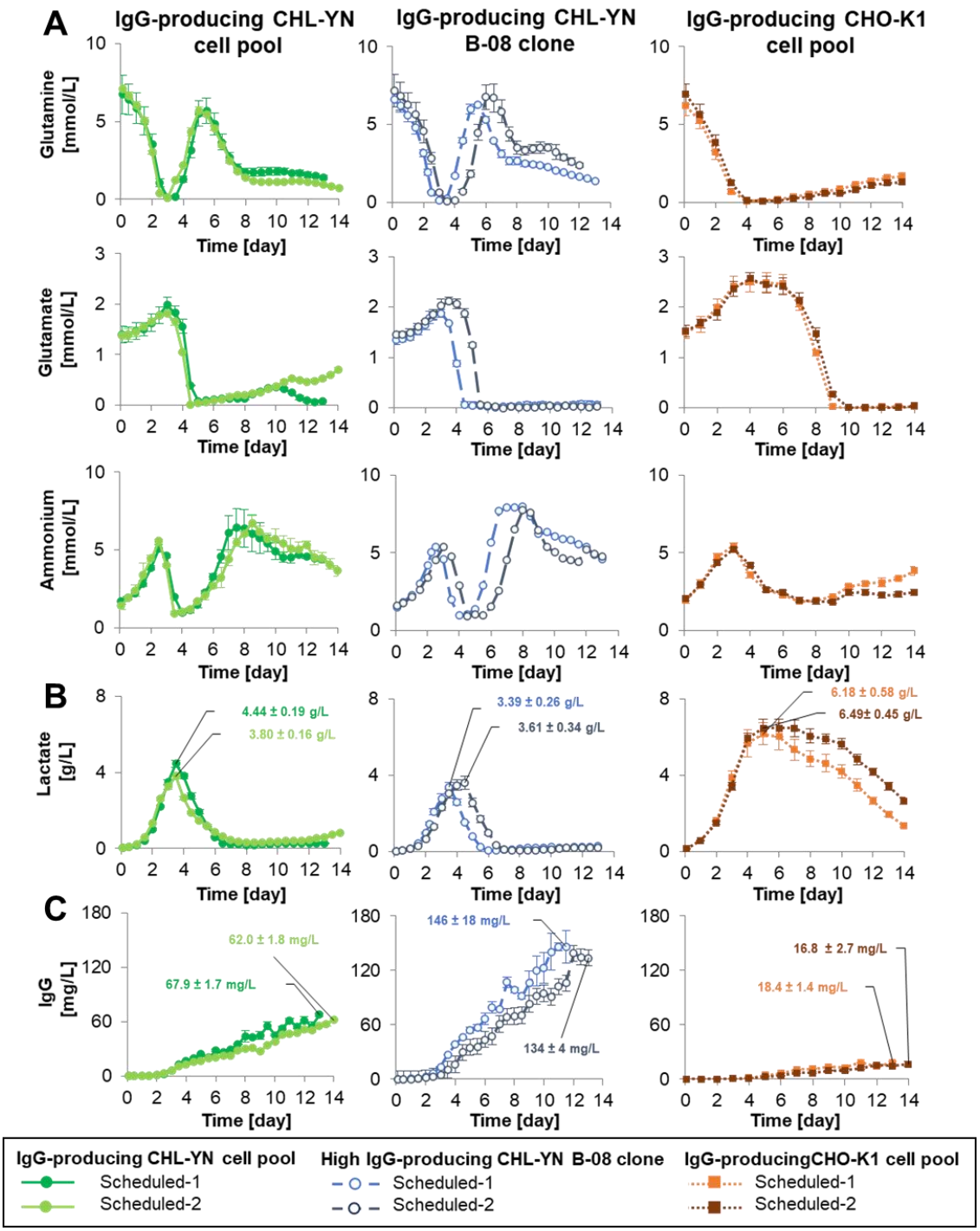

Figure 13. Time-course plots of extracellular metabolic profiles of scheduled glucose feeding fed-batch cultivations. **A)** Extracellular glutamine, glutamate, and ammonium concentrations. **B)** Extracellular lactate concentration. Data labels indicate the maximum lactate concentration. **C)**

IgG concentration. Data labels indicate the maximum IgG concentration. Error bars showed the standard deviation of triplicated measurements. These plots have been published and are available in Sukwattananipaat et al., 2024.

Considering specific rate calculations, overall metabolic profiles could ensure the hypothesis of unique features of IgG-producing CHL-YN cells' metabolic backgrounds. Glucose consumption rates showed correspondent results with the glucose feed rate design. Four different glucose consumption rates (Phase I–IV) were shown at IgG-producing CHL-YN cell cultures, whereas only two glucose consumption rates (Phase I–II) were presented in IgG-producing CHO-K1 cell cultures (Table 5A and Figure 14). Significantly low (p-value = 6.51×10^{-14}) glucose consumption of IgG-producing CHL-YN cells during phase II of glucose consumption (Days 3.5–6) compared to phase II of IgG-producing CHO-K1 cells (Day 4-end), indicated the specific characteristics of IgG-producing CHL-YN cells over the IgG-producing CHO-K1 cells. Glucose consumption was shown in the highest rates in both IgG-producing CHL-YN and CHO-K1 cell cultures during phase I (Day 1–3.5 of IgG-producing CHL-YN cultures and Day 1–4 of IgG-producing CHO-K1 cultures). The glucose consumption of IgG-producing CHO-K1 cells was a significantly higher (p-value = 6.24×10^{-5}) than IgG-producing CHL-YN cells. Lactate production rates were comparable (p-value = 0.498) between IgG-producing CHL-YN and CHO-K1 cell cultures during the early stages (Days 1–3.5). However, lactate consumption rates after lactate shift were shown in difference. Lactate consumption rates in CHL-YN cells were significantly higher (p-value = 2.60×10^{-7}) than CHO-K1 cells (Table 5B and Figure 14). Additionally, calculation-specific glutamine consumption assured the ability of strong glutamine production during Days 3.5–5.5. In comparison to the rates between IgG-producing CHL-YN and CHO-K1 cells, CHL-

YN cells showed about 10-fold higher glutamine production rates (p-value = 1.08×10^{-12}) compared to CHO-K1 cells. In this early stage, IgG-producing CHL-YN cells consumed glutamine at significantly higher rates (p-value = 1.50×10^{-6}) than IgG-producing CHO-K1 cells. Also, the glutamine re-consumption stage was only available in CHL-YN cells (Table 5C and Figure 14). IgG productivity revealed that productivity during the glutamine consumption stage was shown at the highest rates. IgG production of IgG-producing CHL-YN cells was significantly dropped during glutamine production stage (p-value = 1.22×10^{-3}). In addition, the scheduled glucose feeding did not provide an advantage in terms of IgG productivity compared to the preliminary cultures (Table 5D). In this study, production rates of CHL-YN cells were significantly higher than CHO-K1 cells (p-value = 1.35×10^{-4}). The significantly higher IgG production of B-08 clone (p-value = 2.04×10^{-8}) confirmed a benefit on high-producing clone isolation from the cell pool (Figure 14).

Table 5. Calculations of specific metabolic rates. **A)** glucose consumption; **B)** glutamine consumption; **C)** lactate consumption; and **D)** IgG productivity. This table has been published and is available in Sukwattananipaat et al., 2024.

Remarks

- Single asterisk (*) indicates 1-day delayed glucose metabolic pattern of B-08 clone-Scheduled-2 culture; phase I (Days 1–4.5), phase II (Days 4.5–7), phase III (Days 7–10), and phase IV (Days 10–end).

- Double asterisk (**) indicates 1-day delayed lactate metabolic pattern of B-08 clone-Scheduled-2 culture: Lac production (Days 1–4.5), Lac consumption (Days 4.5–8), and cell decline (Days 8–end).

- Triple asterisk (***) indicates 1-day delayed glutamine metabolic and IgG productivity patterns of B-08 clone-Scheduled-2 culture;

A.) Specific glucose consumption rates [pmol·cell^{-1}·day^{-1}]

	Phase I (1–3.5 d)	Phase II (3.5–6 d)	Phase III (6–9 d)	Phase IV (9 d–end)
Scheduled glucose feed control				
IgG-producing CHL-YN cells				
Cell pool – Scheduled-1	3.21 ± 0.14	0.24 ± 0.01	0.50 ± 0.01	0.63 ± 0.01
Cell pool – Scheduled-2	3.29 ± 0.03	0.34 ± 0.02	0.53 ± 0.02	0.75 ± 0.01
B-08 clone – Scheduled-1	2.67 ± 0.15	0.26 ± 0.01	0.59 ± 0.02	0.77 ± 0.00
B-08 clone – Scheduled-2*	3.47 ± 0.11	0.23 ± 0.01	0.62 ± 0.02	0.81 ± 0.02

	Phase I (1–4 d)	Phase II (4 d–end)
Scheduled glucose feed control		
IgG-producing CHO-K1 cells		
Cell pool – Scheduled-1	3.77 ± 0.12	0.67 ± 0.01
Cell pool – Scheduled-2	4.20 ± 0.03	0.69 ± 0.01

B.) Specific lactate consumption rate [pmol·cell^{-1}·day^{-1}], lactate molecular weight = 89.07 g/mol

	Lac production (1 – 3.5 d)	Lac consumption (3.5 – 7 d)	Late stage (7 d – end)
Scheduled glucose feed control			
IgG-producing CHL-YN cells			
Cell pool – Scheduled-1	-4.13 ± 0.15	0.67 ± 0.03	-0.01 ± 0.00
Cell pool – Scheduled-2	-3.14 ± 0.14	0.47 ± 0.01	-0.02 ± 0.00
B-08 clone – Scheduled-1	-3.34 ± 0.31	0.55 ± 0.04	-0.02 ± 0.00
B-08 clone – Scheduled-2**	-2.99 ± 0.23	0.60 ± 0.06	-0.03 ± 0.00

	Lac production (1 – 5 d)	Lac consumption (5 d – end)
Scheduled glucose feed control		
IgG-producing CHO-K1 cells		
Cell pool – Scheduled 1	-2.90 ± 0.42	0.30 ± 0.04

Cell pool – Scheduled 2	-3.56 ± 0.19	0.20 ± 0.02

C.) Specific glutamine consumption rate [pmol·cell^{-1}·day^{-1}]

	Gln consumption (1–3 d)	Gln production (3.5–5.5 d)	Gln re-consumption (5.5–8 d)	Gln stable (8 d–end)
Scheduled glucose feed control				
IgG-producing CHL-YN cells				
Cell pool – Scheduled-1	1.18 ± 0.18	-0.16 ± 0.02	0.08 ± 0.01	0.001 ± 0.001
Cell pool – Scheduled-2	0.90 ± 0.04	-0.16 ± 0.02	0.08 ± 0.00	0.002 ± 0.000
B-08 clone – Scheduled-1	1.27 ± 0.10	-0.17 ± 0.01	0.08 ± 0.01	0.012 ± 0.001
B-08 clone – Scheduled-2***	1.57 ± 0.21	-0.16 ± 0.02	0.10 ± 0.02	0.016 ± 0.001

	Gln consumption (1–4 d)	Gln production (4 d–end)
Scheduled glucose feed control		
IgG-producing CHO-K1 cells		
Cell pool – Scheduled-1	0.50 ± 0.05	-0.01 ± 0.00
Cell pool – Scheduled-2	0.56 ± 0.07	-0.01 ± 0.00

D.) Specific productivity [pg·cell^{-1}·day^{-1}]

	Gln consumption (1–3 d)	Gln production (3.5–5.5 d)	Gln re-consumption (5.5–8 d)
Preliminary glucose feed control			
IgG-producing CHL-YN cells			
Cell pool – Automated-1	0.42 ± 0.02	0.16 ± 0.02	0.27 ± 0.02
Cell pool – Automated-2	0.58 ± 0.01	0.19 ± 0.04	0.35 ± 0.03
Scheduled glucose feed control			
IgG-producing CHL-YN cells			
Cell pool – Scheduled-1	0.65 ± 0.02	0.26 ± 0.02	0.33 ± 0.08
Cell pool – Scheduled-2	0.44 ± 0.03	0.18 ± 0.01	0.20 ± 0.03
B-08 clone – Scheduled-1	1.51 ± 0.09	0.63 ± 0.04	0.89 ± 0.03
B-08 clone – Scheduled-2***	1.41 ± 0.02	0.50 ± 0.03	0.56 ± 0.01

	Gln consumption (1–4 d)	Gln production (4 d–end)
Scheduled glucose feed control		
IgG-producing CHO-K1 cells		
Cell pool – Scheduled-1	0.09 ± 0.01	0.08 ± 0.01
Cell pool – Scheduled-2	0.05 ± 0.01	0.08 ± 0.01

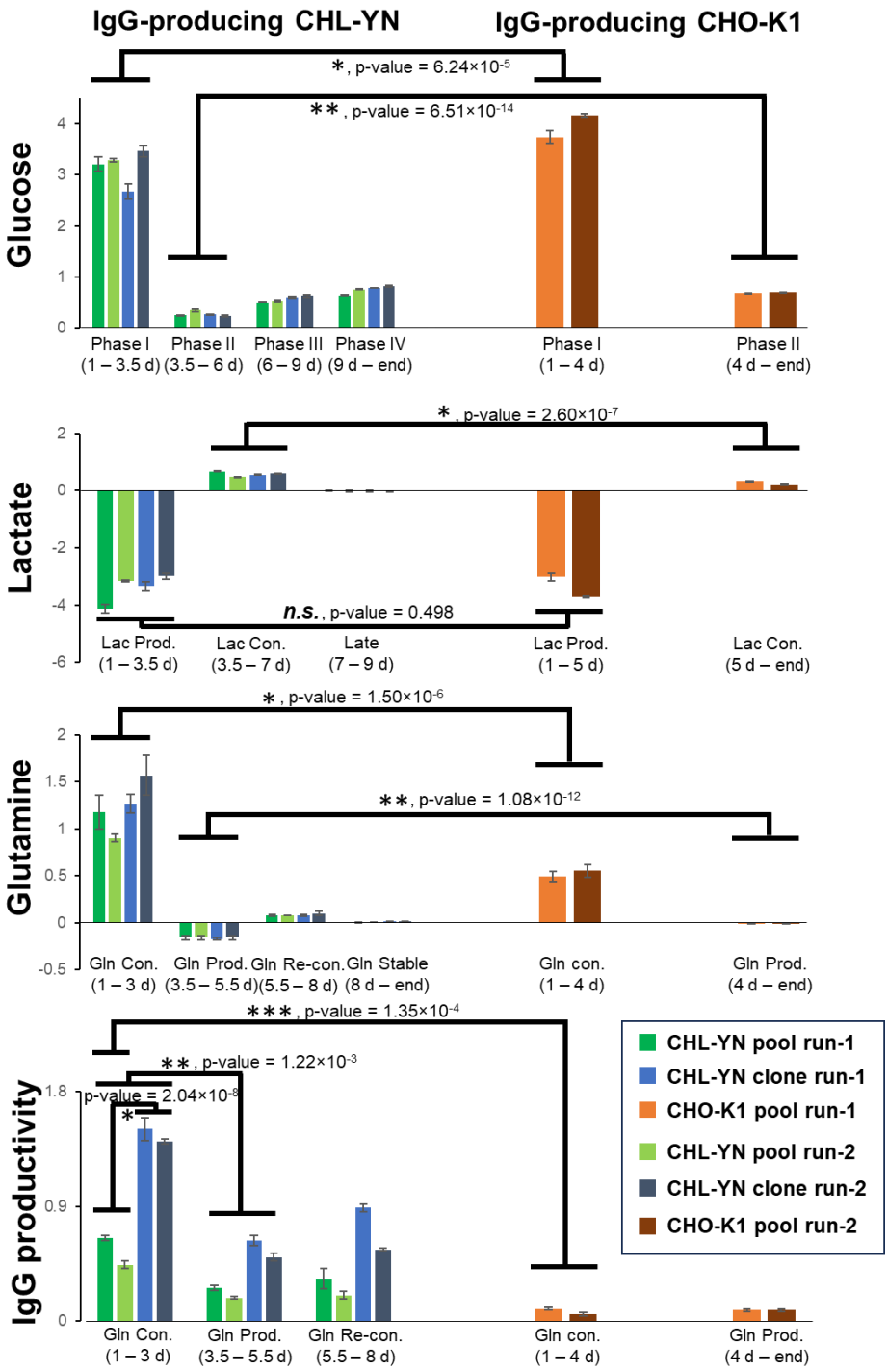

Figure 14. Bar charts of specific extracellular metabolic consumption rates and IgG productivity of scheduled glucose fed-batch cell cultures. Error bars represent the mean ± standard deviation of data. Asterisks indicate the p-value < 0.05 and the *n.s.* means non-significant (p-value ≥ 0.05).

2.4 Discussion

In this chapter, I developed glucose feeding strategies suitable for serum-free fed-batch of IgG-producing CHL-YN cell cultures. Initially, automated glucose feeding was preliminarily developed. Overwhelming amounts of glucose feed had been available since Day 3.5 of CHL-YN cell cultivations. Then, the scheduled glucose feeding was evaluated for IgG-producing CHL-YN cells. Scheduled glucose feeding was created by calculating the consumed glucose amount and then estimating the volume of additional glucose for finalizing the glucose concentration at 3.00 g/L. The goal of 3.00 g/L glucose concentration derived from the previous fed-batch CHO cell cultures, which sustained the glucose concentration by supplying glucose, aimed at finalizing the concentration to 4.00 g/L when the glucose level of cell cultures dropped to 2.00 g/L. Calculated results suggest that three distinct glucose feed rates fluctuated in accordance with glutamine metabolism. However, biological variability available among each bioreactor run leads to different timepoints of glutamine shift. Therefore, scheduling glucose feed rate adjustment on timepoints is recommended. Then, scheduled glucose feeding for IgG-producing CHL-YN cell pool cultures was set at 31.9 mL/d approximately on Days 2–4, 8.62 mL/d approximately on Days 4–6, and 18.0 mL/d approximately on Day 6 onward. The high IgG-producing CHL-YN B-08 clone cultures were set at 24.3 mL/d approximately on Days 2–4, 7.15 mL/d approximately on Days 4–6, and 18.4 mL/d approximately on Day 6 onward. Both the CHL-YN cell pool and the B-08 clone showed the dynamics of glucose feeding, which were different from the IgG-producing CHO-K1 cell pool cultures, which scheduled only one rate at 21.5 mL/d on Day 2 onward. To overcome the biological variability from each culture, a scheduled glucose feeding schedule was used together with a glucose adjustment equation. As a result, CHL-YN cell cultures, both cell pool and B-08 clone, successfully regulated glucose levels along with the cultivation.

Then, cultivation profile analyses revealed that scheduled glucose feeding usage could provide an advantage in slightly prolonging IgG-producing CHL-YN cell cultures up to 13–14 days with above 70.0% cell viability compared to the preliminary automated cultures (**Supporting information 1B**). This culture extension might be caused by avoiding excessive glucose supplementation. Overwhelming glucose feeding into cell culture causes high lactate production and an increase in osmotic stress (Lee et al., 2015; Alhuthali et al., 2021). In the comparison of the maximum lactate concentration between automated and scheduled glucose feedings, lactate peaks showed no change (**Supporting information 1B**). Hence, it suggests that scheduled glucose feeding could not reduce lactate production, and 3.00 g/L of glucose might not be considered a low glucose condition for CHL-YN cells. In addition, glucose overfeeding had been available on Day 3.5 of cultivation, which was available later than lactate shift (Day 3). Hence, high glucose amounts were not utilized as a source for lactate production. The advantage of cell culture extension might be caused by a reduction in osmolarity. To confirm this statement, osmolarity measurement is compulsory.

Furthermore, a study on glycosylation profiles of IgG products derived from controllable glucose condition of fed-batch operation is needed. According to the previous research, controlling glucose concentration could be advantageous to glycosylation pattern of IgG product by avoiding lactate and osmolarity increase. Additionally, limited glucose at low level (approximately 1.0 g/L) could reduce mannosylation on IgG, leading to enhance efficacy and prolong the IgG exposure (Horvat et al., 2020). Thus, scheduled low glucose feeding strategy (targeted at 1.00 g/L) would propose as a future perspective.

In comparison between IgG-producing CHL-YN and CHO-K1 cells, results suggest that IgG-producing CHL-YN cells have both similar and different metabolic characteristics to IgG-

producing CHO-K1 cells. The similar features of both cell lines include high glucose and glutamine consumption during the exponential stage of growth and also lactate production. After glutamine exhaustion, a metabolic shift had then occurred. This metabolic shift was shown in distinct ways between IgG-producing CHL-YN and CHO-K1 cells. IgG-producing CHL-YN cells could produce glutamine at high levels. This ability might be from strong glutamine synthetase expression (Yamano-Adachi et al., 2020). Glutamine was produced from glutamate and ammonium. Intriguingly, glutamine production was continuously observed during Days 3.5–5.5 of cultivation in CHL-YN cell cultures. However, extracellular glutamate was exhausted since Day 4. Therefore, CHL-YN cells may have regulatory mechanism to support glutamine production until Day 5.5 of cultivation. Further study on more associated metabolites, such as metabolomics approaches, may clarify this phenomenon. Moreover, low consumed glucose rates during the glutamine production stage were only observed in CHL-YN cells. This phenomenon might be related to higher lactate consumption in CHL-YN cells during this stage compared to CHO-K1 cells. Furthermore, metabolic analysis also revealed that CHL-YN cells could produce lactate in lower levels, whereas ammonium production was higher compared to CHO-K1 cells. Finally, IgG production in this study suggests that CHL-YN could produce in higher levels than CHO-K1 cells. The high IgG-producing CHL-YN B-08 clone indicated the possibility of obtaining high-productivity clones from CHL-YN cell pools as well as in CHO cell lines. In the industrial aspect, 146±18 mg/L of Trastuzumab antibody from fed-batch CHL-YN B-08 culture was lower than a previous report, which showed over 4 g/L of Trastuzumab production via a high-producing CHO clone (Boulenouar et al., 2023). Hence, CHL-YN cells required several further improvements, such as proper expressing vectors, optimal promotors and selection markers, cultivation process optimization, feed strategies, etc.

2.5 Conclusion

In conclusion of Chapter 2, I attempted to develop continuous glucose feeding system to IgG-producing CHL-YN cells aimed at achieving regulable glucose concentrations at 3.00±1.00 g/L. The scheduled glucose feeding was evaluated based on their glucose consumption. This scheduled feeding for IgG-producing CHL-YN cell cultures showed the dynamic glucose supplements following their glutamine metabolism. With this strategy, the glucose concentrations were controlled within the targeted range along with the cultivation. After that, further investigation on cell counts and metabolic profiles showed that IgG-producing CHL-YN cells have different glucose, lactate, and glutamine metabolism compared to IgG-producing CHO-K1 cell cultures. However, this chapter only presented the cell cultivation development and information focusing on the critical extracellular component profiles. It is difficult to explain the metabolic phenomenon and cellular metabolic backgrounds. In addition, understanding metabolic profiles during the first glutamine shift is necessary to improve the IgG-producing CHL-YN cell culture, because IgG-producing CHL-YN cells started declining viability and IgG productivity in this period. Therefore, in the next chapter, I proposed a deeper investigation focusing on glucose and glutamine metabolism during the first glutamine metabolic shift via targeted metabolomics analyses.

Chapter 3:

Combination CE-MS and LC-MS based metabolic profiling of IgG-producing CHL-YN cells in regulated glucose fed-batch conditions

Chapter 3: Combination CE-MS and LC-MS based metabolic profiling of IgG-producing CHL-YN cells in regulated glucose fed-batch conditions

3.1 Introduction

In Chapter 2, an exclusive glucose-consuming feature of IgG-producing CHL-YN cells in accordance with glutamine metabolism was discovered, coinciding with a decrease in cell viability during the same period. These observations necessitate further investigation of the relationship between glucose and glutamine metabolism. An important role of glutamine has been reported in various cancers and CHO cell studies. Glutamine plays a supporting role in the TCA cycle by converting to glutamate and entering the TCA cycle through α-ketoglutarate (Lieu et al., 2020; Jin et al., 2023). Additionally, glutamine can support cell proliferation and cell survival mechanisms through nucleotide, glutathione, and other non-essential amino acid biosynthesis (Yoo et al., 2020).

Since glucose and glutamine are key cellular energy sources, this study focuses on metabolites involved in central energy pathways like glycolysis, the TCA cycle, and amino acid metabolism. Therefore, targeted metabolic analysis is determined. The liquid chromatography-mass spectrometry (LC-MS) method, with its broad applicability and high sensitivity, is widely used in metabolomics studies. Despite its versatility, using the LC-MS encounters a challenge in difficulty to detect several sugar phosphates, including glycolysis intermediates, which have similar structures, high polarity, and strong negative charge properties. These characteristics of sugar phosphates lead to ion suppression in the LC-MS-based analysis, resulting in less measurement accuracy (Li et al., 2022; Jia et al., 2023; Soga, 2023). In contrast, the capillary electrophoresis-mass spectrometry (CE-MS) approach for metabolomics offers an alternative

approach for analyzing sugar phosphates. CE-MS technology separates the samples based on their size and charge, potentially mitigating the ion suppression effects, which are found in the LC-MS method. However, the CE-MS alone is not sufficient for comprehensive metabolite profiling, as it has limitations in detecting certain classes of phospholipids and fatty acids. Therefore, a combined approach using both LC-MS and CE-MS is employed to achieve a more comprehensive metabolic background of the cultivated cell metabolites (Kudo et al., 2022).

Hereby, this study conducted CE-MS-based intracellular and LC-MS-based extracellular metabolomics analyses for investigating metabolic profiles of regulated glucose fed-batch cultivation of IgG-producing CHL-YN and CHO-K1 cell pools. In addition, the high IgG-producing clone was compared to the cell pool aimed at searching for critical metabolites, which may affect productivity.

3.2 Materials and Methods

3.2.1 Samples and metabolomics analysis preparation

Samples for intracellular and extracellular metabolomics analysis were acquired from serum-free fed-batch operation with regulable glucose conditions. Cell samples consisting of 1.0×10^7 viable cells from each culture were collected for capillary electrophoresis-mass spectrometry (CE-MS) techniques. While supernatant samples from each cell cultivation were collected by centrifugation at 14,000 ×*g* speed for 5 minutes at 4 °C, they were analyzed via liquid chromatography-tandem mass spectrometry (LC-MS/MS) method. The different approaches for intracellular and extracellular metabolomics analysis were because of the capabilities of these tools, which detect distinct sets of metabolites. Four timepoints of each cell line model were

selected aimed at comprehending the first glutamine metabolic shift and representing distinct stages of cell growth. Thereby, samples of the IgG-producing CHL-YN cell culture cell pool and the B-08 clone were from Days 2, 3, 4, and 5 of cell cultivation. Whereas Days 2, 4, 6, and 8 were selected in IgG-producing CHO-K1 cell cultures (Fig. 15).

Sample preparation for the metabolic studies depended on the metabolomic instrument. The cell samples for intracellular CE-MS analysis were pretreated following guidance from Human Metabolome Technologies, HMT (Yamagata, Japan). The cell samples were first rinsed to remove culture medium via 5% mannitol solution (Fujifilm Wako Pure). After that, cell extraction was proceeded by 99.7% methanol solution (Fujifilm Wako Pure). Next, the internal standard reagent provided by HMT was added and mixed before centrifugating at 2,300 ×*g* speed for 5 minutes at 4 °C. Then, the supernatant was through the filter column kit from HMT by centrifugation at 9,100 ×*g* speed for 180 min at 4°C, aiming to collect the intracellular metabolites. The samples were kept at -80 °C before delivering to the HMT company.

Regarding extracellular metabolites, the sample preparation protocol was kindly provided by Shimadzu Corporation. The supernatant samples were first treated for protein precipitation via acetonitrile solution (Fujifilm Wako Pure). Then, acetonitrile-treated samples were centrifuged at 15,000 rpm, for 5 minutes at 25 °C. After pellet removal, centrifuged samples were 10-fold diluted with ultrapure water (Fujifilm Wako Pure).

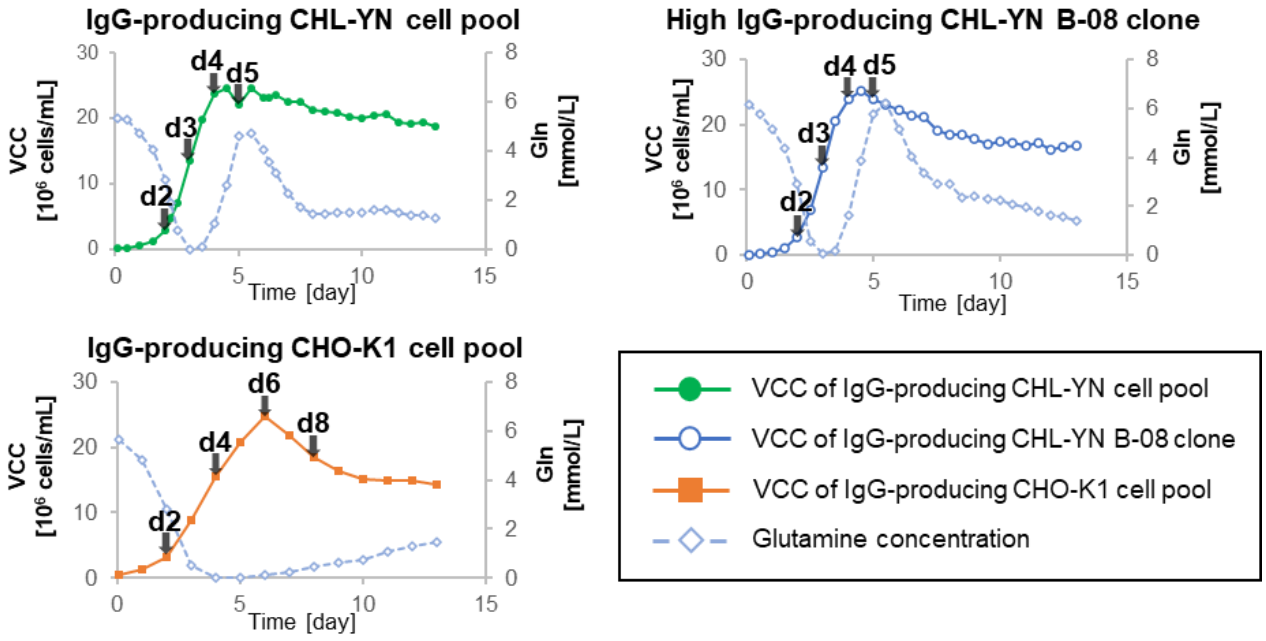

Figure 15. Samples for metabolomics analyses collected from the glucose-regulated fed-batch cell cultures. The sampling point was selected to represent four stages of cell growth (early, Ear; exponential, Exp; stationary, Sta; and decline, Del) and comprehend glutamine metabolic change from consumption to production. These criteria were determined from the time course of off-line viable cell concentration (VCC) and extracellular glutamine concentration. Black arrows labeled with the day indicate sampling timepoints.

3.2.2 Metabolomics analyses

Pretreated intracellular samples were delivered to HMT for the C-SCOPE quantitative analysis package. This method detects a total of 116 ionic metabolites associated with central energy metabolic pathways consisting of glycolysis, the tricarboxylic acid (TCA) cycle, amino acids, and purine metabolisms. Time-of-flight mass spectrometry and triple quadrupole mass

spectrometry were CE-MS-based tools for analyzing these samples. The quantitative metabolic results were described in a unit of concentration per cell (pmol/10^6 cells).

Whilst pretreated extracellular samples were investigated via the LC/MS/MS Method Package for Cell Culture Profiling Ver. 3 (Shimadzu Corporation, Kyoto, Japan). The LCMS-8060NX, triple quadrupole mass spectrometry, was a platform for investigating a total of 144 metabolites in amino acids, TCA cycle, nucleic acids, etc. The software used for identifying LC-MS/MS peaks on a chromatogram and creating data collection was LabSolutions InsightTM LCMS data analysis combined with Peakintelligence^{TM}, an artificial intelligence accommodating chromatographic peak picking, provided by Shimadzu Corp. Without referring to standard solutions, the quantitative data of extracellular metabolites was presented in the peak area.

3.2.3 Data analysis

3.2.3.1 Data processing

The intracellular and extracellular metabolic data was analyzed independently. A universal metabolomics information analysis and interpreting website, MetaboAnalyst (www.metaboanalyst.ca), was chosen as a platform for this study. The Statistical Analysis [one factor] module was selected. The collection of metabolic concentration data, which provided categorized samples and data groups by the cell lines and sampling time, was used. Then, data processing was executed via missing value estimation and data scaling.

To estimate the missing value, two steps are required. First, the metabolites, which have missing over 75% of values, had vanished. After that, missing values of remaining metabolites were replaced by the value calculated from 20% of the minimum detected values of that metabolite,

which assumed that the metabolomics tools could not detect these low amounts. This data compensation was conducted aimed at reducing the complexity of limited data.

Data scaling was proceeded via the auto-scaling method, which centers the mean value and is divided by the standard deviation on each metabolite. This process is a type of data normalization, which can reduce the dispersion from raw metabolic data and facilitate easier comparison between data values.

3.2.3.2 Statistical and enrichment analyses

After data processing, processed data was subsequently investigated for statistical analysis. Clustering data based on metabolic profiles was first evaluated by principal component analysis (PCA) with K-means. The K-means were clustered into 3 groups. Then, metabolic profile comparison between data clusters was explained by a volcano plot, a scatter plot displaying fold change and significance *p*-value. The cut-off criteria for the volcano plots was set at above 1.23 of $-\log_{10}(p\text{-value})$ and over 0.05 of $\log_2(\text{fold change})$. Metabolites, which showed significantly different between two sample clusters, were noted for enrichment analysis. Enrichment analysis was used for searching metabolic pathways that related to significant increased and decreased metabolites. Due to targeted metabolomics analyses, the metabolic library was customized, covering only measurable metabolites. Therefore, two specified databases for each metabolomic approach were constructed. These self-defined databases were a reduced version of the metabolic pathway database of the Chinese hamster (*C. griseus*) available on the Kyoto Encyclopedia of Genes and Genomes (KEGG; Kanehisa Laboratories, Kyoto University, Kyoto, Japan).

3.2.3.3 Integral data interpretation

Aiming at creating hypothetical metabolic models for further explanation, the previous study on transcriptomics analysis from flask-batch host CHL-YN and CHO-K1 cells was provided by Mr. Rintaro Arishima. Additionally, additional LC-MS/MS metabolic results from flask-batch IgG-producing CHL-YN and CHO-K1 were kindly provided by Mr. Kuroda Hirotaka. The LC-MS/MS data of triplicated flask-batch cultures were used for strengthening the hypothesis reliability that was observed from the fed-batch cultivation.

3.3 Results

3.3.1 Data acquisition and sample clustering analyses

The total of 12 samples includes IgG-producing CHL-YN cell pool Day 2–5 (CHL-YN D2–D5); IgG-producing CHL-YN B-08 clone Day 2–5 (B-08 D2–D5); and IgG-producing CHO-K1 Day 2, 4, 6, and 8 (CHO-K1 D2, D4, D6, and D8). These samples were separately analyzed for intracellular and extracellular components via CE-MS and LC-MS/MS, respectively.

Targeted CE-MS metabolomics analysis detected 101 identified peaks. Then, processed metabolic datasets were used to conduct principal component analysis (PCA) with K-means cluster analysis. The results showed that samples were categorized into three groups: 1) glutamine consumption group, which contains 5 samples (CHL-YN D2–D3, B-08 D2–D3, and CHO-K1 D2); 2) glutamine production of CHL-YN cell group, which includes 4 samples (CHL-YN D4–D5 and B-08 D4–D5); and 3) glutamine production of CHO-K1 cell group, which consists of 3 samples (CHO-K1 D4, D6, and D8) (Fig. 16A).

Targeted LC-MS/MS metabolomics approach detected 136 identified peaks. The data was processed and then clustered the sample groups with the exacted methodologies for intracellular metabolomics. The results are also similar to the intracellular investigation. Three groups of samples relying on glutamine metabolism were shown. The extracellular metabolites of CHO-K1 D4 were set in the glutamine consumption group, while intracellular analysis was in the glutamine production group (Fig. 16B). From the statistical analysis, results suggest that the metabolic components in CHL-YN and CHO-K1 were similar during the early stage when extracellular glutamine was available. Later, the metabolic profiles of CHL-YN and CHO-K1 cells were shown differently when glutamine was exhausted. Furthermore, differences between the IgG-producing CHL-YN cell pool and the high IgG-producing CHL-YN clone, B-08, were not observed in this study.

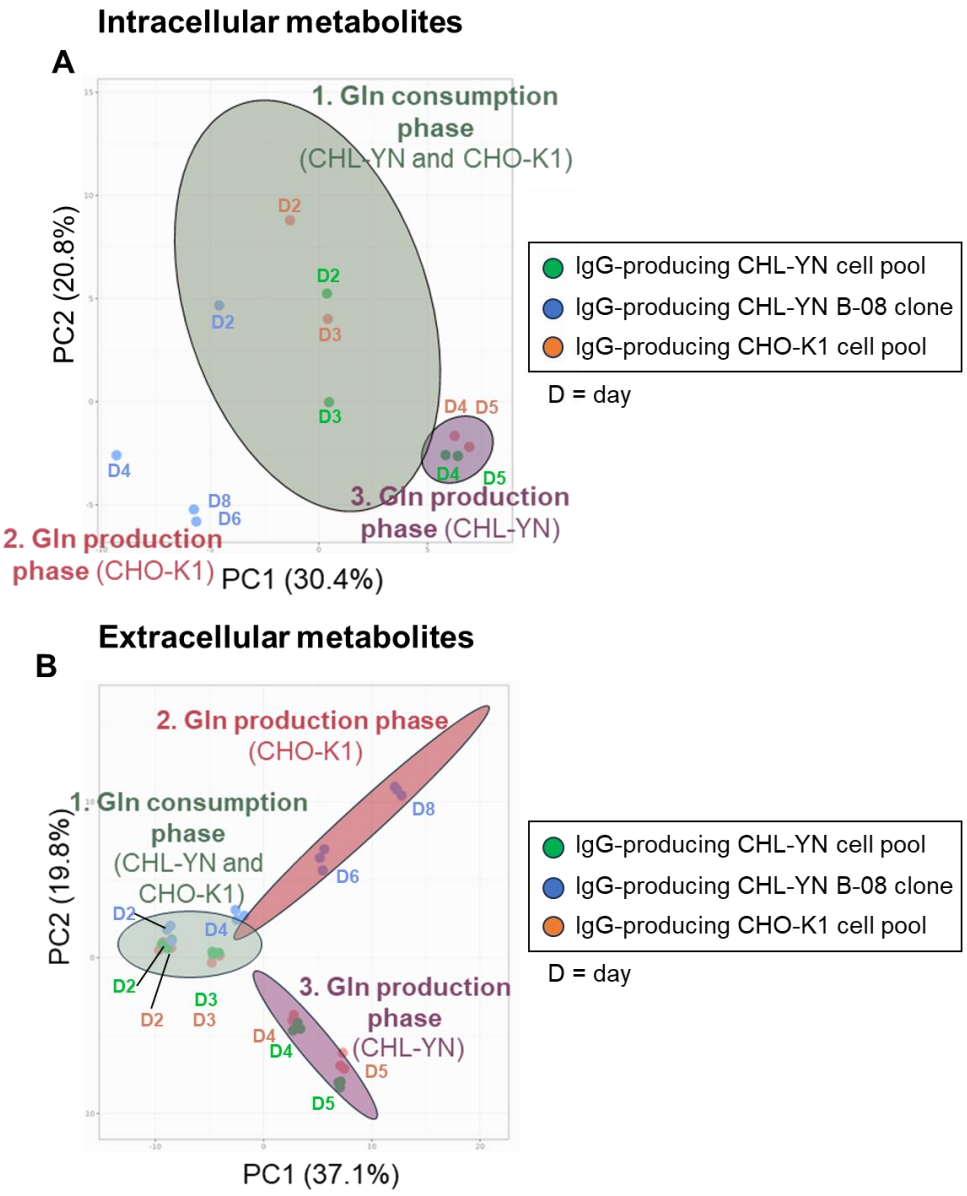

Figure 16. Three distinct sample clusters of both intracellular (CE-MS) and extracellular (LC-MS/MS) metabolomic samples. Metabolomic samples were clustered by principal component analysis (PCA) with K-mean clustering. **A)** Intracellular metabolites and **B)** Extracellular metabolites. These figures have been published and are available in Sukwattananipaat et al., 2024.

3.3.2 Comparison metabolic profiles of IgG-producing CHL-YN cells between glutamine consumption and production stages

After sample groups were formed, further investigation on different metabolic information among each sample group was then conducted. The volcano plot of intracellular metabolites showed that a total of 20 metabolites were significantly decreased when CHL-YN cells produced glutamine, whereas 5 metabolites were significantly increased during glutamine production (Fig. 17A). The enrichment analysis on those 25 differential metabolites revealed that protein biosynthesis (p-value = 0.0041) and aspartate metabolism (p-value = 0.043) were enriched (Fig. 17B).

Investigation on extracellular metabolic profiles: the volcano plot showed that 26 metabolites were significantly decreased when CHL-YN cells produced glutamine, whereas 38 metabolites were significantly increased during glutamine production (Fig. 18A). The enrichment analysis from those 64 shift metabolites disclosed four enriched pathways, including protein biosynthesis (p-value = 0.0081); urea cycle (p-value = 0.0082); phenylalanine and tyrosine metabolism (p-value = 0.030); and valine, leucine, and isoleucine metabolism (p-value = 0.030) (Fig. 18B).

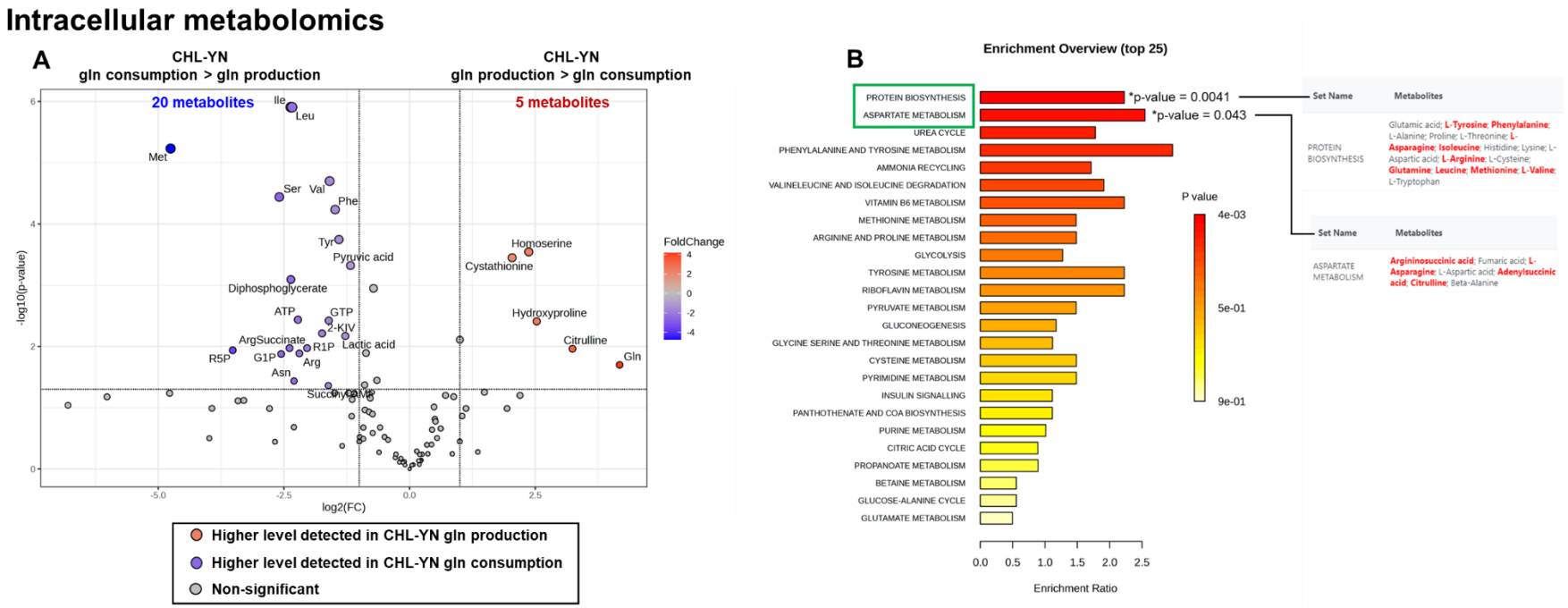

Figure 17. Comparison of intracellular metabolites and associated pathways between CHL-YN cells during glutamine consumption and production stages. **A)** The volcano plot of differential intracellular metabolites. **B)** The enrichment analysis revealed the top 25 pathways that related to significantly differential metabolites available in the volcano plot. The *p*-values and associated metabolic information are shown only for significantly enriched pathways (*p*-value ≤ 0.05). The green rectangle represents enriched pathways. Red metabolic names show significantly differential metabolites.

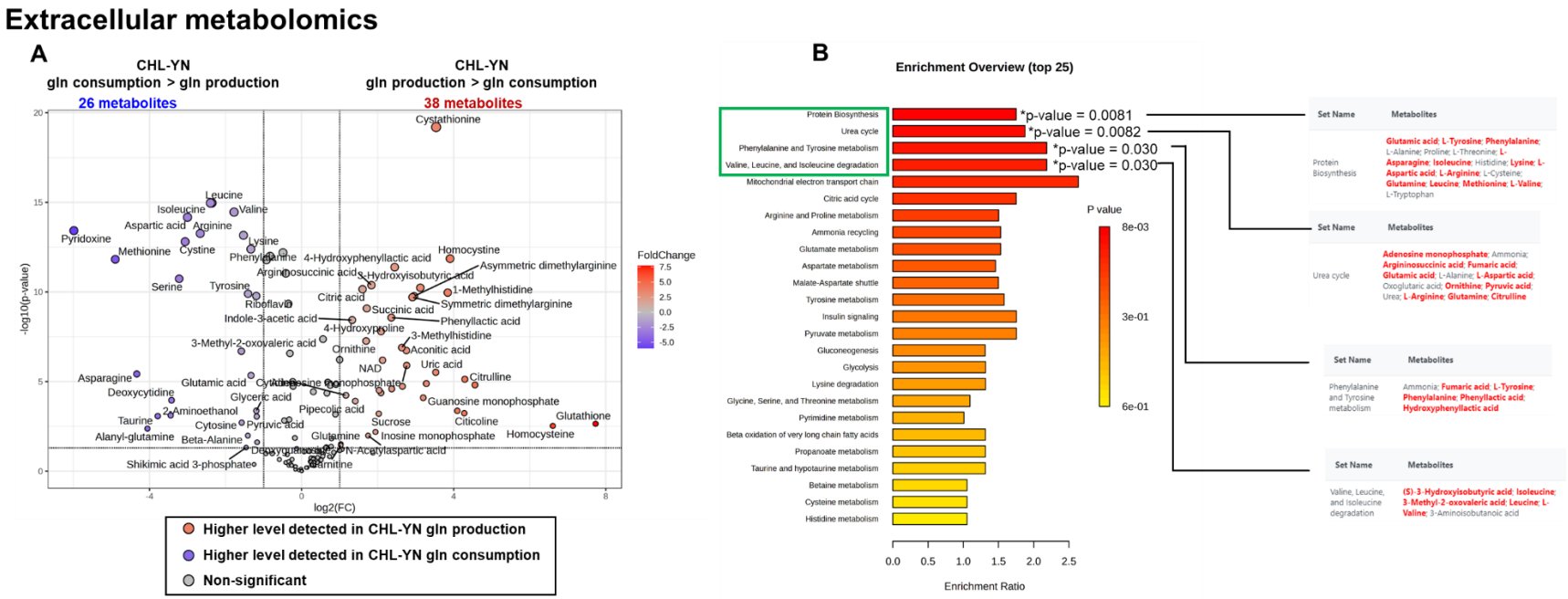

Figure 18. Comparison of extracellular metabolites and associated pathways between CHL-YN cell cultures during glutamine consumption and production stages. **A)** The volcano plot of differential extracellular metabolites. **B)** The enrichment analysis revealed the top 25 pathways that related to significantly differential metabolites available in the volcano plot. The *p*-values and associated metabolic information are shown only for significantly enriched pathways (*p*-value ≤ 0.05). The green rectangle represents enriched pathways. Red metabolic names show significantly differential metabolites.

3.3.3 Comparison metabolic profiles between IgG-producing CHL-YN and CHO-K1 cells during glutamine production stage

Another sample grouping result exposed the different metabolic features between CHL-YN and CHO-K1 cells during glutamine production stage. Then, volcano plots and enrichment analyses were conducted aimed at searching for distinct metabolites and related pathways. The volcano plot for comparing these two cell lines showed that a total of 30 intracellular metabolites were significantly higher in CHO-K1 cells, whereas 7 intracellular metabolites were significantly higher in CHL-YN cells (Fig. 19A). The enrichment analysis of those 37 intracellular metabolites revealed that glycolysis (p-value = 0.0093), gluconeogenesis (p-value = 0.011), and protein biosynthesis (p-value = 0.024) were overrepresented (Fig. 19B).

Inspection of extracellular metabolic information among both cell lines during glutamine production, the volcano plot illustrated a total of 39 extracellular metabolites were significantly presented at a higher level in CHO-K1 cell cultures. Whilst 24 extracellular metabolites were available in CHL-YN cell cultures with significantly greater levels (Fig. 20A). Those 63 metabolites were then utilized for the enrichment analysis. As a result, methionine metabolism (p-value = 0.014) and pyrimidine metabolism (p-value = 0.015) were enriched (Fig. 20B).

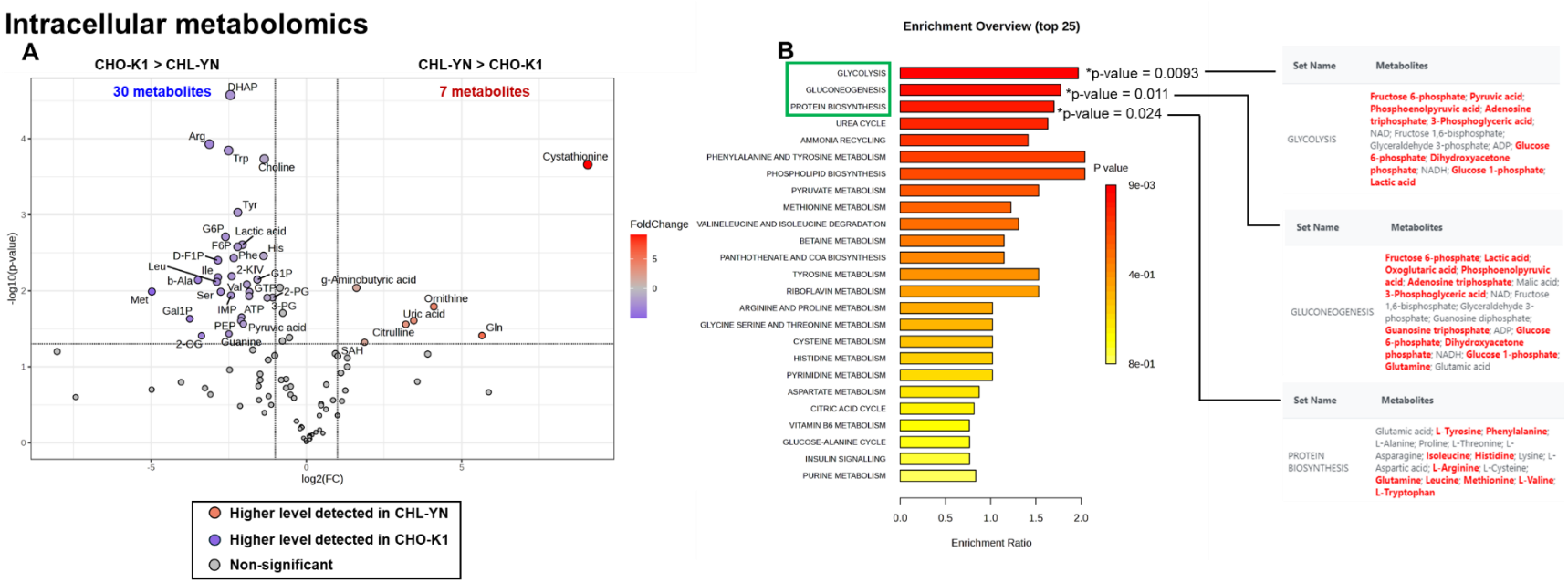

Figure 19. Comparison of intracellular metabolites and associated pathways between IgG-producing CHL-YN and CHO-K1 cells during production stages. **A)** The volcano plot of differential intracellular metabolites. **B)** The enrichment analysis revealed the top 25 pathways that related to significantly differential metabolites available in the volcano plot. The *p*-values and associated metabolic information are shown only for significantly enriched pathways (*p*-value ≤ 0.05). The green rectangle represents enriched pathways. Red metabolic names show significantly differential metabolites.

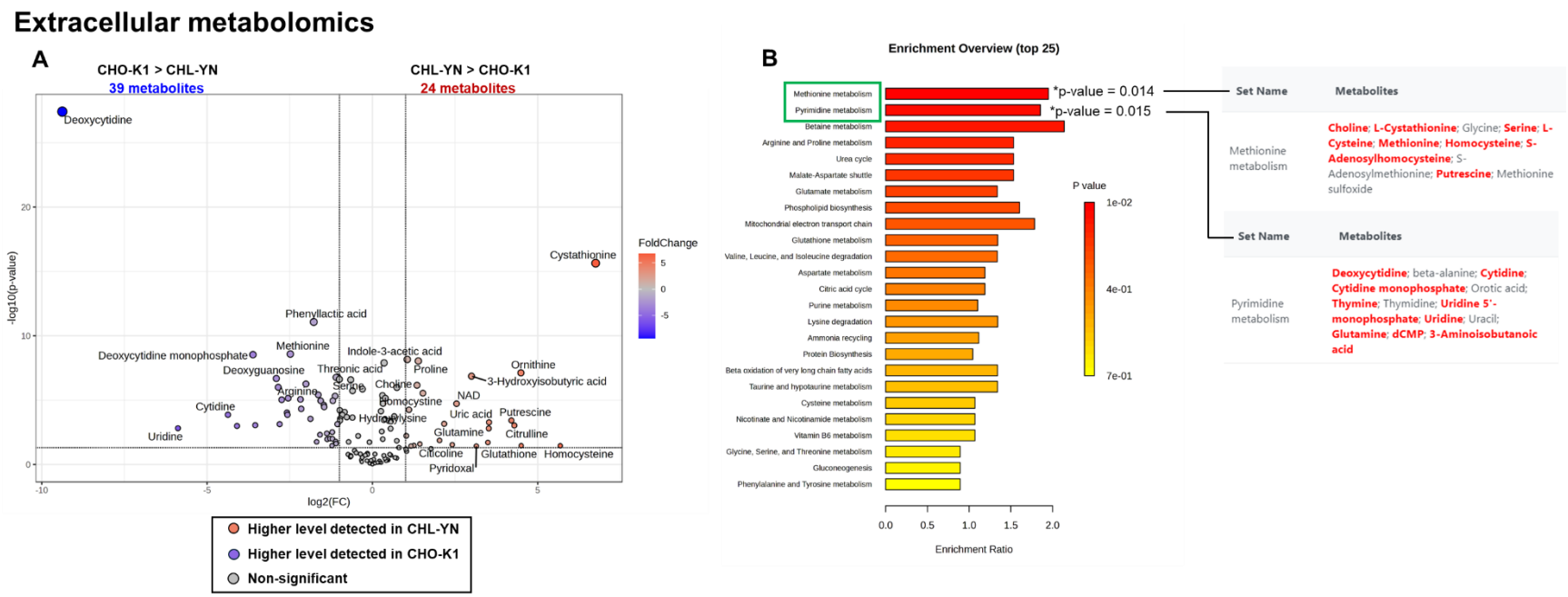

Figure 20. Comparison of extracellular metabolites and associated pathways between IgG-producing CHL-YN and CHO-K1 cell cultures during production stages **A)** The volcano plot of differential extracellular metabolites. **B)** The enrichment analysis revealed the top 25 pathways that related to significantly differential metabolites available in the volcano plot. The *p*-values and associated metabolic information are shown only for significantly enriched pathways (*p*-value ≤ 0.05). The green rectangle represents enriched pathways. Red metabolic names show significantly differential metabolites.

3.3.4 Data interpretation

3.3.4.1 Metabolic investigation specified on amino acids and derivatives

Overall, metabolomic analyses indicated that protein biosynthesis was the most highlighted pathway among those distinct metabolic backgrounds. In addition, the top ten significantly highest fold-change metabolites on volcano plots presented the tremendous change of several amino acids among sample groups, such as methionine, asparagine, serine, and glutamine (Table 6). Hence, this study was then reviewed on concentrations of amino acid metabolisms.

Table 6. The top ten significantly differential metabolites showed the highest fold-change values on volcano plots in Figures 17-20. Red represents a negative value of the fold change (glutamine consumption > glutamine production; CHO-K1 > CHL-YN). Green represents a positive value of the fold change (glutamine consumption < glutamine production; CHO-K1 < CHL-YN). Bold metabolites indicate proteinogenic amino acids. Values in Parentheses indicated the absolute $\log_2$ (fold-change) values.

CHL-YN: Gln production / Gln consumption		CHL-YN / CHO-K1	
CE-MS intracellular	LC-MS extracellular	CE-MS intracellular	LC-MS extracellular
Methionine (4.75)	Glutathione (7.73)	Cystathionine (9.06)	Deoxycytidine (9.38)
Glutamine (4.18)	Homocysteine (6.61)	**Glutamine** (5.65)	Cystathionine (6.75)
Ribose 5-phosphate (3.52)	Pyridoxine (5.99)	**Methionine** (4.98)	Uridine (5.88)
Citrulline (3.24)	**Methionine** (4.90)	Ornithine (4.10)	Homocysteine (5.68)
Serine (2.59)	Oxidized glutathione (4.56)	Galactose 1-Phosphate (3.76)	Glutathione (4.50)
Glucose 1-phosphate (2.55)	**Asparagine** (4.34)	β-Alanine (3.49)	Ornithine (4.49)

Table 6. Continued.

CHL-YN: Gln production / Gln consumption		CHL-YN / CHO-K1	
CE-MS intracellular	LC-MS extracellular	CE-MS intracellular	LC-MS extracellular
Hydroxyproline (2.53)	Citrulline (4.29)	Uric acid (3.46)	Cytidine (4.37)
Argininosuccinate (2.39)	Citicoline (4.28)	α-Ketoglutarate (3.38)	Citrulline (4.29)
Homoserine (2.37)	Guanosine monophosphate (4.09)	Citrulline (3.20)	Putrescine (4.20)
Isoleucine (2.36)	Alanyl-glutamine (4.06)	**Arginine** (3.13)	Argininosuccinate (4.10)

Investigation on concentrations of all amino acids and combined metabolomics studies revealed that there were nine amino acids significantly reduced when glutamine metabolism of CHL-YN cells first shifts from consumption to production. These nine amino acids consist of arginine, aspartate, isoleucine, leucine, methionine, phenylalanine, serine, tyrosine, and valine (**Supporting information 3–4**). Among these decreased amino acids, four amino acids were tremendously dropped after glutamine shift exclusively occurred in CHL-YN cells: arginine, aspartate, methionine, and serine (Fig. 21). Interestingly, arginine and methionine-associated compounds such as ornithine and cystathionine were also remarkable increased in the CHL-YN study. This finding led to the next investigation on involved pathways: arginine and methionine metabolisms.

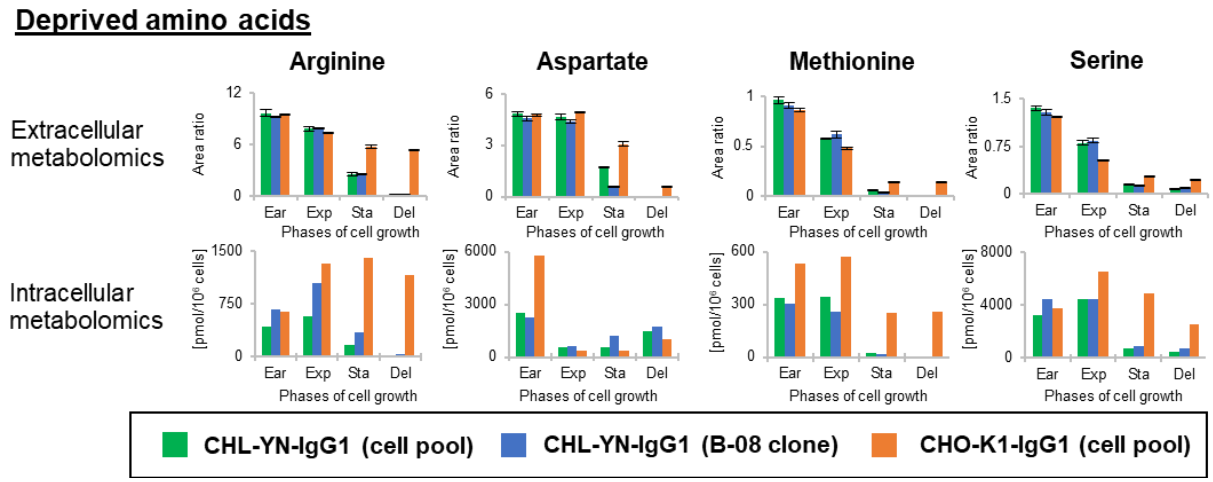

Figure 21. Bar charts illustrate extracellular and intracellular concentrations of deprived amino acids across four cell growth stages. Ear represents the early stage (CHL-YN D2; CHO-K1 D2); Exp represents the exponential stage (CHL-YN D3; CHO-K1 D4); Sta represents the stationary stage (CHL-YN D4; CHO-K1 D6); and Del represents the decline stage (CHL-YN D5; CHO-K1 D8). This figure has been published and is available in Sukwattananipaat et al., 2024.

The concentrations of several metabolic compounds involved in arginine metabolism and related pathways such as the urea cycle, proline biosynthesis, and polyamine anabolism were shown to be distinct between CHL-YN and CHO-K1 cells. Combined metabolic results suggest that CHL-YN cells may have strong capabilities of these pathways. For instance, citrulline, ornithine, glutamine, and putrescine were remarkably increased only in CHL-YN cells. In addition, intracellular argininosuccinate showed strongly reduced activity during the glutamine metabolic shift (between Exp and Sta stages), whereas intracellular argininosuccinate content of CHO-K1 cells was sustained during the same period. Proline reduction was also observed only in CHO-K1 cells. While CHL-YN cells could be raised as well as putrescine (Fig. 22).

Not only arginine metabolism but also methionine metabolism were noticeable in CHL-YN cells compared to CHO-K1 cells. Cystathionine concentration was strongly increased only in CHL-YN cells. Furthermore, glutathione biosynthesis, which is connected to the methionine cycle through the transsulfuration pathway, was also considered. Both reduced and oxidized glutathione (GSH and GSSG) were available in CHL-YN cells with a higher level than CHO-K1 cells (Fig. 23). However, only metabolomics analyses can provide insufficient evidence to confirm the metabolic activity. Therefore, integration with other investigations, such as transcriptomics, was then considered. Also, metabolic information from flask-batch IgG-producing CHL-YN and CHO-K1 cell cultures was used for ensuring metabolic hypotheses from this study.

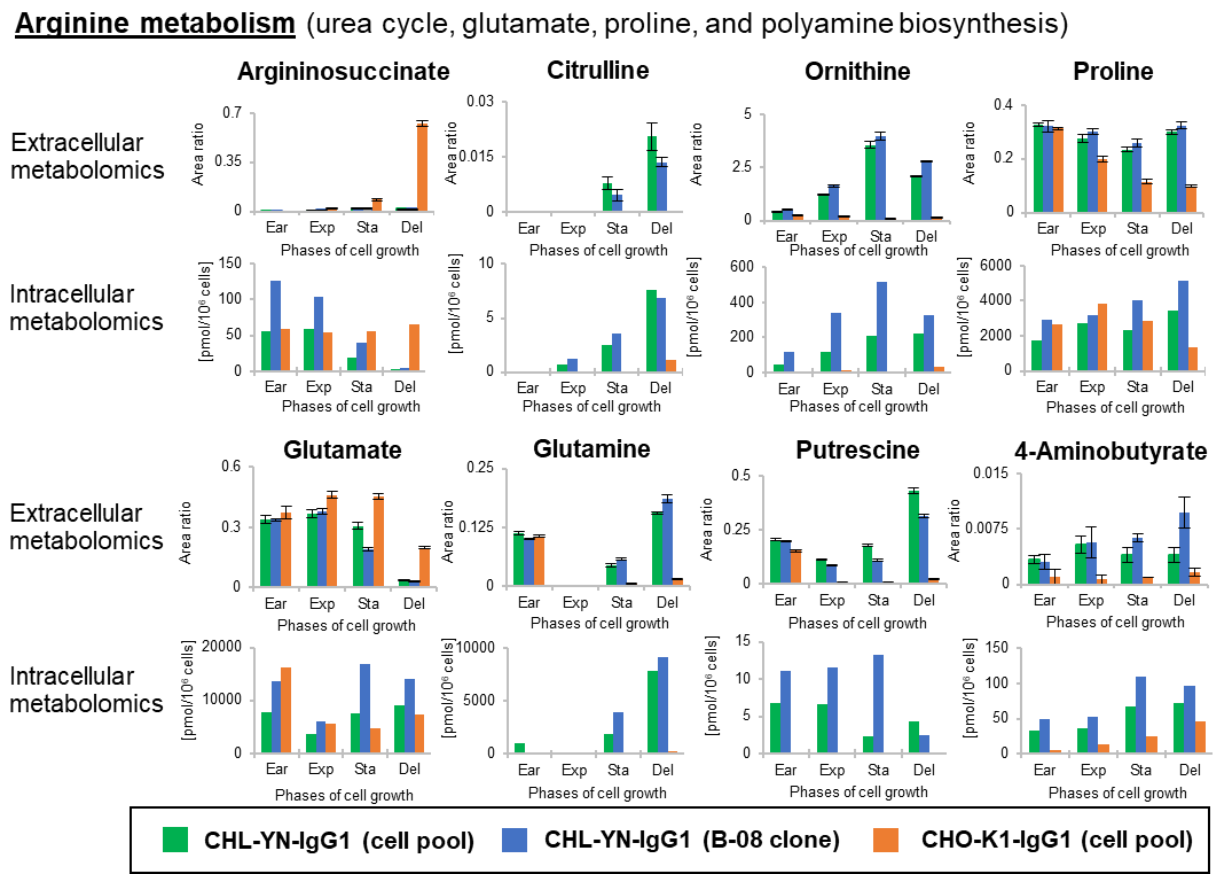

Figure 22. Bar charts illustrate extracellular and intracellular concentrations of metabolites involved in arginine metabolism across four cell growth stages. Ear represents the early stage (CHL-YN D2; CHO-K1 D2); Exp represents the exponential stage (CHL-YN D3; CHO-K1 D4); Sta represents the stationary stage (CHL-YN D4; CHO-K1 D6); and Del represents the decline stage (CHL-YN D5; CHO-K1 D8). This figure has been published and is available in Sukwattananipaat et al., 2024.

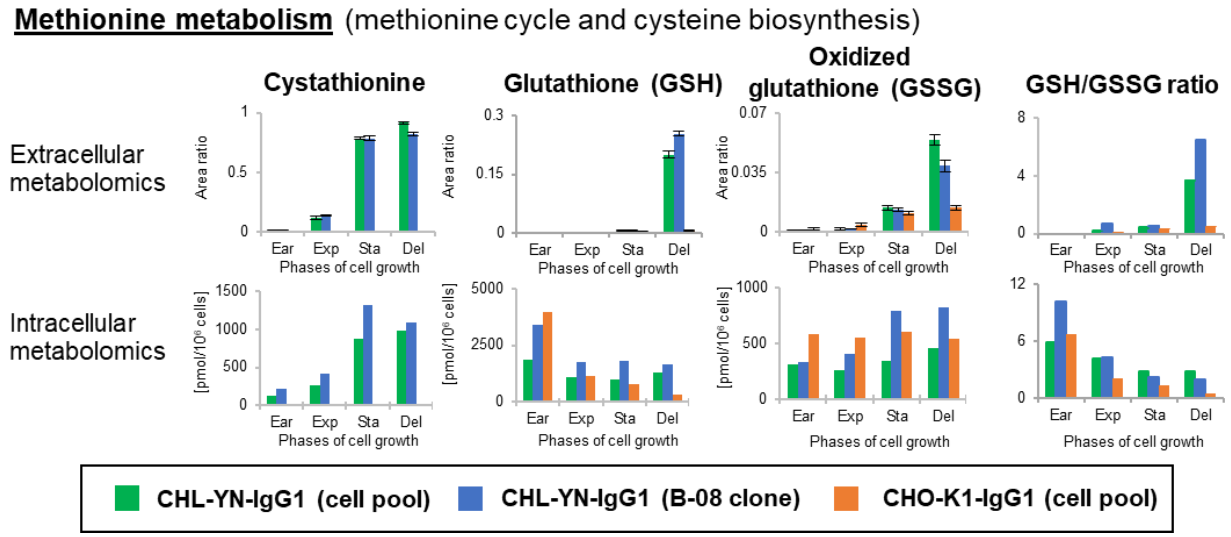

Figure 23. Bar charts illustrate extracellular and intracellular concentrations of metabolites involved in methionine metabolism across four cell growth stages. Ear represents the early stage (CHL-YN D2; CHO-K1 D2); Exp represents the exponential stage (CHL-YN D3; CHO-K1 D4); Sta represents the stationary stage (CHL-YN D4; CHO-K1 D6); and Del represents the decline stage (CHL-YN D5; CHO-K1 D8). This figure has been published and is available in Sukwattananipaat et al., 2024.

3.3.4.2 Integration of multi-omics data and hypothetical metabolic model creation

From the results received from target metabolomics analyses of bioreactor-based fed-batch CHL-YN cell cultures, data interpretation was explained by using hypothetical metabolic models. However, only metabolomics analysis could not be sufficient to understand the phenomena. Then, relevant information from other CHL-YN cell studies was used to clarify the metabolic incident and strengthen the hypothetical models. In this study, hypothetical models of CHL-YN arginine and methionine metabolisms were elaborated by knowledge collected from former studies on flask-batch transcriptomes and metabolomes. Transcriptomics information of flask-batch host CHL-YN cell cultures was previously reported in a term of reads per kilobase per million mapped reads-normalized data by Mr. Arishima Rintaro and partially published in Yamano-Adachi et al., 2020 (**Supporting information 5**). Furthermore, the LC-MS/MS-based targeted metabolomics analysis of intracellular and extracellular compounds of flask-batch IgG-producing CHL-YN and CHO-K1 cells was conducted by Mr. Kuroda Hirotaka (**Supporting information 6–7**).

From the results, CHL-YN cells have stronger urea cycle gene expressions than CHO-K1 cells, leading to an increase in urea cycle intermediate amounts such as citrulline and argininosuccinate. However, CHL-YN cells seem to use ornithine mainly out of the urea cycle. CHL-YN cells can utilize arginine through arginase-2 and convert to ornithine. Ornithine can be then converted to several metabolites, including putrescine via ornithine decarboxylase and glutamate 5-semialdehyde via ornithine aminotransferase. Putrescine is a crucial polyamine precursor and a substrate of 4-aminobutyrate (GABA) biosynthesis through amiloride-sensitive amine oxidase and aldehyde dehydrogenase 7A1. Although GABA could be converted from glutamate via glutamate decarboxylase, transcriptomics analysis showed that CHL-YN cells lacked mRNA expression of both glutamate decarboxylase 1 and 2 (**Supporting information 5**).

In addition, glutamate 5-semialdehyde can be further changed to proline and glutamine through pyrroline-5-carboxylase reductase and pyrroline-5-carboxylase dehydrogenase, respectively. Glutamate is then turned into glutamine via glutamine synthetase. Additionally, glutamate 5-semialdehyde, glutamine, and glutamate are reversible interactions (Fig. 24A). On the other hand, the CHO-K1 cell model showed that CHO-K1 cells lack ornithine production ability in both transcriptome and metabolic levels, resulting in an inability to produce putrescine and proline. An increase in glutamine with very low levels may be caused by glutamine synthetase activity, which showed diminutive gene expressions compared to CHL-YN cells (Fig. 24B).

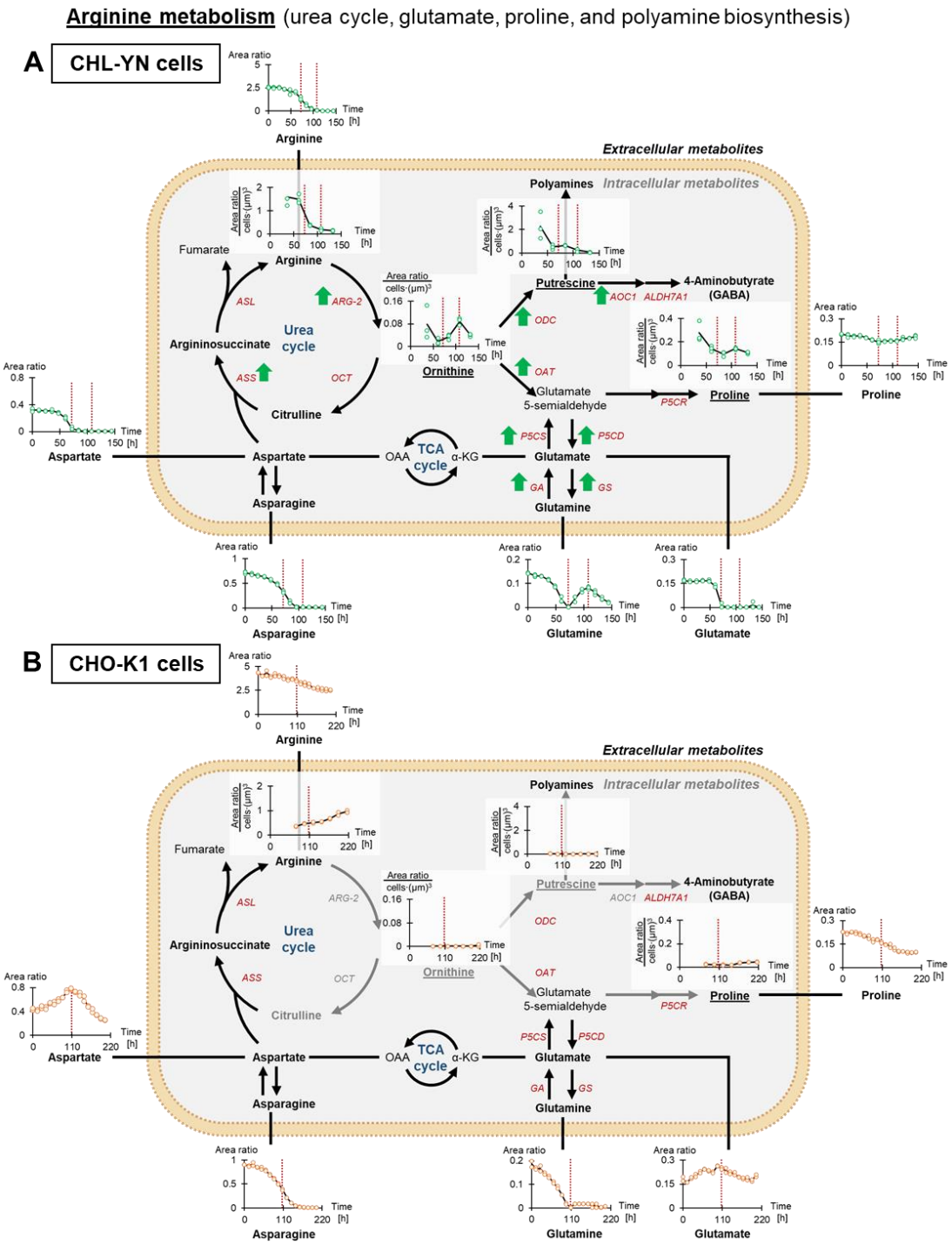

Figure 24. Hypothetical metabolic models present distinctions on arginine metabolism and related pathways. The models generated from transcriptome and metabolome studies on flask-batch cultivation. **A)** CHL-YN cells. **B)** CHO-K1 cells. Intermediate names in bold indicate the

availability of metabolic data; italic red colors indicate measurable mRNA transcripts expressing the enzyme; gray colors indicate undetectable compounds and/or transcripts expressing associated enzymes; black arrows show the available enzymatic function on the metabolic interaction; green arrows show increased gene expressions of that enzyme in CHL-YN cells compared to CHO-K1 cells estimated by over 1.0 of log2 [CHL-YN (Exp) / CHO-K1 (Exp)]. The time-course of explained metabolites was shown. Red-dotted lines indicate the first (Day 3) and second (Day 5.5) of glutamine metabolic switch. More information about transcripts and metabolites is available in supporting information 5–7. This figure has been published and is available in Sukwattananipaat et al., 2024.

Considering methionine metabolism of CHL-YN cells, CHL-YN cells have higher gene expressions of enzymes involved in methionine cycle such as methionine adenosyltransferase 2A and adenosyl homocysteinase to generate homocysteine. Homocysteine can be then converted to cystathionine only in CHL-YN cells which is available of cystathionine β-synthetase (CBS) transcripts. Cystathionine is further turned into cysteine via cystathionine γ-lyase (CTH). In addition, glutathione, an antioxidant produced from cysteine, glycine, and glutamate, is increased in CHL-YN cells in both reduced and oxidized forms (GSH and GSSG) compared to CHO-K1 cells (Fig. 25A). Whilst the integrated results suggest that CHO-K1 cells have very low gene expressions of CBS and lack of CTH transcript. Also, a lower glutathione production is found in CHO-K1 cells compared to CHL-YN cells (Fig. 25B).

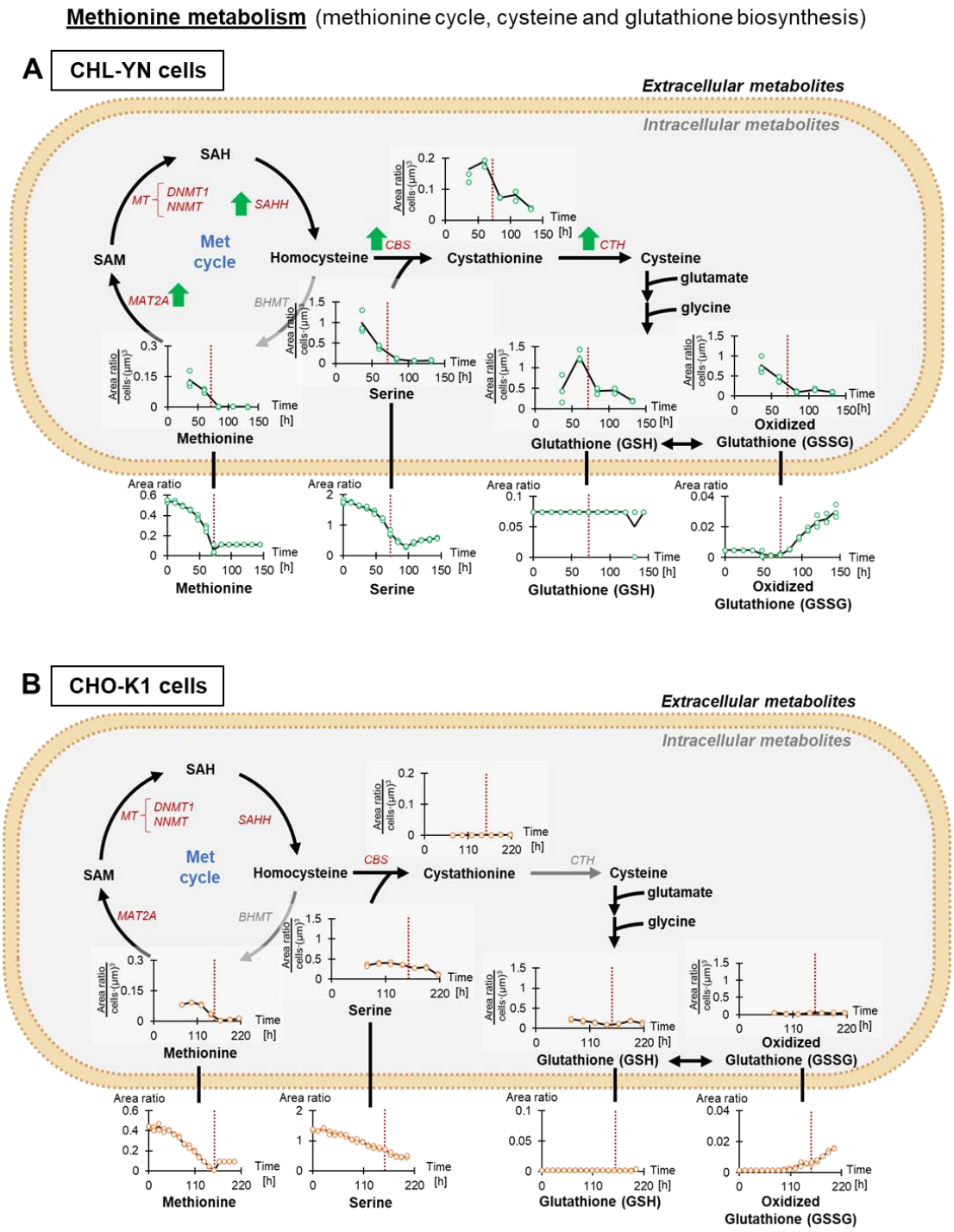

Figure 25. Hypothetical metabolic models present distinctions on methionine metabolism and related pathways. The models generated from transcriptome and metabolome studies on flask-batch cultivation. **A)** CHL-YN cells. **B)** CHO-K1 cells. Intermediate names in bold indicate the

availability of metabolic data; italic red colors indicate measurable mRNA transcripts expressing the enzyme; gray colors indicate undetectable compounds and/or transcripts expressing associated enzymes; black arrows show the available enzymatic function on the metabolic interaction; green arrows show increased gene expressions of that enzyme in CHL-YN cells compared to CHO-K1 cells estimated by over 1.0 of log2 [CHL-YN (Exp) / CHO-K1 (Exp)]. The time-course of explained metabolites was shown. The red dotted line indicates the methionine exhaustion on each culture (Day 3 of CHL-YN cultures and Day 6.5 of CHO-K1 cell cultures). More information about transcripts and metabolites is available in supporting information 5–7. This figure has been published and is available in Sukwattananipaat et al., 2024.

3.4 Discussion

In this chapter, I investigated the metabolic profiles of bioreactor-scale fed-batch operation of IgG-producing CHL-YN cell cultures with stabilized glucose concentration by the scheduled glucose feed strategy. A combination of targeted CE-MS-based intracellular and LC-MS-based extracellular metabolomic approaches was chosen for comprehensively analyzing central energy pathway intermediates, amino acids, and derivatives. As the results, sample clustering analyses suggest that both intracellular and extracellular metabolic profiles between CHL-YN and CHO-K1 cells were shown at similarity during the glutamine consumption stage. When the extracellular glutamine became exhausted and the cell entered the glutamine production stage, metabolic features between CHL-YN and CHO-K1 cells were distinguished. Then, further examination of differentiated metabolites between sample groups was conducted using a volcano plot. After that, searching associated metabolic pathways of those noted metabolites was performed by enrichment analysis. Comparison between CHL-YN in glutamine consumption and production stages showed

that intracellular concentrations of amino acids and aspartate metabolically associated compounds had been significantly changed during this glutamine shift. While extracellular metabolomics results shed light on intermediates involved in amino acid metabolism, urea cycle, phenylalanine and tyrosine metabolism, and branched chain amino acid (BCAA) metabolism. It suggests that CHL-YN cells may alter their metabolic properties to compensate glutamine during exhaustion. This glutamine metabolic change to production might be related to cell proliferation arrest and entering the stationary stage, as well as studies in mammalian-immortalized cells and CHO cells (Fitzpatrick et al., 1993; Fomina-Yadlin et al., 2013; Malakar et al., 2023).

Aspartate utilization in CHL-YN cells might be used by two cellular mechanisms: TCA cycle support and argininosuccinate biosynthesis. The first mechanism has been previously reported in a study on metabolic fluxes of CHO-K1 cells. Flux analysis revealed that aspartate could be converted from asparagine after uptake and subsequently fluxed into the TCA cycles through oxaloacetate. Both aspartate and glutamine were utilized as TCA cycle supporters during the exponential stage of cell growth, although glutamine was superiorly favored beyond aspartate during exponential growth (Kirsch et al., 2021). Therefore, it is possible that extracellular aspartate was strongly decreased when glutamine had already been consumed. Another reason might be the availability of asparagine during the exponential stage. Asparagine could be turned into aspartate after being uptaken by cells. Hence, aspartate was strongly uptaken when asparagine was exhausted in the stationary stage. Secondly, aspartate could be associated with arginine metabolism via the urea cycle. Aspartate and citrulline could be metabolized to argininosuccinate by the activity of the argininosuccinate synthase (ASS) enzyme. Then, argininosuccinate could be converted to fumarate and arginine by the argininosuccinate lyase (ASL) enzyme. In CHL-YN cells, gene expression analysis revealed mRNA transcripts where both enzymes were expressed.

Whereas CHO-K1 cells transcribed very low levels of ASS and comparable levels of ASL genes compared to CHL-YN cells. In this study, when aspartate was presented at a low-level during glutamine production in CHL-YN cell cultures, reductions of argininosuccinate and arginine concentrations were observed.

Further investigation on the urea cycle found that arginine catabolic activity was specially available in CHL-YN cells compared to CHO-K1 cells. Arginase-2 (ARG-2) transcripts, encoding an enzyme to convert arginine to ornithine, were shown at a very high level in CHL-YN, while no expression was available in CHO-K1 cells. From this statement, it could be assumed that CHL-YN cells might have strong activities of urea cycle over CHO-K1 cells. However, CHL-YN cells seemed to have high expressions only in partial urea cycle genes. For instance, the ornithine carbamoyl transferase (OCT) gene, which converts ornithine to citrulline, was found at a very low level. Therefore, this incident might lead to an imbalance of urea cycle intermediates and incomplete activity of the cycle. Ornithine might be converted to metabolites in another pathway, such as proline, glutamate, and putrescine, rather than utilized in the urea cycle. As previously reported, the roles of ARG-2 that could be influent in polyamines, glutamate, and proline production (Deignan et al., 2006; Marselli et al., 2021). Ornithine could be metabolized to putrescine, a precursor of polyamines, through the ornithine decarboxylase (ODC) enzyme. Putrescine and polyamines have been reported as a crucial supplement for CHO cells to support cell proliferation and antibody production since CHO-K1 cells lack the ability to produce ornithine (Roca et al., 2019; Xu et al., 2023; Miyajima et al., 2023). In addition, gamma-aminobutyrate (4-aminobutyrate, GABA), which could be produced from putrescine through amiloride-sensitive amine oxidase (AOC1) and aldehyde dehydrogenase 7A1 (ALDH7A1) enzymes, was presented at higher levels in CHL-YN cells over CHO-K1 cells. Although the benefit of GABA production in

CHL-YN cells is still unclear from this study, it may be evidence to prove the ability of putrescine production in CHL-YN cells. Glutamate and proline were connected to ornithine through glutamate 5-semialdehyde conversion. Strong expression of the ornithine aminotransferase-encoding gene was observed in CHL-YN cells, assuming strong glutamate 5-semialdehyde might be available. Although glutamate 5-semialdehyde could not be detected in this study, subsequent metabolites such as proline and glutamate were increased in CHL-YN cells. The proline biosynthetic ability is exclusively reported in CHL-YN cells since several CHO cells have been mentioned for their dysfunction of proline production (Hefzi et al., 2016; Sun et al., 2020; Budge et al., 2021). Glutamine was highly converted from glutamate in CHL-YN over CHO-K1 cells through glutamine synthetase, leading to distinct extracellular glutamine observation between two cell lines. This information has been previously reported (Yamano-Adachi et al., 2020). As all results showed, typical urea cycle intermediates and derivatives were increased, while some metabolites such as arginine and argininosuccinate were decreased during the stationary stage.

Furthermore, another five amino acids, phenylalanine, tyrosine, leucine, isoleucine, and valine, were significantly decreased during the glutamine production stage. Phenylalanine, tyrosine, and BCAA were consumed as well as in CHO cells for biomass and anaplerosis (Ahn and Antoniewicz, 2011). In mammalian cells, anaplerosis has been described as phenylalanine and tyrosine being fluxed into the TCA cycle through fumarate conversion, while isoleucine and valine could be metabolized to succinyl-CoA. In addition, these five amino acids could also be converted to acetyl-CoA (Owen et al., 2002). Although metabolic flux analysis of Ahn and Antoniewicz (2011) reported that anaplerosis was reduced during the stationary phase of CHO cells, this study found that anaplerosis seemed to increase in both CHL-YN and CHO-K1 cells. The distinction of anaplerosis results might be from different cell lines, medium composition, and cultivation

procedures. Intriguingly, consumption of these amino acids could lead to cell growth inhibitor accumulation such as 4-hydroxyphenyllactate derived from phenylalanine and tyrosine, phenyllactate from phenylalanine, and isobutyrate from valine (Mulukutla et al., 2017; Mulukutla et al., 2019; Harrington et al., 2021; Coulet et al., 2022). These growth inhibitors may impact cell death on CHL-YN cell cultures. Hence, regulation of amino acids aiming to reduce inhibitor production may be a further perspective to improve cell performance of CHL-YN cell culture.

In comparison between CHL-YN and CHO-K1 cells, statistical analyses found that glycolysis intermediates were decreased in CHL-YN cells compared to CHO-K1 cells. This study suggests that lower glycolytic compounds might be from lower glucose consumption during the glutamine production stage of CHL-YN cells, together with a higher lactate consumption rate when compared to CHO-K1 cells. In addition, the methionine metabolism of both cell lines showed action at different levels. For instance, results from volcano plots shed light on cystathionine. Cystathionine was available only in CHL-YN cells, while not present in CHO-K1 cells. As further investigations on methionine metabolism suggest, results suggest that higher methionine cycle and transsulfuration pathways were found in CHL-YN cells over CHO-K1 cells. In the methionine cycle, methionine could convert to S-adenosylmethionine (SAM) through methionine adenosyltransferase 2A (MAT2A). High gene expressions on the MAT2A in CHL-YN cells over CHO-K1 cells were observed. Then, SAM could metabolize to S-adenosylhomocysteine (SAH) by methyltransferase enzymes such as DNA (cytosine-5-)-methyltransferase 1 (DNMT1) and Nicotinamide N-methyltransferase (NNMT). SAH was then turned into homocysteine by adenosyl homocysteinase (SAHH). Homocysteine was shifted to the transsulfuration pathway through combining with serine to produce cystathionine via cystathionine β-synthase (CBS). Eventually, Cystathionine was converted into cysteine via Cystathionine γ-lyase (CTH). In this

study, CHL-YN cells showed high gene expressions of CBS, while very low expression was found in CHO-K1. Furthermore, CTH transcript was highly observed in CHL-YN cells, whereas no transcript was available in CHO-K1 cells. The dysfunction of CBS and CTH, leading to cysteine auxotrophic characteristic in previous studies on CHO cells (Hefzi et al., 2016; Chen and Betenbaugh, 2023; Greenfield et al., 2024). Cysteine could be further metabolized by combining glutamate and glycine to produce glutathione. Glutathione was shown at a higher level in CHL-YN cells, suggesting a higher cysteine production ability in CHL-YN over CHO-K1 cells. These results also suggest the advantage of cysteine production capability over glutathione production. Despite the increase in glutathione, it could not lead to sustainable cell viability in CHL-YN cells during the late stage. Glutathione in CHL-YN cells could protect against oxidative stress, as noticed by the increasing of oxidized glutathione (GSSG). However, it is complicated to define the cause of cell death of CHL-YN cells due to data limitations.

Additionally, pyrimidine metabolism was shown at a decreased level in CHL-YN cell cultures over CHO-K1 cells. This phenomenon might be caused by exhaustion of amino acid sources for pyrimidine production such as aspartate and glutamine (Li et al., 2021; Kirsch et al., 2021). Although glutamine was produced, the fluxes might not go to the pyrimidine metabolism. Instead, CHL-YN cells seemed to uptake pyrimidine sources from extracellular, resulting in a strong decrease in deoxycytidine, cytidine, and uridine in volcano plots.

As this study used targeted metabolomics approaches, these could only be specified on about a hundred central energy metabolites and amino acids. Also, limitations on replication of CE-MS data acquisition had occurred. Therefore, limitations on these data make it difficult to gain comprehensive information and well-explain the cause of metabolic shift beyond the amino acid aspect. Also, it is difficult to define the cause of the decrease in cell viability. Furthermore, since

this study only analyzes based on concentrations of metabolites, it cannot understand the metabolic fluxes and conclude the metabolic state. Hence, construction of kinetic equations for CHL-YN cells is further required for processing metabolic flux analysis aiming at in-depth investigating metabolic profiles of CHL-YN cells. Also, protein levels and enzyme activities should be analyzed in the future to ensure hypothetical metabolic models.

3.5 Conclusion

In conclusion, findings from combination CE-MS and LC-MS/MS targeted metabolomic approaches suggest that metabolic profiles of IgG-producing CHL-YN and CHO-K1 cells were distinct during the late stage when the cells produced glutamine. While the metabolic backgrounds were comparable during the early stage when cells consumed glutamine. Several amino acid metabolisms were exclusively found in CHL-YN cells, particularly in arginine and methionine-associated metabolisms. Arginine utilization was observed during glutamine production of CHL-YN cells, possibly through ARG-2 enzyme activity. Resulting in ornithine production and increasing in ornithine derivatives such as putrescine, GABA, glutamate, glutamine, and proline. Additionally, cysteine biosynthesis seemed to be available in CHL-YN cells through cystathionine biosynthesis ability. The transcriptomics study in previous studies suggests the CHL-YN cells are capable of mRNA transcribing genes involved in cystathionine-associated enzymes (CBS and CTH). Moreover, several amino acids were highly reduced during glutamine production, suggesting that amino acid compensation for glutamine production may have occurred through anaplerosis. Also, cell growth inhibitor accumulations may occur and impact cell viability, as well as stress from nutrient limitations. Future studies on metabolic flux analysis and broader metabolomics investigations are recommended.

Chapter 4:

Conclusion and future perspectives

Chapter 4: Conclusion and future perspectives

Due to limited information on distinctive metabolic backgrounds between IgG-producing CHL-YN and CHO-K1 cell cultures, this study proposed a metabolomics analysis focusing on glucose and glutamine metabolisms. To investigate metabolomes, the development of a cultivation prototype was first needed. Hence, the development of IgG-producing CHL-YN cell cultures in serum-free fed-batch operation with stabilized glucose conditions, which represents a prototype of industrial-scale IgG production, was also proposed herewith in this dissertation.

Aiming at achieving a regulated glucose condition, a continuous glucose feeding strategy was evaluated for IgG-producing CHL-YN cell cultures. From preliminary fed-batch of IgG-producing CHL-YN cell cultures, extracellular metabolic observation led to hypothesize on the relationship between glucose and glutamine metabolism because immediate stagnation of consumed glucose has been found after approximately 12 h glutamine exhaustion. Moreover, schedule glucose feeding was constructed from the consumed glucose data. Three distinct glucose feeding rates were evaluated following glutamine metabolism. From the scheduled feeding and using the glucose adjustment equation to neutralize biological variability among batches, the glucose concentration of IgG-producing CHL-YN cell cultures could be successfully regulated within the desired range of 3.00±1.00 g/L. This glucose feed strategy could be assured in a high IgG-producing clone, CHL-YN B-08. On the other hand, in a case of IgG-producing CHO-K1 cell culture, evaluation of scheduled glucose feeding was shown at a constant rate on Day 2 onward. From cell profiling results, scheduled glucose feeding on IgG-producing CHL-YN cells could slightly extend the cell culture with above 70.0% cell viability up to 13–14 days compared to the

preliminary glucose feeding practice. This extension led to an increase in the final IgG concentration. The improved cell viability by avoiding overwhelming glucose levels is possibly related to reducing osmotic stress rather than reducing lactate concentration. Another point noticed from the development glucose stabilized condition of serum-free fed-batch culture is the metabolic shift of IgG-producing CHL-YN cells during glutamine exhaustion. This glutamine metabolic change may relate to a reduction in glucose consumption and decreases in viability and IgG productivity of IgG-producing CHL-YN cells.

Therefore, further investigation on metabolic profiles targeted at glucose and glutamine-associated pathways was then conducted. Combination of intracellular CE-MS and extracellular LC-MS/MS metabolomics analyses revealed that both intracellular and extracellular metabolic profiles of IgG-producing CHL-YN and CHO-K1 cells were similar during the glutamine consumption stage in the early cell growth. However, the metabolic profiles of IgG-producing CHL-YN and CHO-K1 were set apart during the glutamine production stage. Comparison between a high IgG-producing CHL-YN B-08 clone and heterogenous cell pool, this study could not obviously present. Besides that, comparison between IgG-producing CHL-YN cells between glutamine consumption and production stages revealed that metabolites involved in several amino acid metabolisms, including the urea cycle, aspartate, phenylalanine, tyrosine, and branched-chain amino acid metabolisms, were significantly changed during glutamine production of CHL-YN cells. Typical amino acids and derivatives were decreased, while some of the urea cycle and derivatives were increased. Furthermore, in comparison between IgG-producing CHL-YN and CHO-K1 cells, the results showed that a significant decrease in intracellular glycolytic intermediates was found. This incident may be caused by higher lactate utilization and lower glucose consumption during glutamine production stage in CHL-YN cells. Moreover, CHL-YN

cells have strong methionine and pyrimidine utilization over CHO-K1 cells. As these results suggest the significance of amino acids, considering these amino acid concentrations was then focused. The results showed that nine amino acids (arginine, aspartate, isoleucine, leucine, methionine, phenylalanine, serine, tyrosine, and valine) significantly decreased in CHL-YN cells and/or cultures during glutamine production.

Intriguingly, four amino acids, including arginine, aspartate, methionine, and serine, were tremendously dropped after glutamine shift exclusively occurred in IgG-producing CHL-YN cells. Also, ornithine and cystathionine were significantly higher in CHL-YN cells over CHO-K1 cells. In previous studies on several CHO cell lines reported lacking associated enzymes: ARG-2 for ornithine production and CBS for cystathionine production, leading to proline and cysteine auxotrophic characteristics (Hefzi et al., 2016; Sun et al., 2020; Budge et al., 2021; Chen and Betenbaugh, 2023; Greenfield et al., 2024). This study also proposed the hypothetical metabolic models of arginine and methionine metabolism between CHL-YN and CHO-K1 cells via using further information from flask-batch cultivations. The ability on ornithine production from arginine leads to an increase in derivatives: putrescine, GABA, glutamate, glutamine, and proline in CHL-YN cells. This ability may be a cause of overwhelming glutamine production compared to CHO-K1 cells. Also, putrescine could be a beneficial component supporting cell proliferation and IgG production in CHL-YN cells (Roca et al., 2019; Xu et al., 2023; Miyajima et al., 2023). On the other hand, cysteine production was not directly reported in this study. Instead, glutathione, an antioxidant metabolite derived from cysteine, glutamate, and glycine, was shown to have a significant increase in CHL-YN cells. Although an increase in glutathione was found in CHL-YN cells, it could not sustain cell viability during the glutamine production stage. Higher oxidized glutathione in CHL-YN cells suggests that glutathione could be used in cells to encounter reactive

oxygen species. However, oxidative stress may not be a major cause of cell death in CHL-YN cells. Another possibility of cell death may relate to strong utilization of phenylalanine, tyrosine and branched chain amino acids, which have reported in studies on CHO cell culture about the growth inhibitor production from these amino acids (Mulukutla et al., 2017; Mulukutla et al., 2019; Harrington et al., 2021; Coulet et al., 2022). Nevertheless, due to a complexity to define the exact cause of cell death, further analyses on types of cell death are recommended to disclose the major cause of cell death. Additionally, construction of kinetic equations for CHL-YN cells and metabolic flux analysis are required for completely concluding the metabolic reactions.

Regarding the future perspectives, several aspects from this study need to be considered. Firstly, this study only targeted central energy metabolism and amino acids during this first glutamine shift. To further comprehend metabolomics investigation, an untargeted metabolomics approach is suggested to acquire metabolic information with broader aspects. Also, a study on the second glutamine shift from production to re-consumption should be studied, aiming to clarify the metabolic background of CHL-YN cells. This knowledge of metabolic background could lead to better design of the cultivation conditions and platform suitable for CHL-YN cells and increase productivity. Secondly, early cell death occurred in CHL-YN cells during glutamine production, leading to a viability drop that needs to be further analyzed on the types and causes of cell death. Thirdly, CHL-YN cells still produced trastuzumab IgG at a low level compared to current practices by CHO cells (Boulenouar et al., 2023). Hence, enhancement of expression capability in CHL-YN cells is preferred. For instance, CHL-YN cell line developments such as genetic modifications and selection of IgG expression vectors, promotors, and selection markers are required. Also, cell culture conditions, medium components, feed strategies, and procedures are considered. From this study, the highest productivity of CHL-YN cells during the glutamine consumption stage was

observed. Hence, the development of a perfusion approach is preferred for CHL-YN cells aiming at gaining higher IgG production.

References

Ahn, W. S., & Antoniewicz, M. R. (2011). Metabolic flux analysis of CHO cells at growth and non-growth phases using isotopic tracers and mass spectrometry. *Metabolic Engineering*, *13*(5), 598–609. https://doi.org/10.1016/j.ymben.2011.07.002

Alhuthali, S., Kotidis, P., & Kontoravdi, C. (2021). Osmolality effects on CHO cell growth, cell volume, antibody productivity and glycosylation. *International Journal of Molecular Sciences*, *22*(7). https://doi.org/10.3390/ijms22073290

Baker, M. (2016). Reproducibility: Respect Your Cells! *Nature*, *537*, 433–435. https://doi.org/10.1038/537433a

Bauermeister, A., Mannochio-Russo, H., Costa-Lotufo, L. V., Jarmusch, A. K., & Dorrestein, P. C. (2022). Mass spectrometry-based metabolomics in microbiome investigations. In *Nature Reviews Microbiology* (Vol. 20, Issue 3). https://doi.org/10.1038/s41579-021-00621-9

Berting, A., Farcet, M. R., & Kreil, T. R. (2010). Virus susceptibility of Chinese hamster ovary (CHO) cells and detection of viral contaminations by adventitious agent testing. *Biotechnology and Bioengineering*, *106*(4), 598–607. https://doi.org/10.1002/bit.22723

Boulenouar, H., Bouchoutrouch, N., Amar, Y., Faouzi, M. E. A., Cherrah, Y., Sefrioui, H., & Benhassou, H. A. (2023). Strategy for Developing a Stable CHO Cell Line that Produces Large Titers of Trastuzumab Antibody. *Frontiers in Bioscience (Elite Edition)*, *15*(4), 24. https://doi.org/10.31083/j.fbe1504024

Boune, S., Hu, P., Epstein, A. L., & Khawli, L. A. (2020). Principles of N-linked glycosylation variations of IgG-based therapeutics: Pharmacokinetic and functional considerations. *Antibodies*, *9*(2), 1–20. https://doi.org/10.3390/antib9020022

Bowler, A. L., Bakalis, S., & Watson, N. J. (2020). A review of in-line and on-line measurement techniques to monitor industrial mixing processes. *Chemical Engineering Research and Design*, *153*, 463–495. https://doi.org/10.1016/j.cherd.2019.10.045

Bryan, L., Clynes, M., & Meleady, P. (2021). The emerging role of cellular post-translational modifications in modulating growth and productivity of recombinant Chinese hamster ovary cells. *Biotechnology Advances*, *49*(December 2020), 107757. https://doi.org/10.1016/j.biotechadv.2021.107757

Budge, J. D., Roobol, J., Singh, G., Mozzanino, T., Knight, T. J., Povey, J., Dean, A., Turner, S. J., Jaques, C. M., Young, R. J., Racher, A. J., & Smales, C. M. (2021). A proline metabolism selection system and its application to the engineering of lipid biosynthesis in Chinese hamster ovary cells. *Metabolic Engineering Communications*, *13*(April). https://doi.org/10.1016/j.mec.2021.e00179

Castelli, F. A., Rosati, G., Moguet, C., Fuentes, C., Marrugo-Ramírez, J., Lefebvre, T., Volland, H., Merkoçi, A., Simon, S., Fenaille, F., & Junot, C. (2022). Metabolomics for personalized medicine: the input of analytical chemistry from biomarker discovery to point-of-care tests. In *Analytical and Bioanalytical Chemistry* (Vol. 414, Issue 2). Analytical and Bioanalytical Chemistry. https://doi.org/10.1007/s00216-021-03586-z

Castelli, M. S., McGonigle, P., & Hornby, P. J. (2019). The pharmacology and therapeutic applications of monoclonal antibodies. *Pharmacology Research & Perspectives, 7*(6), e00535. https://doi.org/10.1002/prp2.535

Chakrabarti, L., Chaerkady, R., Wang, J., Weng, S. H. S., Wang, C., Qian, C., Cazares, L., Hess, S., Amaya, P., Zhu, J., & Hatton, D. (2022). Mitochondrial membrane potential-enriched CHO host: a novel and powerful tool for improving biomanufacturing capability. *MAbs*, *14*(1), 1–16. https://doi.org/10.1080/19420862.2021.2020081

Chen, Y., & Betenbaugh, M. J. (2023). Reconstruction of reverse transsulfuration pathway enables cysteine biosynthesis and enhances resilience to oxidative stress in Chinese Hamster Ovary cells. *Metabolic Engineering*, *76*(December 2022), 204–214. https://doi.org/10.1016/j.ymben.2023.02.010

Clish, C. B. (2015). Metabolomics: an emerging but powerful tool for precision medicine. *Molecular Case Studies*, *1*(1), a000588. https://doi.org/10.1101/mcs.a000588

Coulet, M., Kepp, O., Kroemer, G., & Basmaciogullari, S. (2022). Metabolic Profiling of CHO Cells during the Production of Biotherapeutics. *Cells*, *11*(12), 1–21. https://doi.org/10.3390/cells11121929

Deignan, J. L., Livesay, J. C., Yoo, P. K., Goodman, S. I., O'Brien, W. E., Iyer, R. K., Cederbaum, S. D., & Grody, W. W. (2006). Ornithine deficiency in the arginase double knockout mouse. *Molecular Genetics and Metabolism*, *89*(1–2), 87–96. https://doi.org/10.1016/j.ymgme.2006.04.007

Dettmer, K., Aronov, P. A., & Hammock, B. D. (2007). Mass spectrometry-based metabolomics. *Mass Spectrometry Reviews*, *26*(1), 51-78. https://doi.org/10.1002/mas.20108

Finkle, B. (1988). New medicines from industry. *Journal of Chemical Technology & Biotechnology*, *43*(4), 313–327. https://doi.org/10.1002/jctb.280430411

Fitzpatrick, L., Jenkins, H. A., & Butler, M. (1993). Glucose and glutamine metabolism of a murine B-lymphocyte hybridoma grown in batch culture. *Applied Biochemistry and Biotechnology*, *43*(2), 93–116. https://doi.org/10.1007/BF02916435

Fomina-Yadlin, D., Gosink, J. J., McCoy, R., Follstad, B., Morris, A., Russell, C. B., & McGrew, J. T. (2014). Cellular responses to individual amino-acid depletion in antibody-expressing and parental CHO cell lines. *Biotechnology and Bioengineering*, *111*(5), 965–979. https://doi.org/10.1002/bit.25155

Geng, S. L., Zhao, X. J., Zhang, X., Zhang, J. H., Mi, C. L., & Wang, T. Y. (2024). Recombinant therapeutic proteins degradation and overcoming strategies in CHO cells. *Applied Microbiology and Biotechnology*, *108*(1). https://doi.org/10.1007/s00253-024-13008-6

Gerzon, G., Sheng, Y., & Kirkitadze, M. (2022). Process Analytical Technologies – Advances in bioprocess integration and future perspectives. *Journal of Pharmaceutical and Biomedical Analysis*, *207*, 114379. https://doi.org/10.1016/j.jpba.2021.114379

Gowtham, Y. K., Saski, C. A., & Harcum, S. W. (2017). Low glucose concentrations within typical industrial operating conditions have minimal effect on the transcriptome of

recombinant CHO cells. *Biotechnology Progress*, *33*(3), 771–785. https://doi.org/10.1002/btpr.2462

Greenfield, L., Brantley, M., Geoffroy, P., Mitchell, J., DeWitt, D., Zhang, F., & Mulukutla, B. C. (2024). Metabolic Engineering of CHO Cells Towards Cysteine Prototrophy and Systems Analysis of The Ensuing Phenotype. *Metabolic Engineering*, *84*(June), 128–144. https://doi.org/10.1016/j.ymben.2024.06.003

Harrington, C., Jacobs, M., Bethune, Q., Kalomeris, T., Hiller, G. W., & Mulukutla, B. C. (2021). Production of butyrate and branched-chain amino acid catabolic byproducts by CHO cells in fed-batch culture enhances their specific productivity. *Biotechnology and Bioengineering*, *118*(12), 4786–4799. https://doi.org/10.1002/bit.27942

Hefzi, H., Ang, K. S., Hanscho, M., Bordbar, A., Ruckerbauer, D., Lakshmanan, M., Orellana, C. A., Baycin-Hizal, D., Huang, Y., Ley, D., Martinez, V. S., Kyriakopoulos, S., Jiménez, N. E., Zielinski, D. C., Quek, L. E., Wulff, T., Arnsdorf, J., Li, S., Lee, J. S., … Lewis, N. E. (2016). A Consensus Genome-scale Reconstruction of Chinese Hamster Ovary Cell Metabolism. *Cell Systems*, *3*(5), 434-443.e8. https://doi.org/10.1016/j.cels.2016.10.020

Horie, M., Yamano-Adachi, N., Kawabe, Y., Kaneoka, H., Fujita, H., Nagamori, E., Iwai, R., Sato, Y., Kanie, K., & Ohta, S. (2022). Recent advances in animal cell technologies for industrial and medical applications. *Journal of Bioscience and Bioengineering*, *xxx*(xxx). https://doi.org/10.1016/j.jbiosc.2022.03.005

Horvat, J., Narat, M., & Spadiut, O. (2020). The effect of amino acid supplementation in an industrial Chinese Hamster Ovary process. *Biotechnology Progress*, 36(5). https://doi.org/10.1002/btpr.3001

Huang, Y. M., Hu, W., Rustandi, E., Chang, K., Yusuf-Makagiansar, H., & Ryll, T. (2010). Maximizing productivity of CHO cell-based fed-batch culture using chemically defined media conditions and typical manufacturing equipment. *Biotechnology Progress*, *26*(5), 1400–1410. https://doi.org/10.1002/btpr.436

Idle, J. R., & Gonzalez, F. J. (2007). Metabolomics. *Cell Metabolism*, November 6(5), 348-351. https://doi.org/10.1016/j.cmet.2007.10.005

Jia, Z., Qiu, Q., He, R., Zhou, T., & Chen, L. (2023). Identification of Metabolite Interference Is Necessary for Accurate LC-MS Targeted Metabolomics Analysis. *Analytical Chemistry*, *95*(20), 7985–7992. https://doi.org/10.1021/acs.analchem.3c00804

Jiang, H., Horwitz, A. A., Wright, C., Tai, A., Znameroski, E. A., Tsegaye, Y., Warbington, H., Bower, B. S., Alves, C., Co, C., Jonnalagadda, K., Platt, D., Walter, J. M., Natarajan, V., Ubersax, J. A., Cherry, J. R., & Love, J. C. (2019). Challenging the workhorse: Comparative analysis of eukaryotic micro-organisms for expressing monoclonal antibodies. *Biotechnology and Bioengineering*, *116*(6), 1449–1462. https://doi.org/10.1002/bit.26951

Jin, J., Byun, J. K., Choi, Y. K., & Park, K. G. (2023). Targeting glutamine metabolism as a therapeutic strategy for cancer. *Experimental and Molecular Medicine*, *55*(4), 706–715. https://doi.org/10.1038/s12276-023-00971-9

Kałuzna-Czaplińska, J. (2011). Current medical research with the application of coupled techniques with mass spectrometry. *Medical Science Monitor*, *17*(5), 117–123. https://doi.org/10.12659/msm.881756

Kirsch, B. J., Bennun, S. V., Mendez, A., Johnson, A. S., Wang, H., Qiu, H., Li, N., Lawrence, S. M., Bak, H., & Betenbaugh, M. J. (2022). Metabolic analysis of the asparagine and glutamine dynamics in an industrial Chinese hamster ovary fed-batch process. *Biotechnology and Bioengineering*, *119*(3), 807–819. https://doi.org/10.1002/bit.27993

Kudo, R., Igarashi, K., Soga, T., Ishikawa, T., & Saito, Y. (2022). Comprehensive metabolome analysis of intracellular metabolites in cultured cells. In *STAR Protocols* (Vol. 3, Issue 3). The Author(s). https://doi.org/10.1016/j.xpro.2022.101531

Lai, Z., Choudhury, F. K., Tang, D., Liang, X., Dean, B., Misaghi, S., & Sangaraju, D. (2022). LC-HRMS-based targeted metabolomics for high-throughput and quantitative analysis of 21 growth inhibition-related metabolites in Chinese hamster ovary cell fed-batch cultures. *Biomedical Chromatography*, *36*(5), 1–16. https://doi.org/10.1002/bmc.5348

Lee, T. Y., Lin, H. H., Chen, C. L., Hwang, S. M., & Tseng, C. P. (2015). Inhibitory Effect of Excessive Glucose on Its Biochemical Pathway and the Growth of Chinese Hamster Ovary (CHO) Cells. *Journal of Carbohydrate Chemistry*, *34*(1), 1–11. https://doi.org/10.1080/07328303.2014.977908

Lewis, N. E., Liu, X., Li, Y., Nagarajan, H., Yerganian, G., O'Brien, E., Bordbar, A., Roth, A. M., Rosenbloom, J., Bian, C., Xie, M., Chen, W., Li, N., Baycin-Hizal, D., Latif, H., Forster, J., Betenbaugh, M. J., Famili, I., Xu, X., … Palsson, B. O. (2013). Genomic

landscapes of Chinese hamster ovary cell lines as revealed by the Cricetulus griseus draft genome. *Nature Biotechnology*, *31*(8), 759–765. https://doi.org/10.1038/nbt.2624

Li, G., Li, D., Wang, T., & He, S. (2021). Pyrimidine biosynthetic enzyme CAD: Its function, regulation, and diagnostic potential. *International Journal of Molecular Sciences*, *22*(19). https://doi.org/10.3390/ijms221910253

Li, M., Ebel, B., Chauchard, F., Guédon, E., & Marc, A. (2018). Parallel comparison of in situ Raman and NIR spectroscopies to simultaneously measure multiple variables toward real-time monitoring of CHO cell bioreactor cultures. *Biochemical Engineering Journal*, *137*, 205–213. https://doi.org/10.1016/j.bej.2018.06.005

Li, P., Su, M., Chatterjee, M., & Lämmerhofer, M. (2022). Targeted analysis of sugar phosphates from glycolysis pathway by phosphate methylation with liquid chromatography coupled to tandem mass spectrometry. *Analytica Chimica Acta*, *1221*(March). https://doi.org/10.1016/j.aca.2022.340099

Li, W., Fan, Z., Lin, Y., & Wang, T. Y. (2021). Serum-Free Medium for Recombinant Protein Expression in Chinese Hamster Ovary Cells. *Frontiers in Bioengineering and Biotechnology*, *9*(March). https://doi.org/10.3389/fbioe.2021.646363

Lieu, E. L., Nguyen, T., Rhyne, S., & Kim, J. (2020). Amino acids in cancer. *Experimental and Molecular Medicine*, *52*(1), 15–30. https://doi.org/10.1038/s12276-020-0375-3

Liu, B., Spearman, M., Doering, J., Lattová, E., Perreault, H., & Butler, M. (2014). The availability of glucose to CHO cells affects the intracellular lipid-linked oligosaccharide distribution, site

occupancy and the N-glycosylation profile of a monoclonal antibody. *Journal of Biotechnology*, *170*(1), 17–27. https://doi.org/10.1016/j.jbiotec.2013.11.007

Lu, S., Sun, X., & Zhang, Y. (2005). Insight into metabolism of CHO cells at low glucose concentration on the basis of the determination of intracellular metabolites. *Process Biochemistry*, *40*(5), 1917–1921. https://doi.org/10.1016/j.procbio.2004.07.004

Malakar, P., Singha, D., Choudhury, D., & Shukla, S. (2023). Glutamine regulates the cellular proliferation and cell cycle progression by modulating the mTOR mediated protein levels of β-TrCP. *Cell Cycle*, *22*(17), 1937–1950. https://doi.org/10.1080/15384101.2023.2260166

Marselli, L., Bosi, E., De Luca, C., Del Guerra, S., Tesi, M., Suleiman, M., & Marchetti, P. (2021). Arginase 2 and polyamines in human pancreatic beta cells: Possible role in the pathogenesis of type 2 diabetes. *International Journal of Molecular Sciences*, *22*(22). https://doi.org/10.3390/ijms222212099

Maruthamuthu, M. K., Rudge, S. R., Ardekani, A. M., Ladisch, M. R., & Verma, M. S. (2020). Process Analytical Technologies and Data Analytics for the Manufacture of Monoclonal Antibodies. *Trends in Biotechnology*, *38*(10), 1169–1186. https://doi.org/10.1016/j.tibtech.2020.07.004

Masuda, K., Kubota, M., Nakazawa, Y., Iwama, C., Watanabe, K., Ishikawa, N., Tanabe, Y., Kono, S., Tanemura, H., Takahashi, S., Makino, T., Okumura, T., Horiuchi, T., Nonaka, K., Murakami, S., Kamihira, M., & Omasa, T. (2024). Establishment of a novel cell line, CHO-MK, derived from Chinese hamster ovary tissues for biologics manufacturing. *Journal of*

Bioscience and Bioengineering, *137*(6), 471–479. https://doi.org/10.1016/j.jbiosc.2024.02.005

Mellahi, K., Brochu, D., Gilbert, M., Perrier, M., Ansorge, S., Durocher, Y., & Henry, O. (2019). Assessment of fed-batch cultivation strategies for an inducible CHO cell line. *Journal of Biotechnology*, *298*(April), 45–56. https://doi.org/10.1016/j.jbiotec.2019.04.005

Miyajima, R., Manaka, H., Honda, T., Hashii, N., Suzuki, M., Komeno, M., Takao, K., Ishii-Watabe, A., Igarashi, K., Toida, T., & Higashi, K. (2023). Intracellular polyamine depletion induces N-linked galactosylation of the monoclonal antibody produced by CHO DP-12 cells. *Journal of Biotechnology*, *378*(July), 1–10. https://doi.org/10.1016/j.jbiotec.2023.10.008

Mulukutla, B. C., Kale, J., Kalomeris, T., Jacobs, M., & Hiller, G. W. (2017). Identification and control of novel growth inhibitors in fed-batch cultures of Chinese hamster ovary cells. *Biotechnology and Bioengineering*, *114*(8), 1779–1790. https://doi.org/10.1002/bit.26313

Mulukutla, B. C., Mitchell, J., Geoffroy, P., Harrington, C., Krishnan, M., Kalomeris, T., Morris, C., Zhang, L., Pegman, P., & Hiller, G. W. (2019). Metabolic engineering of Chinese hamster ovary cells towards reduced biosynthesis and accumulation of novel growth inhibitors in fed-batch cultures. *Metabolic Engineering*, *54*(October 2018), 54–68. https://doi.org/10.1016/j.ymben.2019.03.001

Omasa, T., Higashiyama, K., Shioya, S., & Suga, K. (1992). Effects of lactate concentration on hybridoma culture in lactate-controlled fed-batch operation. *Biotechnology and Bioengineering*, *39*(5), 556–564. https://doi.org/10.1002/bit.260390511

Omasa, T., Onitsuka, M., & Kim, W. D. (2010). Cell Engineering and Cultivation of Chinese Hamster Ovary (CHO) Cells. *Current Pharmaceutical Biotechnology*, *11*(3), 233–240. https://doi.org/10.2174/138920110791111960

Onitsuka, M., Kim, W. D., Ozaki, H., Kawaguchi, A., Honda, K., Kajiura, H., Fujiyama, K., Asano, R., Kumagai, I., Ohtake, H., & Omasa, T. (2012). Enhancement of sialylation on humanized IgG-like bispecific antibody by overexpression of α2,6-sialyltransferase derived from Chinese hamster ovary cells. *Applied Microbiology and Biotechnology*, *94*(1), 69–80. https://doi.org/10.1007/s00253-011-3814-1

Owen, O. E., Kalhan, S. C., & Hanson, R. W. (2002). The key role of anaplerosis and cataplerosis for citric acid cycle function. *Journal of Biological Chemistry*, *277*(34), 30409–30412. https://doi.org/10.1074/jbc.R200006200

Park, J. U., Han, H. J., & Baik, J. Y. (2022). Energy metabolism in Chinese hamster ovary (CHO) cells: Productivity and beyond. *Korean Journal of Chemical Engineering*, *39*(5), 1097–1106. https://doi.org/10.1007/s11814-022-1062-y

Pereira, S., Kildegaard, H. F., & Andersen, M. R. (2018). Impact of CHO Metabolism on Cell Growth and Protein Production: An Overview of Toxic and Inhibiting Metabolites and Nutrients. *Biotechnology Journal*, *13*(3). https://doi.org/10.1002/biot.201700499

Poulain, A., Mullick, A., Massie, B., & Durocher, Y. (2019). Reducing recombinant protein expression during CHO pool selection enhances frequency of high-producing cells. *Journal of Biotechnology*, *296*(March), 32–41. https://doi.org/10.1016/j.jbiotec.2019.03.009

PUCK, T. T., Cieciura, S. J., & Robinson, A. (1958). Puck, J Exp Med. 1958 Dec 1;108(6):945-56. *Journal of Experimental Medicine*, *108*(77), 945–956.

Rajendra, Y., Peery, R. B., & Barnard, G. C. (2016). Generation of stable Chinese hamster ovary pools yielding antibody titers of up to 7.6 g/L using the piggyBac transposon system. *Biotechnology Progress*, *32*(5), 1301–1307. https://doi.org/10.1002/btpr.2307

Ramautar, R., Somsen, G. W., & de Jong, G. J. (2019). CE-MS for metabolomics: Developments and applications in the period 2016–2018. *Electrophoresis*, *40*(1), 165–179. https://doi.org/10.1002/elps.201800323

Reinhart, D., Damjanovic, L., Kaisermayer, C., Sommeregger, W., Gili, A., Gasselhuber, B., Castan, A., Mayrhofer, P., Grünwald-Gruber, C., & Kunert, R. (2019). Bioprocessing of Recombinant CHO-K1, CHO-DG44, and CHO-S: CHO Expression Hosts Favor Either mAb Production or Biomass Synthesis. *Biotechnology Journal*, *14*(3), 1–11. https://doi.org/10.1002/biot.201700686

Ritacco, F. V., Wu, Y., & Khetan, A. (2018). Cell culture media for recombinant protein expression in Chinese hamster ovary (CHO) cells: History, key components, and optimization strategies. *Biotechnology Progress*, *34*(6), 1407–1426. https://doi.org/10.1002/btpr.2706

Roca, B. C., Lao, N., Barron, N., Doolan, P., & Clynes, M. (2019). An arginase-based system for selection of transfected CHO cells without the use of toxic chemicals. *Journal of Biological Chemistry*, *294*(49), 18756–18768. https://doi.org/10.1074/jbc.RA119.011162

Romanova, N., Schelletter, L., Hoffrogge, R., & Noll, T. (2022). Hyperosmolality in CHO cell culture: effects on the proteome. *Applied Microbiology and Biotechnology*, *106*(7), 2569–2586. https://doi.org/10.1007/s00253-022-11861-x

Sakaki, A., Namatame, T., Nakaya, M., & Omasa, T. (2023). Model-based control system design to manage process parameters in mammalian cell culture for biopharmaceutical manufacturing. *Biotechnology and Bioengineering*, *October*. https://doi.org/10.1002/bit.28593

Salcedo, N., Reddy, A., Gomez, A. R., Bosch, I., & Herrera, B. B. (2022). Monoclonal antibody pairs against SARS-CoV- 2 for rapid antigen test development. *PLoS Neglected Tropical Diseases*, *16*(3), 1–19. https://doi.org/10.1371/journal.pntd.0010311

Samy, A., Kaneyoshi, K., & Omasa, T. (2020). Improvement of Intracellular Traffic System by Overexpression of KDEL Receptor 1 in Antibody-Producing CHO Cells. *Biotechnology Journal*, *15*(6). https://doi.org/10.1002/biot.201900352

Sandomenico, A., Sivaccumar, J. P., & Ruvo, M. (2020). Evolution of *Escherichia coli* expression system in producing antibody recombinant fragments. *International Journal of Molecular Sciences*, *21*(17), 1–39. https://doi.org/10.3390/ijms21176324

Selamat, J., Rozani, N. A. A., & Murugesu, S. (2021). Application of the metabolomics approach in food authentication. *Molecules*, *26*(24), 1–19. https://doi.org/10.3390/molecules26247565

Soga, T. (2023). Advances in capillary electrophoresis mass spectrometry for metabolomics. *TrAC - Trends in Analytical Chemistry*, *158*, 116883. https://doi.org/10.1016/j.trac.2022.116883

Spadiut, O., Capone, S., Krainer, F., Glieder, A., & Herwig, C. (2014). Microbials for the production of monoclonal antibodies and antibody fragments. *Trends in Biotechnology*, *32*(1), 54–60. https://doi.org/10.1016/j.tibtech.2013.10.002

Sun, T., Kwok, W. C., Chua, K. J., Lo, T. M., Potter, J., Yew, W. S., Chesnut, J. D., Hwang, I. Y., & Chang, M. W. (2020). Development of a Proline-Based Selection System for Reliable Genetic Engineering in Chinese Hamster Ovary Cells. *ACS Synthetic Biology*, *9*(7), 1864–1872. https://doi.org/10.1021/acssynbio.0c00221

Tabll, A., Abbas, A. T., El-Kafrawy, S., & Wahid, A. (2015). Monoclonal antibodies: Principles and applications of immmunodiagnosis and immunotherapy for hepatitis C virus. *World Journal of Hepatology*, *7*(22), 2369–2383. https://doi.org/10.4254/wjh.v7.i22.2369

Tang, Y., Cain, P., Anguiano, V., Shih, J. J., Chai, Q., & Feng, Y. (2021). Impact of IgG subclass on molecular properties of monoclonal antibodies. *MAbs*, *13*(1), 1–12. https://doi.org/10.1080/19420862.2021.1993768

Tian, H., Lam, S. M., & Shui, G. (2016). Metabolomics, a powerful tool for agricultural research. *International Journal of Molecular Sciences*, *17*(11). https://doi.org/10.3390/ijms17111871

Tihanyi, B., & Nyitray, L. (2020). Recent advances in CHO cell line development for recombinant protein production. *Drug Discovery Today: Technologies*, *38*, 25–34. https://doi.org/10.1016/j.ddtec.2021.02.003

Vidarsson, G., Dekkers, G., & Rispens, T. (2014). IgG subclasses and allotypes: From structure to effector functions. *Frontiers in Immunology*, *5*(OCT), 1–17. https://doi.org/10.3389/fimmu.2014.00520

Villacrés, C., Tayi, V. S., Lattová, E., Perreault, H., & Butler, M. (2015). Low glucose depletes glycan precursors, reduces site occupancy and galactosylation of a monoclonal antibody in CHO cell culture. *Biotechnology Journal*, *10*(7), 1051-1066. https://doi.org/10.1002/biot.201400662

Vodopivec, M., Lah, L., Narat, M., & Curk, T. (2019). Metabolomic profiling of CHO fed-batch growth phases at 10, 100, and 1,000 L. *Biotechnology and Bioengineering*, *116*(10), 2720–2729. https://doi.org/10.1002/bit.27087

Waldmann, T. A. (1991). *Monoclonal Antibodies Therapy*. *252*(June), 1657–1662. https://doi.org/10.1126/science.2047874

Walsh, G., & Walsh, E. (2022). Biopharmaceutical benchmarks 2022. *Nature Biotechnology*, *40*(12), 1722–1760. https://doi.org/10.1038/s41587-022-01582-x

Xiang, S., Zhang, J., Yu, L., Tian, J., Tang, W., Tang, H., Xu, K., Wang, X., Cui, Y., Ren, K., Cao, W., Su, Y., & Zhou, W. (2024). Developing an ultra-intensified fed-batch cell culture

process with greatly improved performance and productivity. *Biotechnology and Bioengineering*, *121*(2), 696–709. https://doi.org/10.1002/bit.28605

Xiao, S., Ahmed, W., Mohsin, A., & Guo, M. (2021). Continuous feeding reduces the generation of metabolic byproducts and increases antibodies expression in Chinese hamster ovary-k1 cells. *Life*, *11*(9), 1–12. https://doi.org/10.3390/life11090945

Xu, J., Rehmann, M. S., Xu, M., Zheng, S., Hill, C., He, Q., Borys, M. C., & Li, Z. J. (2020). Development of an intensified fed-batch production platform with doubled titers using N-1 perfusion seed for cell culture manufacturing. *Bioresources and Bioprocessing*, *7*(1). https://doi.org/10.1186/s40643-020-00304-y

Xu, W. J., Lin, Y., Mi, C. L., Pang, J. Y., & Wang, T. Y. (2023). Progress in fed-batch culture for recombinant protein production in CHO cells. *Applied Microbiology and Biotechnology*, *107*(4), 1063–1075. https://doi.org/10.1007/s00253-022-12342-x

Yamano-Adachi, N., Arishima, R., Puriwat, S., & Omasa, T. (2020). Establishment of fast-growing serum-free immortalised cells from Chinese hamster lung tissues for biopharmaceutical production. *Scientific Reports*, *10*(1), 1–12. https://doi.org/10.1038/s41598-020-74735-0

Yoo, H. C., Yu, Y. C., Sung, Y., & Han, J. M. (2020). Glutamine reliance in cell metabolism. *Experimental and Molecular Medicine*, *52*(9), 1496–1516. https://doi.org/10.1038/s12276-020-00504-8

Online publication

National Institution of Health Science. (2022). Antibody pharmaceutical products approved in Japan, the US and Europe. Retrieved from https://www.nihs.go.jp/dbcb/mabs.html, Accessed March 13, 2024.

Unpublished reference

Sukwattananipaat, P. (2020). Studies on autophagy of Chinese hamster lung cells in serum-free culture [Unpublished master's thesis]. Osaka University.

List of publications

Original article

1. **Sukwattananipaat, P**., Kuroda, H., Yamano-Adachi, N., & Omasa, T. (2024). Metabolomic characterization of monoclonal antibody-producing Chinese hamster lung (CHL)-YN cells in glucose-controlled serum-free fed-batch operation. Biotechnology and Bioengineering, 1–20. https://doi.org/10.1002/bit.28777

Presentations

1. **Sukwattananipaat, P.**, Yamano-Adachi, N., Koga, Y., & Omasa, T. (2021). Development of monoclonal antibody producing Chinese hamster lung (CHL)-YN cells in serum-free fed-batch cultivation. [Online presentation]. Selected as a the SCEJ award presenter, at the 26th Symposium of Young Asian Biological Engineers' Community.

2. **Sukwattananipaat, P.**, Yamano-Adachi, N., & Omasa, T. (2022). Development of novel fast-growing Chinese hamster lung (CHL)-YN cells in serum-free fed-batch for monoclonal antibody production. [Poster presentation]. Selected as the poster student highlights presenter, at the 27th ESACT Meeting European Society for Animal Cell Technology, Lisbon, Portugal.

3. **Sukwattananipaat, P.**, Yamano-Adachi, N., & Omasa, T. (2024). Metabolic profiling of monoclonal antibody producing CHL-YN cells in fed-batch operation. [Oral presentation] selected as a featured presentation at the 89th International Chemical Engineering Symposia, Osaka, Japan.

4. **Sukwattananipaat, P.**, Yamano-Adachi, N., & Omasa, T. (2024). Metabolic profiling of monoclonal antibody producing CHL-YN cells in fed-batch operation. [Press release] 89th International Chemical Engineering Symposia, Osaka, Japan.

Co-author articles and presentations

1. Yamano-Adachi, N., Arishima, R., **Puriwat, S.**, & Omasa, T. (2020). Establishment of fast-growing serum-free immortalised cells from Chinese hamster lung tissues for biopharmaceutical production. *Scientific Reports*, *10*(1), 1–12. https://doi.org/10.1038/s41598-020-74735-0

2. Kunita, H., **Sukwattananipaat, P.**, Koga, Y., Yamano-Adachi, N., & Omasa, T. (2022, October). CHL-YN 細胞の重力沈降型小型灌流培養. [Oral presentation]. Presented at the 74th Annual Meeting of the Society for Biotechnology, Japan.

3. Yamano-Adachi, N., Arishima, R., **Sukwattananipaat, P.**, Koto, T., Kunita, H., Koga, Y., & Omasa, T. (2021, November). Establishing CHL-YN cells to spread their wings to the world. [Online presentation]. Presented at the 26th Symposium of Young Asian Biological Engineers' Community (YABEC2021).

4. Yamano-Adachi, N., **Sukwattananipaat, P.**, Koga, Y., Kunita, H., & Omasa, T. (2021, October). CHL-YN細胞の重力沈降型小型灌流培養. [Online presentation]. Presented at the 73rd Annual Meeting of the Society for Biotechnology, Japan.

5. Yamano-Adachi, N., Koto, T., **Sukwattananipaat, P.**, Kunita, H., Arishima, R., Koga, Y., & Omasa, T. (2021, September). 高増殖性新規生産宿主細胞Chinese hamster lung (CHL)-YN細胞の特徴とその培養制御. [Online presentation]. Presented at the 52nd Autumn Meeting of the Society of Chemical Engineers,

Acknowledgement

I would like to express my gratitude to Professor Takeshi Omasa for supervising and supporting me during my master's and PhD studies at Osaka University. He offered me excellent opportunities to study in Japan and to attend academic conferences.

I sincerely appreciate Associate Professor Noriko Yamano-Adachi for her kind and warm supervision and advice, as well as providing me with an excellent chance to do research on CHL-YN cells. She also provided me with valuable encouragement and support throughout my studies.

I would like to appreciate the Department of Biotechnology, Graduate School of Engineering, Osaka University for offering great master's and PhD courses. Also, I would like to greatly thank the Japanese Government for providing financial assistance through the Monbugakusho (MEXT) scholarship, which allowed me to pursue my study and live in Japan as an international student.

I would like to thank all Omasa Laboratory's members and alumni for being friendly, supportive, and nice to me. I genuinely enjoyed my life and felt relieved there.

I specially thank Hirotaka Kuroda and Rintaro Arishima for generously sharing information for supporting my Ph.D. research, as well as kindly teaching me how to perform experiments and having great discussions. Also, becoming good friends.

I thank these people who fulfill my wonderful memories of my time in Japan. Kouki Kuroda and Jun Ho Lee for caring for me during the first two years in Japan; Tatsuya Hokimoto for teaching me many things and being one of my best friends; Hiromu Kunita, Koto Takae, Hiroki Sadotomo, Sayaka Nagae, and Shohei Sakai for being nice CHL-YN cell team members; Passaraporn Theeraseematham for kind helping and being nice to me; Sathidaphorn Sungwallek and Junya Leim Anderson for becoming my best seniors in Japan.

Finally, I would be grateful to my family and my friends for their continued support and encouragement during my study journal.

Supporting information

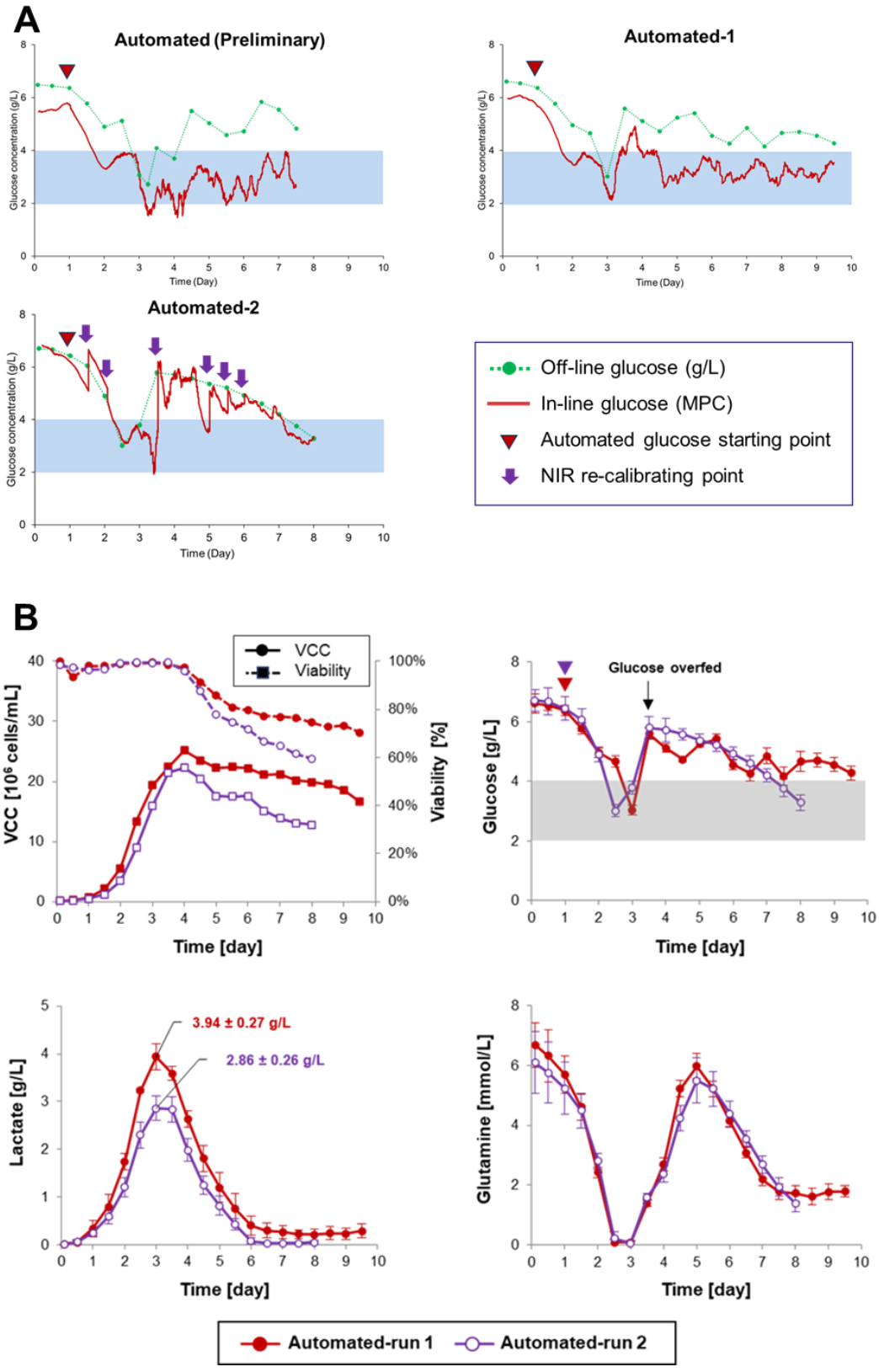

Supporting information 1. Automated glucose feeding for serum-free fed-batch cultivation of IgG-producing CHL-YN cell pool culture showed overfeeding of glucose. **A)** Extracellular glucose concentration profiles. The blue area represents the expected glucose concentration range (3.00±1.00 g/L). **B)** Time course of automated cultivation profiles. Viable cell concentration (VCC) and cell viability measured by Vi-CELL^{TM} XR cell viability analyzer are shown at solid lines and dashed lines, respectively. Extracellular glucose, lactate, and glutamine concentration measured by the YSI 2950 biochemical analyzer. The target glucose range of 3.00 ± 1.00 g/L is shown in the gray zone. Upside-down triangles point to the starting point (Day 1) of automated glucose feed control execution on each cell culture. Numerical data labels on lactate concentration plot show the maximum lactate concentration of each CHL-YN cell culture. Error bars indicate the standard deviation of triplicate measurements. These plots of culture profiles have been published and are available in Sukwattananipaat et al., 2024.

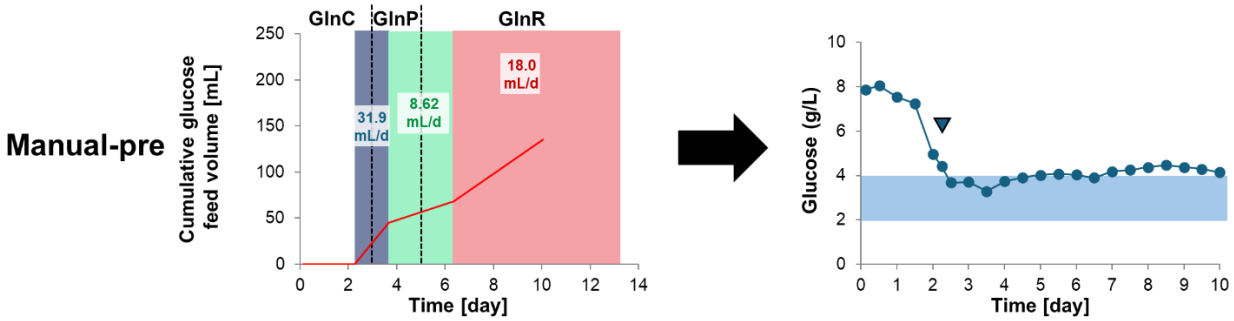

Supporting information 2. Preliminary scheduled glucose feed strategy applied for IgG-producing CHL-YN heterogeneous cell pool cultures. (Left) Time-course of cumulative glucose feed amount on each bioreactor run. Three-different colors (blue, green, and red) represent three distinct glucose feed rates following the change of glutamine metabolism (glutamine consumption, GlnC; glutamine production, GlnP; glutamine re-consumption; GlnR). Black-dashed lines represented turning points of glutamine concentration that occurred in the time-course glutamine plot.

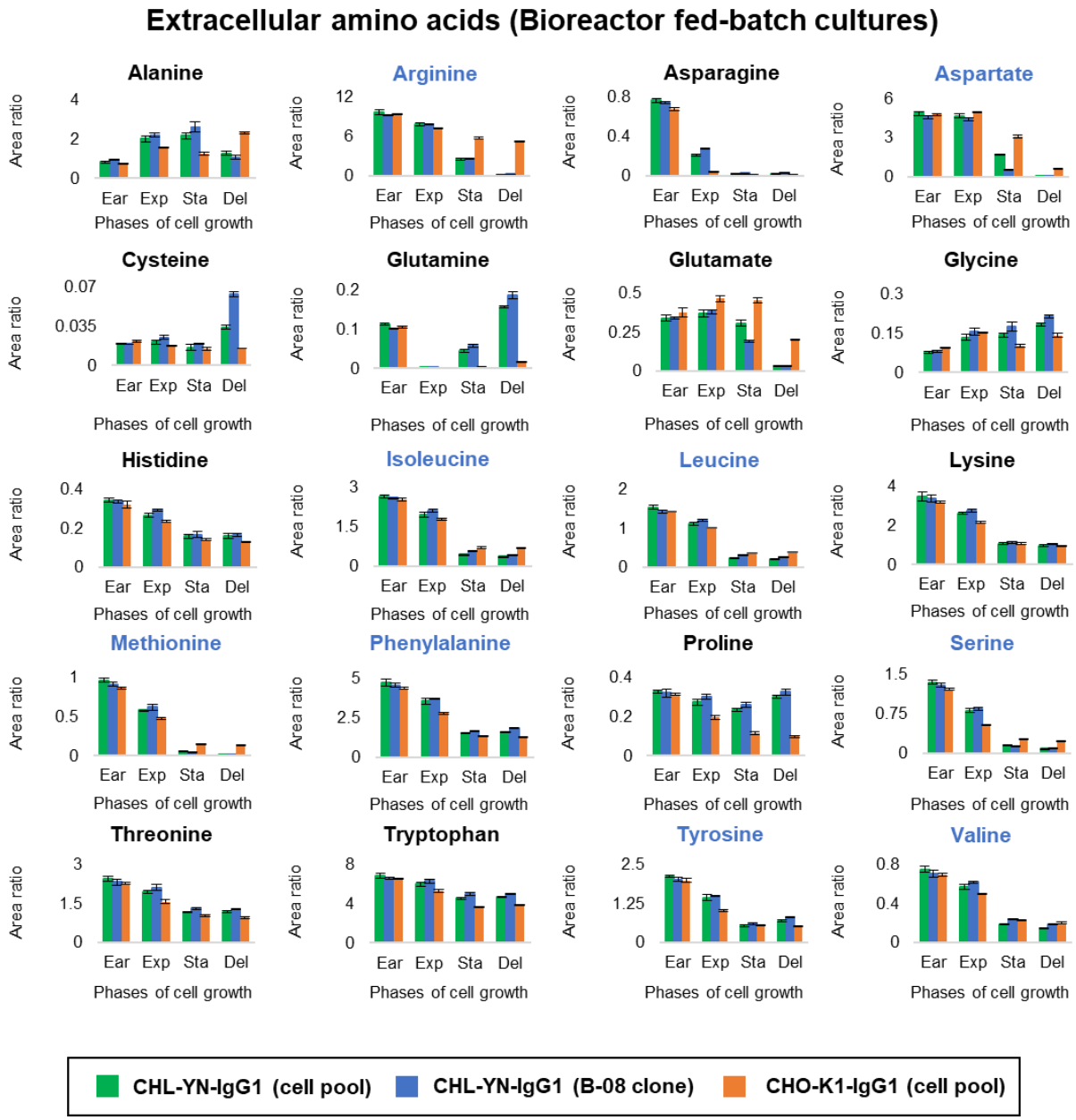

Supporting information 3. Bar charts of bioreactor-scale fed-batch extracellular concentrations of twenty amino acids in different four stages of cell growth. Ear indicates early stage (day 2 of CHL-YN and CHO-K1 cell cultures); Exp indicates exponential stage (day 3 of CHL-YN and day 4 of CHO-K1 cell cultures); Sta indicates stationary stage (day 4 of CHL-YN and day 6 of CHO-K1); and Del indicates decline stage (day 5 of CHL-YN and day 8 of CHO-K1). Blue represents nine amino acids that significantly decreased during the first glutamine shift between days 3 and 4 of CHL-YN cell cultures.

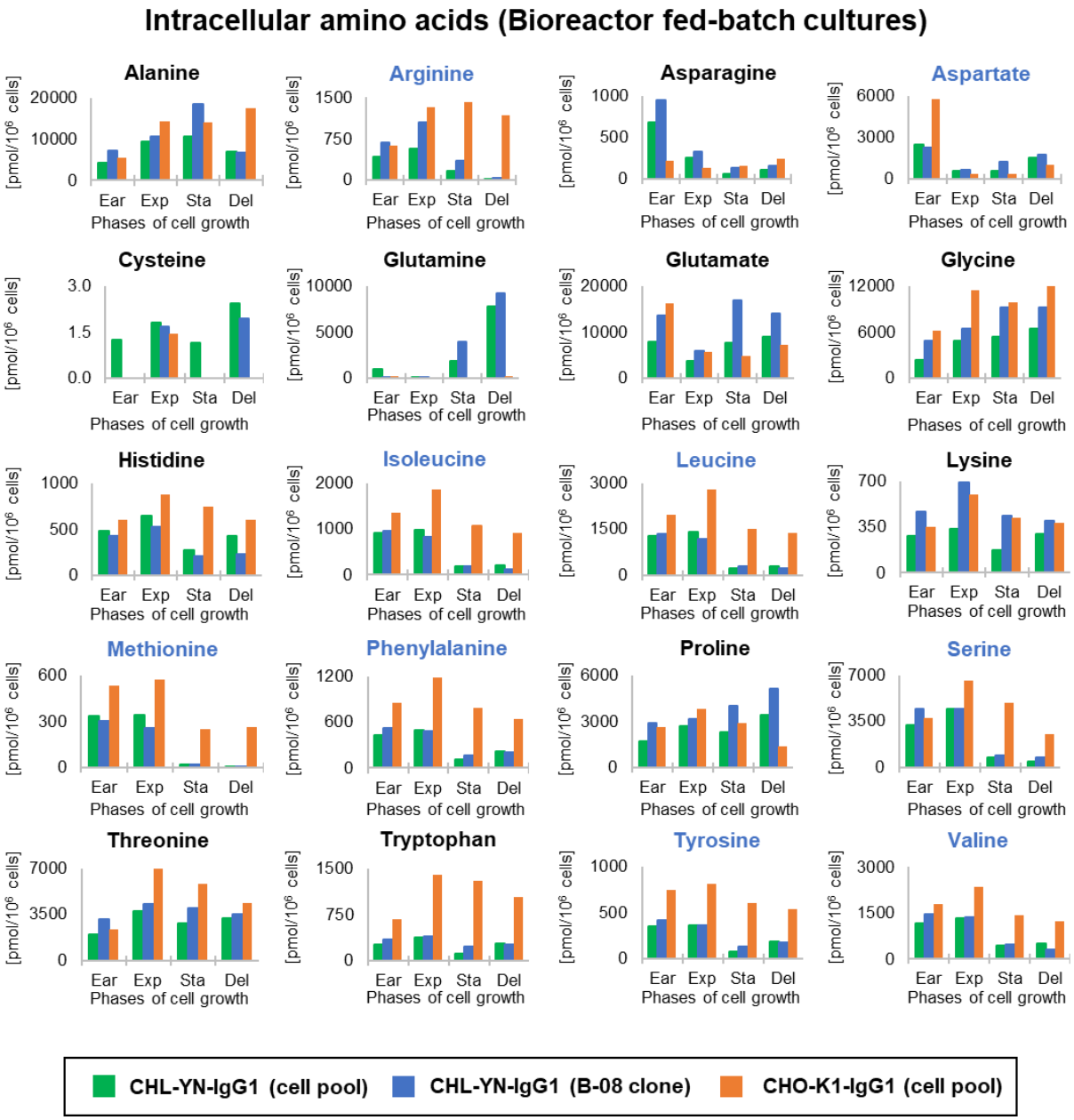

Supporting information 4. Bar charts of bioreactor-scale fed-batch intracellular concentrations of twenty amino acids in different four stages of cell growth. Ear indicates early stage (day 2 of CHL-YN and CHO-K1 cell cultures); Exp indicates exponential stage (day 3 of CHL-YN and day 4 of CHO-K1 cell cultures); Sta indicates stationary stage (day 4 of CHL-YN and day 6 of CHO-K1); and Del indicates decline stage (day 5 of CHL-YN and day 8 of CHO-K1). Blue represents nine amino acids that significantly decreased during the first glutamine shift between days 3 and 4 of CHL-YN cell cultures.

Supporting information 5. Normalized transcriptomics analysis results by reads per kilobase of exon per million mapped reads (RPKM). Flask-batch expression host CHL-YN and CHO-K1 cells cultivated in EX-CELL® CD CHO Fusion medium supplemented with 6 mM L-glutamine. Day 2 and 3 samples of CHL-YN cells were collected to analyze, while only Day 3 of CHO-K1 cells were used. Partial data have been published in Yamano-Adachi et al., 2020. Blue indicates transcript data presented only in CHL-YN cells; green indicates the significance of fold change, which shows above 1.0 of $\log_2$[CHL-YN cells (Exp) / CHO-K1 cells (Exp)]. This data is available in the supporting section of Sukwattananipaat et al., 2024.

RPKM normalized mRNA-sequencing	Samples		
	Flask-batch CHO-K1, day 3 (Exp)	Flask-batch CHL-YN, day 2 (Exp)	Flask-batch CHL-YN, day 3 (Sta)
Proline biosynthesis and urea cycle			
Arginase-2 (mitochondrial); *ARG2*	0	94.69	83.80
Argininosuccinate synthetase; *ASS*	0.02	1.65	0.74
Argininosuccinate lyase; *ASL*	2.99	3.10	3.43
Ornithine aminotransferase; *OAT*	5.18	25.00	9.93
Ornithine decarboxylase; *ODC*	18.39	177.41	110.38
Ornithine carbamoyl transferase; *OCT*	0	0	0.01
Glutamine synthetase; *GS*	0.15	1.03	0.96
Glutaminase; *GA*	9.71	26.17	14.05
Aldehyde dehydrogenase 4 family, member A1 (encoded 1-pyrroline-5-carboxylate dehydrogenase); *P5CD*	6.10	23.49	4.89
Aldehyde dehydrogenase 18 family, member A1 (encoded 1-pyrroline-5-carboxylate synthetase); *P5CS*	0.15	40.68	34.94
Pyrroline 5-carboxylase reductase; *P5CR*	15.93	4.50	3.18
Amiloride-sensitive amine oxidase (copper-containing); *AOC1*	0	0.01	0.04
Aldehyde dehydrogenase 7 family, member A1; *ALDH7A1*	21.34	17.33	7.86
Glutamate decarboxylase; *GDC2* (Glutamate → 4-aminobutyrate)	0.30	0	0

Supporting information 5. Continued.

Methionine cycle and transsulfuration pathway (cysteine biosynthesis)			
Methionine adenosyltransferase 2A; *MAT2A*	42.09	134.93	136.47
DNA (cytosine-5-)-methyltransferase 1; *DNMT1*	34.36	61.75	42.41
Nicotinamide N-methyltransferase; *NNMT*	2.56	3.57	4.71
Glycine N-methyltransferase; *GNMT* (methyltransferase)	0.02	0	0.03
Adenosyl homocysteinase; *SAHH*	67.52	188.75	113.48
Cystathionine β-synthetase; *CBS*	0.01	19.10	10.53
Cystathionine γ-lyase; *CTH*	0	4.30	0.69
Glutamate-cysteine ligase catalytic subunit	15.44	22.63	14.03
Betaine-homocysteine S-methyltransferase; *BHMT*	0	0	0
Others			
Glutamate decarboxylase 1; *GAD1*	0.00	0.00	0.00
Glutamate decarboxylase 2; *GAD2*	0.30	0.00	0.00

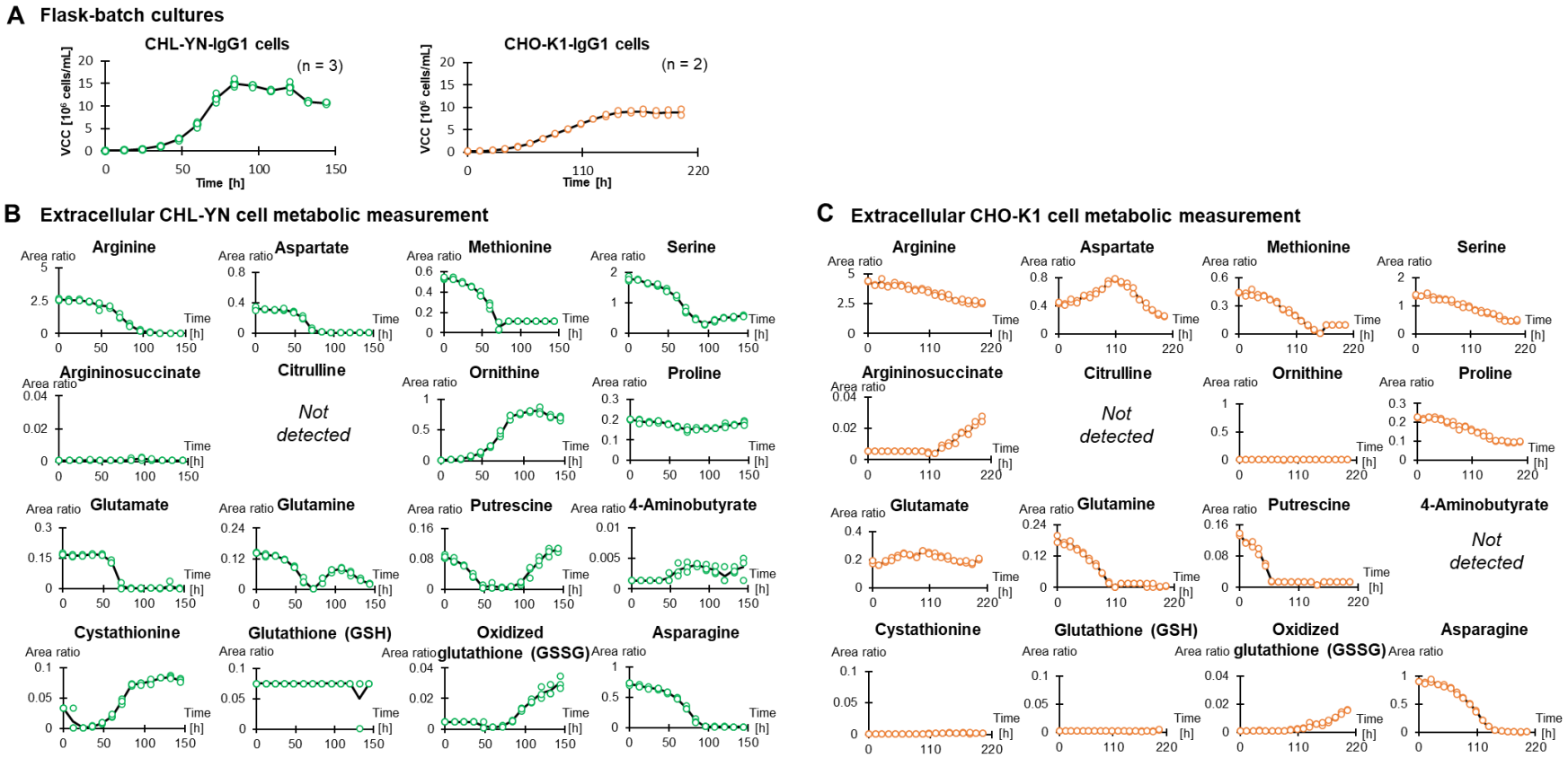

Supporting information 6. Targeted metabolomics for flask-batch extracellular compounds using the LC-MS/MS approach. Flask-batch of IgG-producing CHL-YN and CHO-K1 cells cultivated in EX-CELL® CD CHO Fusion medium supplemented with 6 mM L-glutamine and 5 µg/mL puromycin. Time-course plots of relative area (Area) illustrate highlighted metabolic concentrations involved in arginine and methionine metabolisms. Circles in the plot show processed data of detected metabolites. Whilst black lines show averaged data. **A)** Time course plot of VCC. Black arrows point to the sampling timepoints. **B)** Time course plot of CHL-YN intermediates with triplicated samples. **C)** Time course plot of CHO-K1 intermediates with duplicated samples. This data is available in the supporting section of Sukwattananipaat et al., 2024.

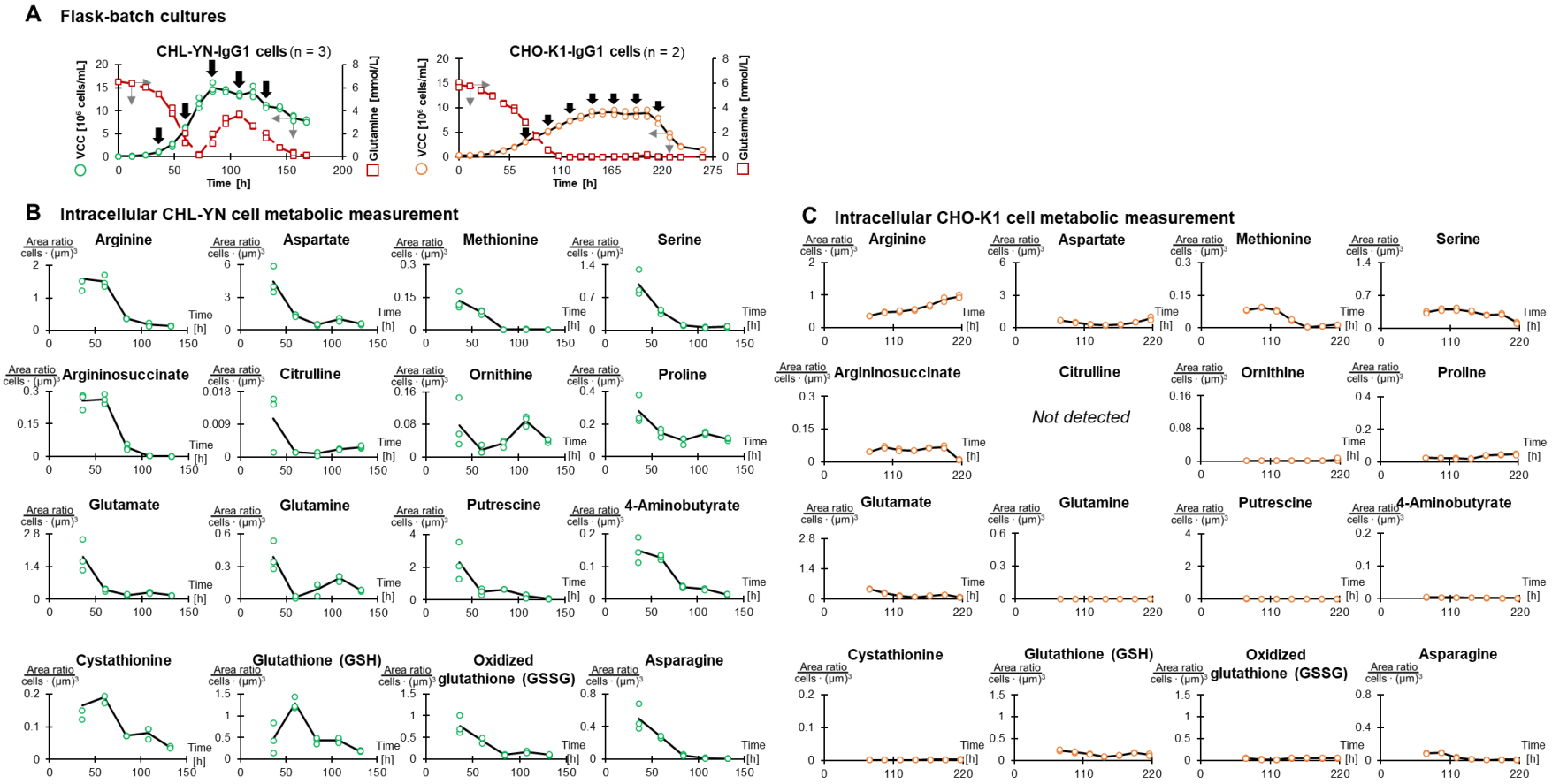

Supporting information 7. Targeted metabolomics for flask-batch intracellular compounds using the LC-MS/MS approach. Flask-batch of IgG-producing CHL-YN and CHO-K1 cells cultivated in EX-CELL® CD CHO Fusion medium supplemented with 6 mM L-glutamine and 5 µg/mL puromycin. Time-course plots of relative area (Area) illustrate highlighted metabolic concentrations involved in arginine and methionine metabolisms. Circles in the plot show processed data of detected metabolites. Whilst black lines show averaged data. **A**) Time course plot of VCC. Black arrows point to the sampling timepoints. **B)** Time course plot of CHL-YN intermediates with triplicated samples. **C)** Time course plot of CHO-K1 intermediates with duplicated samples. This data is available in the supporting section of Sukwattananipaat et al., 2024.